DEPARTMENT OF CIVIL ENGINEERING

DÉPARTEMENT DE GENIE CIVIL

DEPARTMENT OF CIVIL, ARCHITECTURAL

AND ENVIRONMENTAL ENGINEERING

PATCH LOADING AND THE EFFECTS OF ECCENTRICITY ON STEEL GIRDERS

A thesis submitted in partial fulfilment of the requirement for the degree of Masters in Engineering (Meng) in **Civil Engineering**

Curriculum: Structural engineering

Presented by:

EMECHEBE CLINTON CHISOM

Matricule Number:

15TP20960

Supervised by:

Prof. Eng. Carmelo MAJORANA

Co-Supervised by:

Dr. Eng. Emanuele MAJORANA

Dr. Eng. Guillaume Hervé POH'SIE

ACADEMIC YEAR: 2019/2020

DEDICATION

This work is dedicated to my beloved parents

EMECHEBE FEDRICK

&

HASSAN MAGDALINE MBUINFON

ACKNOWLEDGEMENT

The completion of this thesis could not have been possible without the participation and assistance of so many people whose names may not all be enumerated. Their contributions are sincerely appreciated and gratefully acknowledged. However, I would like to express my deep appreciation and indebtedness particularly to the following;

ABBREVIATIONS

a: Transverse stiffener separation

a_1: Horizontal panel width in corrugated members

a_2: Inclined panel width in corrugated members

CAE: Computer-Aided Engineering

D: Depth of section

D_x: Flexural stiffness per unit corrugation about the x-axis

D_y: Flexural stiffness per unit corrugation about the y axis

e: Eccentricity

E: Elastic Modulus

EN: European Standards

f_u: Ultimate tensile strength

f_y: Yield strength of steel

FEM: Finite Element Method

FEA: Finite Element Analysis

G: Shear modulus

t: The thickness of the section

λ: Slenderness parameter

λ_P: Upper limit for compact category

λ_r: Upper limit for non-compact category

C: Depth of the web section

T: Thickness of the section

α : Proportion of the part in compression

ψ : Stress or strain ratio

σ_{Cr} : Critical buckling stress

N_{Cr} : Critical buckling load

b: Plate cross-sectional high

v : Poisson ratio

K_F : Buckling coefficient

F_{cr}: Critical patch load resistance

h_w: Web high

t_w: Web thickness

f_{yw} : yield stress of the web

f_{y_f} : yield stress of the flange

F_u: Ultimate patch load resistance

S_s : Loading length

L_{eff} : Effective loading length

f : Deflected shape length next to the applied load.

M_{plf} : Plastic Moment.

$\tau_{Cr,L}$: Elastic local buckling stress

w Bigger of the horizontal or inclined flat plate sub-panel width

$\tau_{Cr,G}$: Elastic global buckling stress

β: global buckling factor

τ_y: shear stress

LPF: Load proportionality factor

ABSTRACT

The main objective of this study is to analyze the effects of patch loading and load eccentricities on flat and corrugated plate girders in the linear and non-linear elastic fields considering variations in slenderness, aspect ratio, loading length, loading width, corrugated angles, local and global fold ratios. To attain these objectives 35 plate girders were modeled for both linear and nonlinear buckling analysis which consisted of 10 flat and 25 corrugated plate girders. Theoretical values of patch loading resistance were computed using Eurocode and specifications by other authors. Also, a finite element package ABAQUS/CAE program is used to obtain numerical results by geometrical and material nonlinear analysis using geometric imperfections. Model verification is executed by the comparison of the theoretical and Finite element results and also from past experimental results gotten by other authors. Results show that the patch load resistance increases with decreasing aspect ratio and decreasing web slenderness. It also increases with increasing loading length and loading width. In corrugated members, Patch loading resistance increases with increasing corrugated angles and decreases with increasing global fold ratio. It also decreases with increasing local fold ratio and using unequal folds is seen to have a resistance increase when shorter inclined and longer parallel load are used. Flat web girders were seen to show global buckling accompanied by web buckling for high slenderness and web yielding for low slenderness ratios at failure. Corrugated members on the other hand show both interactive and local buckling accompanied by web and flange yielding at failure as critical buckling loads are seen to be way higher than ultimate load. Ultimate patch loading resistance generally decreases with an increase in load eccentricity which are seen to be accompanied by mostly flange buckling and yielding at high eccentricities. The effects of eccentricity is seen to increase with increase loading length and local fold ratio. Also, it decreases with increase Corrugation angle and global fold ratio. The smaller outstand for parallel fold is a more critical location as the maximum reduction in patch load capacity occurs when the patch load is kept adjacent to the edge of the shorter overhang which always accounts for a difference of 3% to 10% as compared to the longer overhang. It was observed that corrugated members show higher patch loading resistance than equivalent flat web members which could result in a 15% material reduction per unit length along the longitudinal span in the use of corrugated plates girders over flat plate girders.

Keywords: Patch loading, Corrugated web, Flat web, Eccentricities, Bridges.

EMECHEBE CLINTON CHISOM/*Master's Thesis in Civil engineering*

RESUME

L'objectif principal de cette étude était d'analyser les des effets du charges concentrées et des excentricités de charge sur les poutres plates et ondulées dans les champs élastiques linéaires et non linéaires en tenant compte des variations d'élancement, de rapport d'aspect, de longueur de chargement, de largeur de chargement, et les taux de pliage globaux. Pour atteindre ces objectifs, 35 poutres à plaques ont été modélisées pour l'analyse de flambement linéaire et non linéaire qui consistait en 10 poutres en plaques plates et 25 en tôles ondulées. Les valeurs théoriques de la résistance aux charges concentrées ont été calculées à l'aide de l'Eurocode et des spécifications d'autres auteurs. De plus, un programme d'éléments finis ABAQUS/CAE a été utilisé pour obtenir des résultats numériques par analyse non linéaire géométrique et matérielle en utilisant des imperfections géométriques. La vérification du modèle est exécutée par la comparaison des résultats théoriques et des éléments finis ainsi que des résultats expérimentaux antérieurs d'autres auteurs. Les résultats montrent que la résistance aux charges concentrées augmente avec la diminution du rapport hauteur/largeur et la diminution de l'élancement de la bande. Il augmente également avec l'augmentation de la longueur et de la largeur de chargement. Dans les éléments ondulés, la résistance au chargement augmente avec l'augmentation des angles ondulés et diminue avec l'augmentation du rapport de pli global. Il diminue également avec l'augmentation du taux de pliage local et l'utilisation de plis inégaux entraîne une augmentation de la résistance lorsque des charges parallèles inclinées plus courtes et plus longues sont utilisées. On a observé que les poutres à âmes plates présentaient un flambage global accompagné d'un flambement de l'âme pour un élancement élevé et d'une élasticité de l'âme pour de faibles rapports d'élancement. Les éléments ondulés, d'autre part, ont montré à la fois un flambement interactif et local accompagné d'une élasticité de l'âme et de la semelle à la rupture, car les charges critiques de flambement étaient bien supérieures à la charge ultime. La résistance ultime aux charges concentrées diminue avec l'augmentation de l'excentricité de la charge, ce qui s'accompagne principalement d'un voilement des brides et d'une plastification à des excentricités élevées. En outre, il a été observé que les éléments ondulés présentent une résistance aux charges concentrées plus élevée que les éléments d'âme plats équivalents, ce qui pourrait entraîner une réduction de 15 % du matériau par unité de longueur le long de la portée longitudinale lors de l'utilisation de poutres en tôle ondulée sur des poutres en tôle plate.

Mots-clés : Charges concentrées, Nappe ondulée, Nappe plate, Excentricités, Ponts.

EMECHEBE CLINTON CHISOM/*Master's Thesis in Civil engineering*

TABLE OF CONTENTS

LIST OF TABLES

LIST OF FIGURES

GENERAL INTRODUCTION

Steel plate girders are widely used in engineering structures; bridges, long spanned buildings, gantry cranes, liquid and gas containers, shipping containers are amongst the engineering applications of plated structural elements. Patch loading or partial edge loading of steel girder webs is a load case where a concentrated force is introduced perpendicular to the flange of a girder. Patch loading and the effects of loading eccentricities are unavoidable in steel structures because this usually induces a local failure of the girder web in the vicinity of the loaded flange. In structural applications, concentrated forces are a common load case for girders introduced for example; at supports, by purlins, from crane wheels, and during the launching of bridges. For fixed loads, the problem of concentrated forces is usually solved by transverse stiffeners but for moving loads, this is not practically possible neither an economical solution. For a bridge girder, the problem concerning resistance to patch loading usually occurs during launching. Bridge incremental launching is a common method to erect steel and composite bridges. This means that the bridge girders are assembled on the ground behind the abutment and then pushed out over launching shoes into the final position. Patch loads are always derived which is always to a magnitude that governs the web thickness and even a small increase of the web thickness can add a substantial amount of steel. Generally, for an applied load, a large portion of the force is carried by the web panel and the bending moment by the flange plates. The induced shear forces in the web are generally lower than the normal forces in the flanges. To obtain a high strength to weight ratio demands the use of deep-section (Ghadami, A., & Broujerdian 2019). This results in the use of slender webs which are susceptible to buckling. Various parameters affect the patch loading resistance for plate girders some of which include slenderness, aspect ratio, loading length, loading width, corrugation angle, local and global fold ratio. The British architect and engineer Henry Palmer in 1929 initiated the idea of using the corrugated metal sheet for webs of plate girders. It was observed that sheets that fold perpendicular to flanges produced web stiffening, which significantly increases critical stress, thus allowing the use of slender walls (Basiński 2019)

Corrugated steel webs have been widely used in various structures due to their several advantages. They can be used to replace the stiffened steel plates in plate girders as they reduce out-of-plane displacements. Also, they improve the performance of beams especially the out-of-plane strength such as lateral-torsional buckling resistance (Abbas, M., Ibrahim, S. M., & Korashy 2019).

Other parameters such as corrugation width and angle of corrugation also influence significantly the load-bearing capacity of corrugated plate girders. Despite the growing numbers of publications on this topic, most of them are centered around investigating how these parameters affect the load resistance and buckling behavior and the use of corrugations to replace stiffeners.

However, the main objective of this study is to analyze and effects of patch loading and resistance reductions due to the presence of load eccentricities in linear elastic and nonlinear elastic fields of plate girders with planar and corrugated webs under the same patch loads and boundary conditions. This will be done considering variations in slenderness, aspect ratio, loading length, loading width, corrugated angles, local and global fold ratios. To attain these objectives, 35 plate girder models were used consisting of 10 flat plate girders and 25 corrugated webs girders. Theoretical values of patch loading resistance were evaluated according to EN 1993-1-5 and specifications from other authors which were computed using MS Excel. A finite element analysis package ABAQUS/CAE was calibrated and used to obtain results by the FEM of analysis.

This study is divided into three main chapters. The first chapter is the literature review which focuses on the definition of plate girders, their general behaviors, classification of plate girders, and further elaborations on plate girders with flat and corrugated webs as well. The second chapter describes the methodology used in the study to obtain results focusing on geometric classification, material properties, theoretical and finite element method for patch loading resistance computation, and the modeling methodology using ABAQUS/CAE FEA package. The last chapter of this work presents the results, analysis, and discussion of these results. Here also, a comparative analysis between flat and corrugated girders will be made.

CHAPTER 1. LITERATURE REVIEW

Introduction

The application of steel in engineering works has rapidly increased in the last decade. This accounts for the lots of research works investigating the behavior of this structural element. This chapter gives a general overview of steel which is used in construction, paying great attention to steel girders, and also presents the state of research works in this area of study. To better talk about it, this chapter is divided into six parts. The first part of this chapter gives the definition of plate girders and a general application in construction. This is followed by the presentation of the different patch loading scenarios in steel construction. Stating their origin and imposed problems. The third part of this chapter talks about the classification of plate girder sections as compact, non-compact, and slender sections as a function of the slenderness parameter according to Eurocode standards. This is followed by the description of the general behavior of plate girders elaborating on their ultimate resistance and their elastic buckling and failure modes. The fifth parts present general aspects and research works for flat plate girders and finally followed by corrugated webs discussing the types of corrugations, failure modes, their design parameters, some research works investigating their behaviors. This part also presents some profiles of corrugated steel bridges constructed around the world.

1.1. STEEL GIRDERS IN CONSTRUCTION

Steel plate girders are widely used in engineering structures. Bridges, long spanned buildings, gantry cranes, liquid and gas containers, shipping containers are amongst the engineering applications of plated structural elements.

1.1.1. Definition of Plate girders

Plate girders are I-beams built up from plates that are joined together by angles and rivets, with or without stiffeners to obtain the desired size. They are also known as deep flexural members which are capable of carrying heavy loads. (Chi 2014)

For making the cross-section efficient to resist in-plane bending it is required that maximum material is placed as far away from the neutral axis as possible. As the depth of section increases, the depth of web increases and it becomes slender, premature failure of girder due to web buckling in shear might occur. Hence to reduce the slenderness ratio created by the high depth and small thickness of the web, instead of using stiffeners, the corrugated web is the possible way to give stability against the elastic buckling of the web. (Rajkumar et al. 2017)
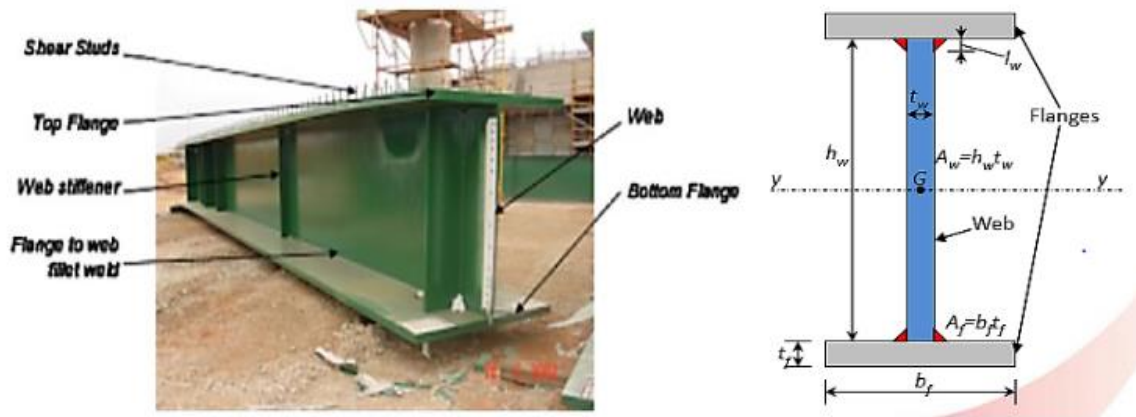
Figure 1.1. Cross section of a typical plate girder (Chi, 2014)

1.2. APPLICATION OF STEEL

In construction applications, the web usually bears most of the compressive stress and transmits shear in the beam while the flanges support the major external loads. In most practical ranges, the induced shearing force is relatively lower than the normal flange forces. (Elgaaly et al. 2000) Therefore, to obtain a high strength to weight ratio, it is common to choose deep slender sections. But slender sections are susceptible to web buckling (Ajeesh 2016). This led to the need for slender sections with stiffeners or corrugations along the web section. The use of corrugations is gradually replacing the use of stiffeners. Various forms of instabilities, such as shear buckling of web plates, lateral beam buckling of girders, compressive buckling of webs, flange-induced buckling of webs, local buckling, and crippling of webs are considered in design procedures (Kala, Z., & Kala 2019). Again, it has been proven that the use of thinner webs results in lower material cost, with an estimated cost savings of 10-30% in comparison with conventionally fabricated sections and more than 30% compared with standard hot rolled universal beams. (Rajkumar et al. 2017)

1.2.1. Construction of long-span Industrial buildings

Industrial buildings and warehouses require unobstructed access and passage to allow the circulation of vehicles and provide convenient and large work surface areas.

This results in the need for lightweight but high-strength steel material. However, to realize steel of high strength to weight ratio requires the use of deep and thin sections making plate girders the best choice for its application.

Figure 1.2. Plate girders in realization of industrial buildings(www. steelconstruction)

1.2.2. Lifting Machines (Gantry crane)

A gantry crane is a type of overhead crane with a single or double girder configuration supported by freestanding legs that move on wheels or along a track or rail system. Gantry cranes are usually considered when there is a reason not to incorporate an overhead runway system. The high strength to weight ratio of steel plate girders allows the possibility and applicability of plate girders as gantry cranes to support large loads

Figure 1.3. Plate girder application in gantry cranes (https://dafangcranez.com)

1.2.3. Bridge Construction

Plate girders became popular in the late 1800s when they were used in the construction of railroads and long-span bridges. The plates were joined together using angles and rivets to obtain plate

girders of desired sizes. By the 1950s welded plate girders replaced riveted and bolted plate girders in the developed world due to their better quality, aesthetics, and economy. The use of plate girders rather than rolled beam sections for the two main girders gives the designer freedom to select the most economical girder for the structure.

Figure 1.4. Application of plate girders in bridge constructions (https://www.indiamart.com)

1.3. PATCH LOADING IN STEEL GIRDER STRUCTURES

Patch loading or partial edge loading of steel girder is a load case where a concentrated force is introduced perpendicular to the flange of a girder. Patch loading and the effects of loading eccentricities are unavoidable in steel structures because this usually induces a local failure of the girder web in the vicinity of the loaded flange. In structural applications, concentrated forces are a common load case for girders introduced for example; at supports, by purlins, from crane wheels and during the launching of bridges

1.3.1. Incremental Launching

One of the most competitive bridge construction methods for long-spans is the incremental launching technique. Different technologies are used for bridge erection around the world, among which, the incremental Launching method appears to be preferred according to the statistics presented by many researchers. (Kövesdi et al., 2014; Graciano and Zapata-Medina,2015; Kövesdi and Dunai, 2016; Tetougueni et al.,2019).

Figure 1.5. Incrementally-launched bridge construction (Valley Bridge Coburg)

For long bridges, bridges high over ground or bridges over water, i.e. when the bridge is either too heavy to lift into position or it is impossible for other reasons, a very common method to erect the bridge girders is to launch it from one or both ends. This means that sections manufactured at the workshop are welded together on the ground and then pushed out over launching shoes into the final position. A launching nose is usually placed in the front of the bridge girder to both get it up on the next support and also to decrease the bending moment and support reaction in the girder at the launching shoe because the launching nose usually consists of a steel truss with low weight.(Egziabher and Edwards 2013)
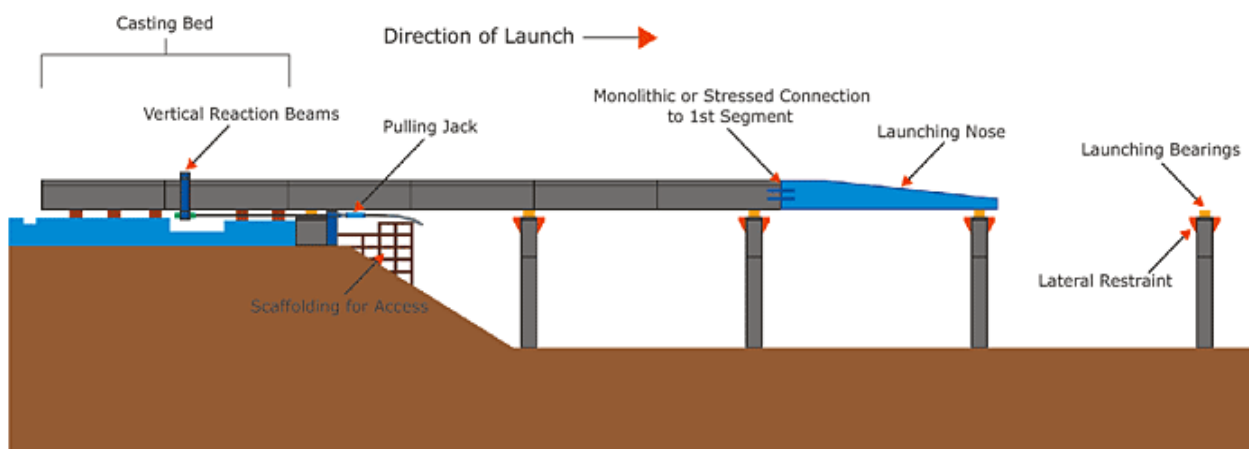
Figure 1.6. Layout for incremental launching

EMECHEBE CLINTON CHISOM/*Master's Thesis in Civil engineering*

For a steel bridge girder, the problem concerning resistance to patch loading occurs during the launching of the girder. The lower flange is subjected to a concentrated force from the launching shoe, along which the girder travels. Also, just before the launching nose reaches the next support large bending moments are present. So high support reactions have to be introduced during the launching process as transverse forces into the girder web which also interacts with shear forces and bending moments. A section of the girder can be subjected to several repeated traveling concentrated forces when passing over several supports during launching. These concentrated forces can be of the magnitude that governs the web thickness and even a small increase of the web thickness can add a substantial amount of steel. Therefore, it is important to find a suitable criterion for resistance evaluation during this process.
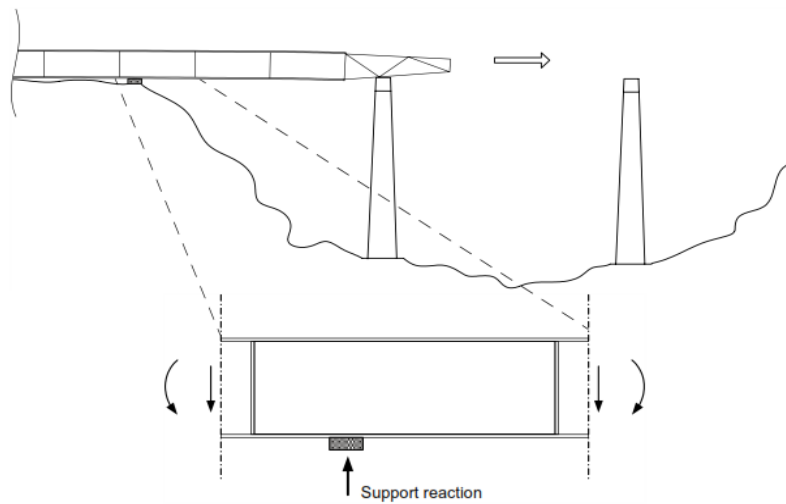
Figure 1.7. Launching of a bridge girder and load situation

1.4. PLATE GIRDERS CLASSIFICATION

1.4.1. Classification of plate girder sections

Plate girders can be classified as compact, non-compact, or slender depending on the type of loading it experienced and the values of the width-to-thickness ratios of its elements(Abdul Siraj,2016). The Euler equation defining the slenderness parameter (λ) is given by equation (1.1)

$$\lambda = {D}/{t} \qquad\qquad (1.1)$$

Where:

D: is the depth of the section,

t: is the thickness of the section.

Compact, non-compact, and slender plates are therefore defined based on the limiting parameters

λ_P (upper limit for the compact category) and

λ_r (upper limit for the non-compact category)

1.4.1.1. Compact plates

Compact or stocky sections are members of the plate having D/t ratios between 0 and λ_P. They are not expected to exhibit any buckling behavior. They yield before buckling and no post-buckling is expected in this aspect. The applied loading history of compact plates is divided into three stages, namely, material reaching the limit of proportionality, plastic buckling, and post-plastic softening (Alinia, Habashi, & Khorram, 2009). Their compressive strength is limited by the material compressive strength.

1.4.1.2. Non-Compact plates

These are members with limiting D/t ratios between λ_P and λ_r. They exhibit both elastic and plastic buckling behavior. In non-compact plates, material yielding and geometric instability are nearly simultaneous. The applied loading history of these plates are divided into two stages; material reaching the limit of proportionality, followed by inelastic post-buckling and softening stage. Their compressive strength is limited by inelastic buckling.

1.4.1.3. Slender plates

Slender plates are with having D/t ratios between greater than λ_r. They exhibit elastic buckling behavior such that a slender plate under shear or patch loading buckles elastically at early stages of loading and may experience material and geometric nonlinearities during its post-buckling behavior. The load-displacement history of such a plate is divided into four stages; elastic buckling, formation of diagonal yield zone, ultimate capacity, and softening. Their compressive strengths are limited by elastic buckling.

1.4.2. Cross section Classification of members

Members of plate girders will be classified according to EC3 Part 1-1, Section 5.5 where cross-sections of plate girders are classified to identify the extent to which the resistance and rotation

capacity of cross-sections is limited by its local buckling resistance. Members are classified as class 1, class 2, class 3, and class 4. Cross-sections. (da Silva, Simões, and Gervásio 2010)
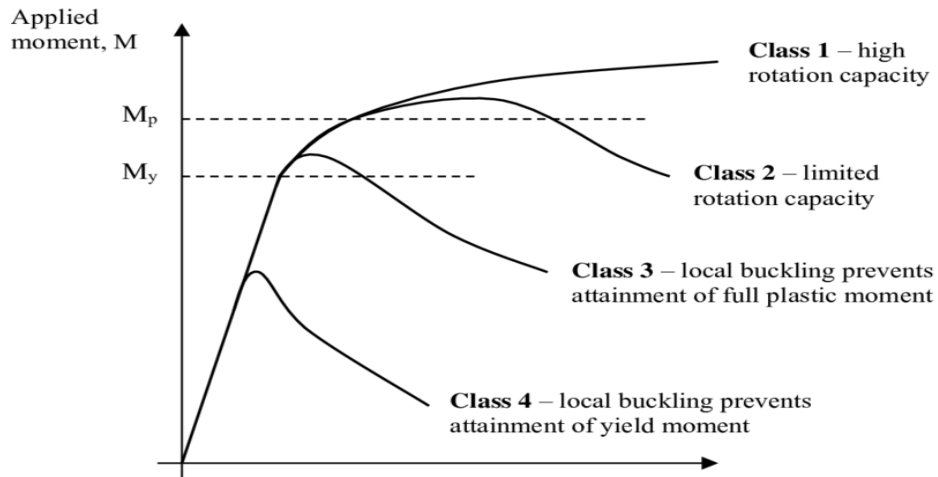
Figure 1.8. Resistance behavior for different steel classes

1.4.2.1. Class 1 Cross section

Class 1 cross-sections are those which can form a plastic hinge with the rotation capacity required from the plastic analysis without reduction of the resistance.

1.4.2.2. Class 2 Cross section

Class 2 cross-sections are those which can develop their plastic moment resistance but have limited rotation capacity because of local buckling.

1.4.2.3. Class 3 Cross section

Class 3 cross-sections are those in which the stress in the extreme compression fiber of the steel member assuming an elastic distribution of stresses can reach the yield strength, but local buckling is liable to prevent the development of plastic moment resistance.

1.4.2.4. Class 4 Cross section

Class 4 cross-sections are those in which local buckling will occur before the attainment of yield stress in one or more parts of the cross-section. The limiting proportions for class 1, 2, and 3 members are obtained from table 5.2 of the Eurocode for internal compression members and the outstanding flanges are summarized in **Error! Reference source not found.** and **Table 1.2** respectively

Table 1.1.Limit proportions for class 1, 2, and 3 sections for web

Class	Parts subjected to Bending	Parts subjected to Compression	Part in bending and in compression
1	$c/t \leq 72\varepsilon$	$c/t \leq 33\alpha$	For $\alpha > 0.5$: $c/t \leq \dfrac{396\varepsilon}{13\alpha-1}$ For $\alpha \leq 0.5$: $c/t \leq \dfrac{36\varepsilon}{\alpha}$
2	$c/t \leq 83\varepsilon$	$c/t \leq 38\varepsilon$	For $\alpha > 0.5$: $c/t \leq \dfrac{456\varepsilon}{13\alpha-1}$ For $\alpha \leq 0.5$: $c/t \leq \dfrac{41.5\varepsilon}{\alpha}$
3	$c/t \leq 12\varepsilon$	$c/t \leq 42\varepsilon$	For $\psi > -1$: $c/t \leq \dfrac{42\varepsilon}{0.67+0.33\psi}$ For $\psi \leq 1$: $c/t \leq 62\varepsilon(1-\psi)\sqrt{(-\psi)}$

$$\varepsilon = \sqrt{(233/f_y)}$$

$$c = h_\omega - 2t_f - 2r \qquad\qquad (1.2)$$

Where

C is the depth of the web section

T is the thickness of the section

f_y is the yield strength

α is a proportion of the part in compression

ψ is the stress or strain ratio

$\Psi \leq -1$ applies where either the compression stress $\sigma \leq f_y$ or the tensile strain $\varepsilon_y > f_{y}/_E$

Table 1.2. Limit proportions for class 1, 2, and 3 sections for outstand flanges

Class	Parts subjected to Bending	Parts subjected to Compression	
		Tip in compression	Tip in tension
1	$c/t \leq 9\varepsilon$	$c/t \leq \dfrac{9\varepsilon}{\alpha}$	$c/t \leq \dfrac{9\varepsilon}{\alpha\sqrt{\alpha}}$
2	$c/t \leq 10\varepsilon$	$c/t \leq \dfrac{10\varepsilon}{\alpha}$	$c/t \leq \dfrac{10\varepsilon}{\alpha\sqrt{\alpha}}$
3	$c/t \leq 14\varepsilon$	$c/t \leq 12\varepsilon\sqrt{K_\sigma}$	

With

$$c = (b_f - t_\omega - 2r)/2 \qquad\qquad (1.3)$$

Below is a summary showing class according to EC with the variation of depth-thickness ratio, susceptibility to buckling, and with BS5950 classification equivalence. (da Silva et al. 2010)

Table 1.3. Classification of section according to EC and BS5950 equivalence

EC3	BS5950
Class 1	Plastic
Class 2	Compact
Class 3	Semi-compact
Class 4	Slender

Increasing c/t (left arrow, downward)

Increasing local buckling susceptibility (right arrow, downward)

1.5. GENERAL BEHAVIOR OF PLATE GIRDERS

1.5.1. The behavior of plate girders

Plated structural members can be subjected to direct stress, shear stresses, or bending.

(a) Combined loading (b) Bending stress (c) Shear stress (d) Transverse stress
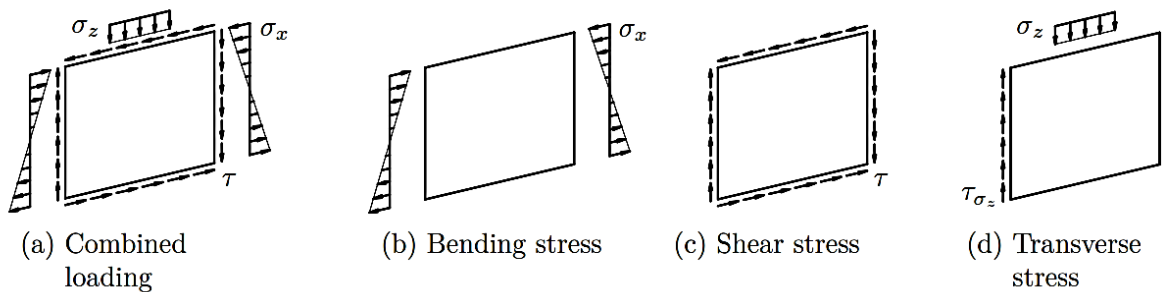
Figure 1.9. Plate under combined loading (a) and basic load effects (b-d)

These plate elements under the actions of stresses are susceptible to buckling. Buckling is defined as a mode of failure under compression of a structural component that is thin with respect to its length Buckling greatly limits the Ultimate compressive strength of plate elements, that is the maximum load that a material can withstand before failure in a compression environment.
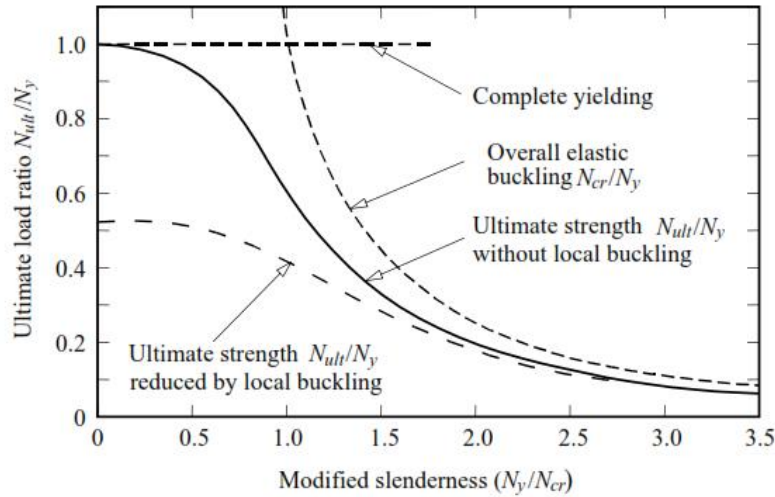
Figure 1.10. Effects of local buckling on the resistances of compression members.

$$\sigma_{Cr} = N_{Cr}/bt \tag{1.4}$$

$$\sigma_{Cr} = \frac{\Pi^2 E}{12(1 - v^2)} \frac{K_F}{(b/t)^2} \tag{1.5}$$

Where,

The lowest value of the buckling coefficient $K_F = 4$

For the hypothetical limiting case of a perfectly straight elastic member, there is no bending until the applied load reaches the elastic buckling value N_{Cr} refers to as the elastic critical force. At this load, the compression member begins to deflect laterally, as shown in **Figure 1.11**

These deflections grow until failure occurs at the beginning of compressive yielding. This action of suddenly deflecting laterally is called flexural buckling. In some cases, plate girders rely on the strength available after the web has buckled, so most of the flexural strength will come from the flanges. This brings in the need to study Post-buckling, Post-buckling has to do with the response of a compression member, beyond the critical buckling load. They are highly non-linear.(Alinia, Gheitasi, and Shakiba 2011)
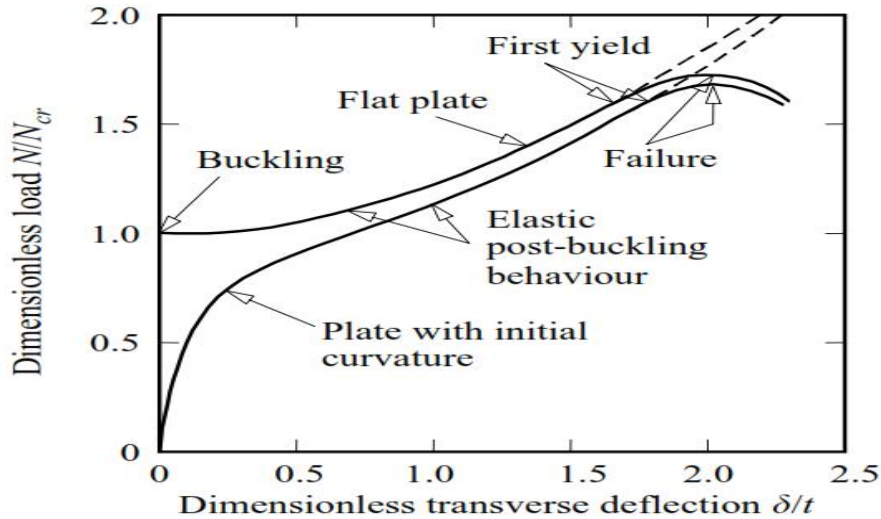
Figure 1.11. Post-buckling behavior of thin plates.

1.5.2. Buckling in plate girders

Buckling in girders is very common as it greatly affects its ultimate load. This varies with different geometrical properties such as aspects, loading, and boundary conditions.

1.5.2.1. Local buckling

Local buckling is normally defined as the mode which involves plate-like deformations alone without the translation of the intersection lines of the adjacent plate elements. Local buckling is characterized by skin buckling between stiffening elements for stiffened members or skin buckling within individual folds for corrugated members. Another important feature of local buckling is that the associated buckling length is the smallest among the three modes, and typically less than the width of any plate that construct the cross-section (Ethod, 2004)

1.5.2.2. Global buckling

Global buckling is a buckling mode where the member deforms with no deformation in its cross-sectional shape. Global is characterized by buckling of the entire panel including stiffening elements for stiffened members or a combination of folds in corrugated plates. Thus, the deformations can be characterized by the displacement and torsion of the system line of the member. Depending on the deformations and the type of loading, further subclasses can be defined such as flexural buckling, torsional buckling, flexural-torsional buckling, and lateral-torsional buckling.

1.5.2.3. Interactive or distortion buckling mode

The interactive or distortionary buckling mode is the combination of local and global buckling mode. Distortion buckling seems to be the most problematic mode. As far as the associated buckling length is concerned it is typically in between the lengths of local and global modes, while the transverse deformations involve both plate-like deformations and the translation of one or multiple intersection lines of adjacent plate elements (Ethod, 2004). Also, it is important to know that each of these buckling modes has its characteristic post-buckling behavior. It is well known that local buckling may have a significant post-buckling reserve (at least for larger slenderness's where the behavior is primarily elastic). Distortion buckling may have a post-buckling reserve, too, but considerably less than for local buckling; while global buckling (such as flexural buckling of a column) has no post-buckling reserve at all, but the real capacity of the member is always less than its elastic critical load. Thus, it is extremely important to classify the various buckling modes to get realistic design resistance (Ethod, 2004)

1.6. PLATE GIRDERS WITH FLAT WEB

Concentrated transverse forces on girders are commonly referred to as patch loads. Such loads occur in many applications and if the loads are moving as for a crane girder or a bridge girder during launching, the load has to be resisted by the web alone that is without the assistance of vertical stiffeners. The design for such loads has traditionally comprised two independent checks, one for yielding and one for buckling. The response from a girder web subjected to a patch load can be described with one of three failure modes i.e. yielding, buckling, or crippling of the web. However, there is no clear distinction between crippling and buckling instead it could be seen as a gradual change of buckling shape. Normally, the buckling mode is first initiated and followed by a local crippling mode at loads in the vicinity of the ultimate load. (Gozzi n.d.)
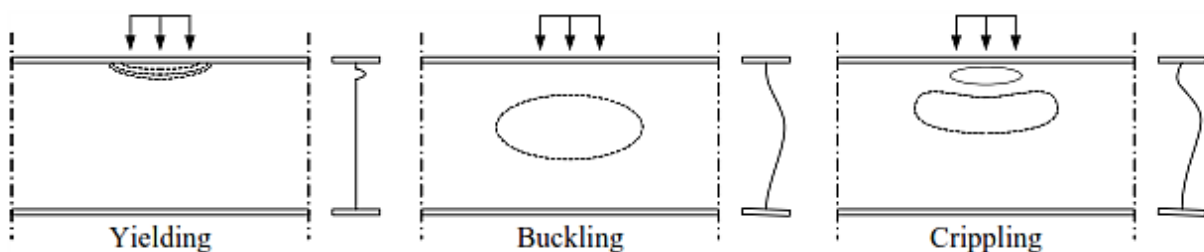
Figure 1.12. Schematic failure modes for girders subjected to patch loading.

1.6.1. Critical Patch loading resistance for flat web girders

The design rules in EN 1993-1-5 cover three different cases of patch loading shown in Figure 1.13
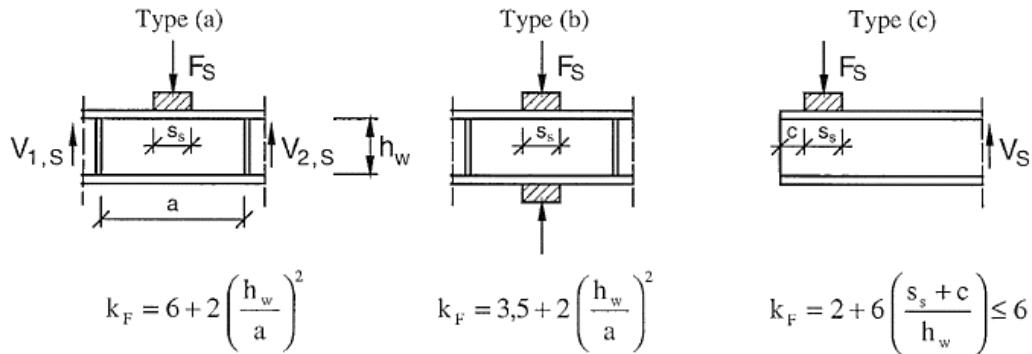
Figure 1.13. Different types of patch loading and approximate buckling

Type (a) is referred to as patch loading, type (b) opposite patch loading, and type (c) end patch loading. The critical patch load resistance can be represented as presented by equation (1.6)

$$F_{Cr} = K_F \frac{\Pi^2 E}{12(1 - v^2)} \frac{t_w^3}{h_w} \approx 0.9 K_F \frac{E t_w^3}{h_w} \tag{1.6}$$

where the coefficient K_F depends on the type of loading and the geometry as shown in **Figure 1.13**

1.6.2. Ultimate patch loading strength for Flat web girders

All test results indicate that the ultimate resistance of a girder subjected to patch loading is almost independent of the web depth h_w. However, the ultimate load is more or less directly proportional to the square of the web thickness and is influenced to a lesser extent by the loaded length, Ss, the flange stiffness, and the yield strength of the web, f_{yw}. One of the first reasonable estimates of the actual resistance was developed by Carl-Adolf Granholm in 1960 at Chalmers University, Sweden. Granholm reported seven tests with concentrated loads on girders with slender webs. He ended up with a resistance to patch load according to the formula:

$$F_u = 0 \cdot 85 t_w^2 \tag{1.7}$$

Where

t_w is the web thickness in mm

The format of the equation was not dimensionally consistent and with present knowledge, it can be converted. Assuming that the girders (S275) that were tested had an average yield strength of 350 MPa the ultimate resistance can be rewritten as soon on equation (1.8)

$$F_u = t_w^2 \sqrt{f_{yw}E}$$

(1.8)

Where

E is the Young's modulus

f_{yw} the yield stress of the web

This formula shows the influence of the most important parameters on the patch loading resistance. This is the same format as the resistance of a slender plate according to von Karman's model and numerically it is about half the resistance of a uniformly compressed plate (actually 1/1,9). Bergfeld and co-workers continued the tradition of studying patch loading at Chalmers University. He went on studying this problem for a long time and proposed step by step several empirical formulae for the patch loading resistance including more and more parameters. At the same time, Rockey and Roberts were working with the same problem in Cardiff. Roberts presented a mechanical model based on a folding mechanism in the web to predict the buckling resistance.
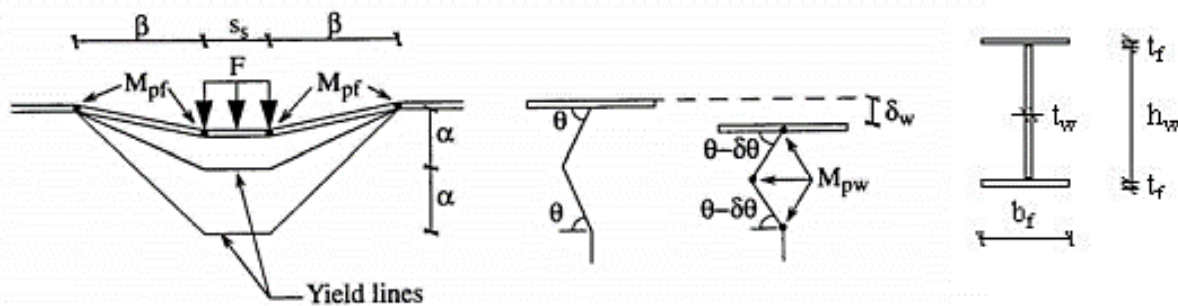
Figure 1.14. Mechanical model for patch loading resistance according to Roberts

A folding mechanism like that in **Figure 1.14** gives a resistance that is decreasing with increasing deformation and to get a fixed value Roberts assumed that the deformation was given by the elastic bending deformation of the flange. This assumption is a bit arbitrary but was justified by tests

results. This model was the basis for the formula in EN 1993-1-1 in which the buckling resistance was given by:

$$F_u = 0.5t_w^2 \sqrt{Ef_{yw}} \left(\sqrt{\frac{t_f}{t_\omega}} + 3\frac{t_w S_s}{t_f h_w} \right) \frac{1}{\gamma_{M_1}}$$

(1.9)

A limitation that S_s should not be taken as more than $0.2S_s$ applies, which makes the contribution from the second term in the brackets quite small. Johansson et al. (2001) present the new design rules that were introduced in Eurocode 3 for plated structures. The design rules for patch loading follow the procedure by Lagerqvist (1994) and Johansson (1996) but with a different reduction Factor. Finally, the design value for Patch loading resistance according to EN 1992-1-5 (2006) was given as shown by equation (1.10) below

$$F_u = \frac{f_{yw} \cdot L_{eff} \cdot t_w}{\gamma_{M1}}$$

(1.10)

Where

$$L_{eff} = \chi_F \cdot l_y \qquad\qquad l_y = s_s + 2 \cdot t_f \cdot \left(1 + \sqrt{m_1 + m_2}\right) \le a$$

$$m_1 = \frac{f_{yf} \cdot b_f}{f_{yw} \cdot t_w}$$

$$m_2 = 0.02 \left(\frac{h_w}{t_f}\right)^2 \qquad for \quad \bar{\lambda}_F > 0.5$$

$$m_2 = 0 \qquad\qquad for \ \bar{\lambda}_F \le 0.5$$

$$\bar{\lambda}_F = \sqrt{\frac{l_y \cdot t_w \cdot f_{yw}}{F_{Cr}}} \qquad\qquad F_{Cr} = K_F \frac{\Pi^2 E}{12(1-v^2)} \frac{t_w^3}{h_w} \approx 0.9 K_F \frac{E t_w^3}{h_w}$$

Table 1.4. Effects of geometric parameters of Flat webs on shear capacity and buckling

(Luo & Edlund, 1996)

Planar-section web

Description	Notation	Effects on Shear Capacity	Effects on buckling
Web thickness	t_w	Increases when t_w increases, but not linearly	Increased post-buckling capacity when t_w increase. t_w smaller = More local buckling
Web Depth	h_w	Increases proportionally with h_w Shear not dependent on web Length/Depth ratio of a Girder	h_w larger = More interactive buckling

1.7. PLATE GIRDERS WITH CORRUGATED WEBS

Corrugated steel webs have been widely used in various structures due to their several advantages. Firstly, they can be used to replace the stiffened steel plates as they reduce out-of-plane displacements and prevent out-of-plane buckling of the web. Secondly, corrugated steel webs improve the performance of beams especially the out-of-plane strength such as lateral-torsional buckling resistance(Abbas, M., Ibrahim, S. M., & Korashy 2019). The types of corrugations failure modes and the design parameters are the most important aspects of corrugated members. These together with the state of research works investigation behavior of corrugated plate girders and profiles of some corrugated steel webs for some constructed bridges will be discussed in this section.

1.7.1. Types of corrugations

The most commonly used types of corrugated plates are trapezoidal, zigzag, and curved or sinusoidal corrugations as soon in Figure 1.15
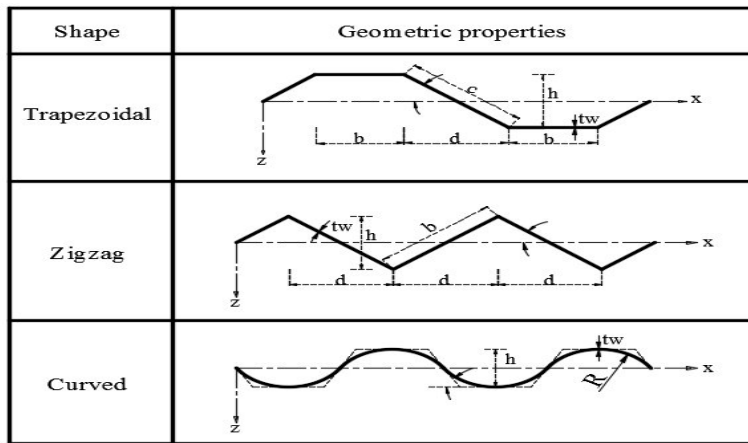
Figure 1.15. Types of corrugations (Kotb & Saddek, 2016)

1.7.2. Design parameters for trapezoidal corrugated webs

The design parameters of plate girders with trapezoidal corrugated webs are the flat folds, inclined folds, and web thickness as shown in Figure 1.16
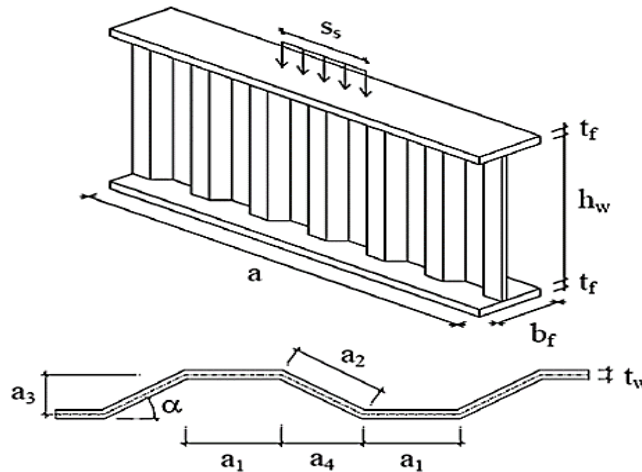
Figure 1.16. Geometrical notations for a trapezoidal web (Luo & Edlund, 1994)

These parameters (a_1, a_2, a_3, a_4, α, h_w, t_w) and their influences on shear strength and buckling from previous research gathered by (Luo & Edlund, 1996), is summarized in Table

Table 1.5. Effects of geometric parameters of corrugated webs on shear capacity and buckling (Luo & Edlund, 1996)

Corrugated Web			
Description	**Notation**	**Effects on Shear Capacity**	**Effects on buckling**
Angle	α	Increased α gives a larger shear capacity	30^0 = more global 45^0 = more interactives 60^0 = more local
Flat fold	a_1	Increased a_1 gives less shear capacity	
Length inclined fold	$a_3 = \dfrac{a_4}{cos\alpha}$		
Corrugation Depth	$a_3 = a_4 \tan \alpha$	No influence on shear capacity	Increased a_3 allows buckling mode to go from interactives to local
Length of Incline fold in x-direction	$a_3 = a_4 \cos \alpha$		

1.7.3. Ultimate resistance for Corrugated webs

Experimental research on the patch loading resistance of girders with trapezoidal corrugated webs started in 1987 by Leiva-Aravena and Edlund were parametric studies were done on three main parameters, namely; the patch load width, the load location, and the web thicknesses. The load was applied across the total width of the flange, as a 50mm wide patch or as a line load at three different locations, namely over a parallel or inclined fold, or at the fold line. An additional test was being conducted by Kähönen on I-girders, where the web crippling was analyzed under patch loading. The influence of web thickness, web depth, and span was examined. In all experiments, the girder was preloaded with two independent concentrated loads, covering the additional shear stress and bending moment for the structure. Based on the experiments Kähönen concluded that the difference between girders with corrugated webs and traditional I-beams is not only in the patch loading resistance, but these I-beams have a special character, which is called by him as "snap through-phenomenon". Its essence described the fact that the failure of the girder appears very quickly after reaching the ultimate load. Elgaaly and Seshadri made five tests in 1997. The tests were performed on a simply supported beam by varying the position of the applied load. All tests focused on typical building structures, where the load is transferred from the purlins to the roof girder, and therefore the loading length is usually very short. In all cases, the failure was due to vertical bending of the flange and crippling of the web under the load. The first design model for patch loading resistance of girders with corrugated webs was recommended by Kähönen in 1988.

This design formula is based on the four plastic hinge failure mechanisms developed by Rockey and Roberts for flat web girders. (Roberts 1979)
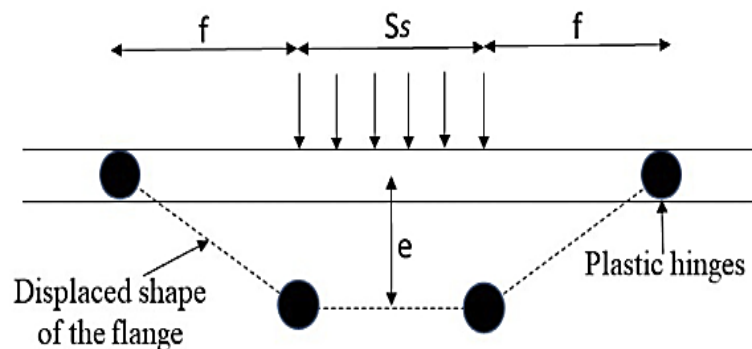
Figure 1.17. Flange mechanism for patch loading failure (Rockey and Roberts)

$$F = 2 \cdot \sqrt{4 \cdot M_{plf} \cdot t_w \cdot f_{yw} + f_{yw} \cdot t_w \cdot (s_s + f)} \tag{1.11}$$

$$M_{plf} = \frac{b_f \cdot t_f^2}{4} \cdot f_{yf} \tag{1.12}$$

$$f = \sqrt{\frac{4M_{plf}}{f_{yw} \cdot t_w}} \tag{1.13}$$

Where

F = Patch load resistance

f_{yf} the yield stress of the flange,

f_{yw} the yield stress of the web

t_w web thickness,

t_f flange thickness,

S_s loading length,

f deflected shape length next to the applied load.

This resistance formula can be subdivided into two parts, the first is the contribution from the flange, and the second is the contribution from the web. Kövesdi et al later modified this formula which was enhanced to consider the influence of the corrugation angle and global buckling to be presented by a geometric limit as a function of the corrugation profile. (Kövesdi et al. 2010)

$$F = 2 \cdot \sqrt{4 \cdot M_{plf} \cdot t_w \cdot \chi \cdot f_{yw} + \chi \cdot t_w \cdot f_{yw} \cdot ss \cdot K_\alpha} \tag{1.14}$$

$$M_{plf} = \frac{b_f \cdot t_f^2}{4} \cdot f_{yf}$$

$$\chi = \frac{1 \cdot 9}{\bar{\lambda}} - \frac{0 \cdot 798}{\bar{\lambda}^2} \quad if \ \bar{\lambda} > 1 \cdot 273 \tag{1.15}$$

$$\chi = 1.00 \quad if \ \bar{\lambda} \leq 1 \cdot 273$$

Where

$$\bar{\lambda} = \sqrt{\frac{f_{yw}}{\sigma_{Cr}}}$$

$$\sigma_{Cr} = \frac{\Pi^2 E}{12(1-v^2)} \cdot \left(\frac{t_w}{a_i}\right)^2 \qquad K_\alpha = \frac{1}{0 \cdot 9} = 1.11$$

Based on the numerical parameter study this design method is valid for corrugation angles $15^0 \leq \alpha \leq 65^0$, loading lengths in the range between $^{ss}/_{h_w} = 0 \cdot 4 \ and \ 0 \cdot 8$, if inclined and parallel folds have the same length ($a_1 = a_2$). This design formula may be used for web slenderness ratios $^{h_w}/_{t_w} = 200 - 500$ if the failure mode is local buckling. This parameter range is relevant for bridges. Elgaaly and Seshadri also developed a design method based on their experimental and numerical investigations. Two distinct failure modes were observed, web crippling and web yielding, for which separate equations were proposed. (Elgaaly et al. 2000) The ultimate load for web crippling consists of two components. One representing the contribution from the flange, which can be determined from the flange collapse mechanism, and the other representing the contribution from the web, which can be calculated based on an empirical equation developed for girders with flat webs. The ultimate capacity for web yielding can be calculated based on the yielding of a width of the web taking into account the loading position. Then the smaller of the two calculated resistances governs. In 1996, Luo and Edlund proposed an empirical design formula based on a simple design model for flat webs. According to their investigations, the most influential parameters are the loading length and the corrugation angle. Recommendations for the influence of those parameters were developed, and they were taken into account in the resistance formula. The parameter range of the previously executed tests and numerical calculations is shown below depending on the loading length and web panel ratio. The grey area illustrates the considered parameter range used in bridges. The majority of the executed experiments until now deal with very short loading lengths where the loads are applied only along one-fold. For bridges, built with an incremental launching process, the launching device at the pier corresponds to the location of load introduction, and its length is usually not limited to one-fold, but it can be significantly longer. By the up to now built bridges the loading length varies in general between 40-80% of the web depth (ss/t_w = 0.4 to 0.8).
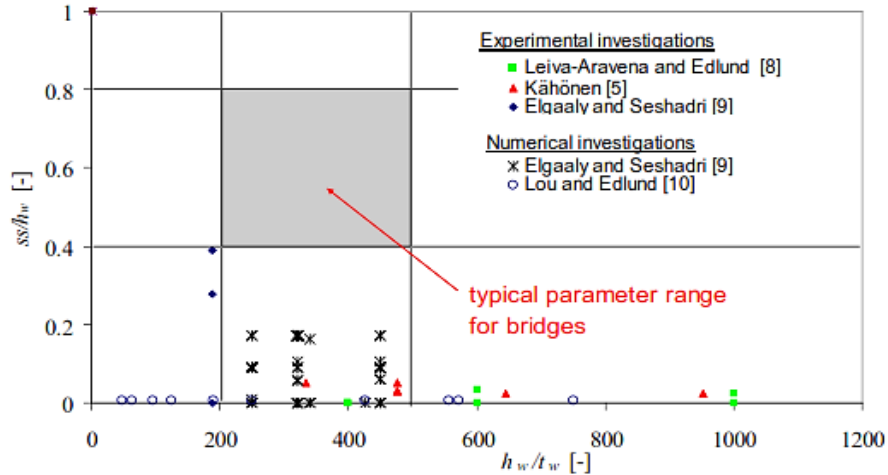
Figure 1.18. Parameter range of experimental and numerical investigations

1.7.4. Buckling and failure of corrugated girders

The buckling modes of corrugated plate girders could be local, global, or interactive depending on the corrugation width, corrugation angle, and magnitude of the acting forces. The corrugated steel webs may fail due to the yielding of the steel or due to patch buckling. Three different shear buckling modes (local, global and interactive) are possible depending on the geometric characteristics of the corrugated steel web (Kotb & Saddek, 2016)

1.7.4.1. Local buckling mode

Local buckling occurs when a flat sub-plate between vertical edges has large width to thickness ratio. Considering the instability of a steel panel simply supported between two folds, the corrugated web in this mode of failure acts as a series of flat plate sub panels that are mutually supported by the flanges at their horizontal (shorter) edges.
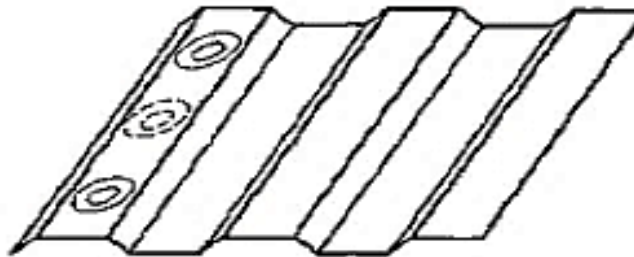
Figure 1.19. Local buckling mode of corrugated plates (Kotb & Saddek, 2016)

These flat-plate sub-panels are subjected to shear. The elastic buckling stress considering these plates as isotropic plates are given by (Galambos, 1998) as defined by equation (1.16)

$$\tau_{Cr,L} = K_L \frac{\pi E}{12(1-v^2)} \left(\frac{t_\omega}{w}\right)^2$$

(1.16)

With

$$K_L = 5.34 + 2.31 \left(\frac{w}{h_w}\right) - 3.44 \left(\frac{w}{h_w}\right)^2 + 8.39 \left(\frac{w}{h_w}\right)^3$$

For long edges simply supported and short edges clamped

Where:

t_ω is the corrugated web plate thickness

w is the bigger of the horizontal or inclined flat plate sub-panel width,

E and v are Young's modulus and the Poisson's ratio for the steel respectively,

K_L is the shear buckling coefficient for the local buckling mode.

However, expressions used by (Saddek, Hamed, & Luxor, 2018) to evaluate the value of K_L is given by Equation (1.17)

$$K_L = \frac{43\Pi}{256} \sqrt{\varphi_{L_1} \varphi_{L_2}}$$

(1.17)

With:

$$\varphi_{L_1} = \frac{1}{2}\left(\frac{3}{8}\left(\frac{h_\omega}{b}\right) + 2\left(\frac{b}{h_w}\right)^3 + \frac{1}{2}\left(\frac{b}{h_w}\right)\right)$$

$$\varphi_{L_2} = \frac{1}{2}\left(16\left(\frac{h_\omega}{b}\right) + 41\left(\frac{b}{h_w}\right)^3 + 40\left(\frac{b}{h_w}\right)\right)$$

1.7.4.2. Global Buckling Mode

Global shear buckling is characterized by the formation of diagonal buckles through the entire web similarly to a flat plate web as shown
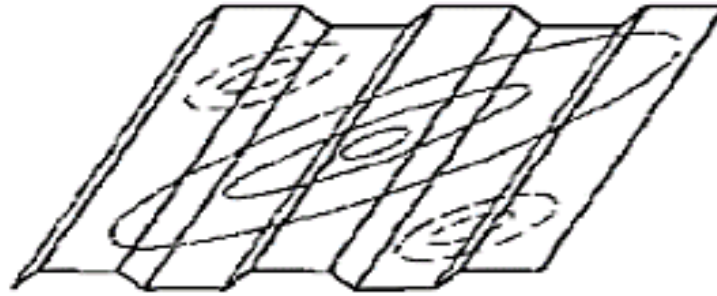
Figure 1.20. Global buckling mode of corrugated plates (Kotb & Saddek, 2016)

Global Buckling mode is the dominant failure mode in the case of dense corrugation defines the global elastic buckling strength expression by (Easley & McFarland, 1969)

$$\tau_{Cr,G} = 36\beta \frac{D_y^{0.25} D_x^{0.75}}{t_\omega h_{xw}^2} \tag{1.18}$$

With:

$$D_x = \frac{E t_w^3 \left[\left(h/t_w \right)^2 + 1 \right]}{6\eta} \qquad D_x = \frac{E t_w^2}{12(1 - v^2)} \eta$$

Where

β is the global buckling factor that depends on the boundary conditions such that;

$\beta = 1$ and $\beta = 1.9$ for simply supported and fixed edges respectively,

Dx and Dy are the flexural stiffness per unit corrugation about the x and y axes respectively,

h is the corrugation depth,

η is the length reduction factor defined as $(b + d)/(b + c)$.

1.7.4.3. Interactive shear buckling

The interactive buckling mode which is the most troublesome includes all the failure criteria (steel yielding, local and global buckling stress).

Figure 1.21. Interactive buckling mode of corrugated plates.

Below is the interaction equation giving the expression by (Metwally & Loov, 1999)

$$\frac{1}{\tau_{Cr,I}{}^n} = \frac{1}{\tau_{Cr,L}{}^n} + \frac{1}{\tau_{Cr,G}{}^n} + \frac{1}{\tau_Y{}^n}$$

(1.19)

Where:

$\tau_{Cr,I}{}^n, \tau_{Cr,L}{}^n, \tau_Y{}^n$ $are\ defined\ in$ (1.17)(1.16)

1.7.4.1. Failure of steel girders

The corrugated steel webs may fail due to the yielding of the steel or due to shear buckling. Three different shear buckling modes (local, global and interactive) are possible depending on the geometric characteristics of corrugated steel web (Kotb & Saddek, 2016). The shear stress which causes an element of the corrugated web to yield when it is subjected to pure patch loading can be determined using von misses yield criterion.

$$\tau_y = \frac{f_y}{\sqrt{3}}$$

(1.20)

Where

τ_y is the shear stress,

f_y is the yield strength of steel.

1.7.5. Research works

In the past decade, many researchers have been involved in studies related to patch loading evaluations and other aspects related to eccentricities.

1.7.5.1. Centric patch loading

The two experiments of Elgaaly and Seshadri were near to the parameter range used in bridges construction. Five test were performed on a simply supported short beam by varying the position of the applied loading on the beam and the profile of the 2 mm thick web is shown in and the web was stiffened over the supports to prevent yielding and/or crippling.
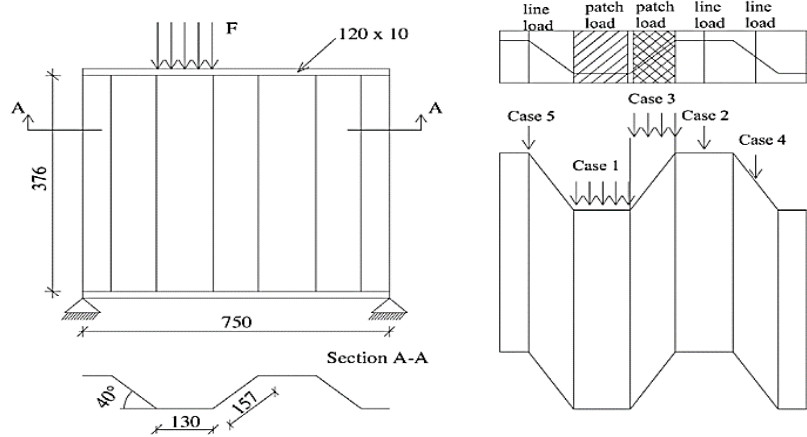
Figure 1.22. Test specimen of Elgaaly and Seshadri

The yield and the ultimate stresses of the flange material were provided by the girder manufacturer, and they are 389 MPa and 563 MPa, respectively. The yield and ultimate stresses of the web were determined from test coupons to be 379 MP and 413 MPa respectively. The five tests were conducted by varying the position of the applied load, as shown in Fig. The patch loads were applied through 25.4 mm thick plates, and the line loads were applied using a 76.2 mm diameter steel rod. In all cases, the load was applied across the total width of the flange.

Figure 1.23. Test specimen arrangement and typical failure mode

Further Numerical Model were also created based on a full shell model using four-node thin shell elements. Model verification was executed by recalculations of all the experimental results. The ultimate loads were determined by geometrical and material nonlinear analysis using imperfections. The applied material model is linear elastic-plastic with a multilinear isotropic hardening rule with a von Mises yield criterion. The material was assumed to behave linear-elastic and to obey Hooke's law with Young's modulus of (E) 200 GPa up to the yield stress. Reaching the ultimate stress, the material was assumed to follow linear hardening with a reduced modulus equal to 0.01E. The material was assumed to be perfectly plastic when it reaches the ultimate stress.
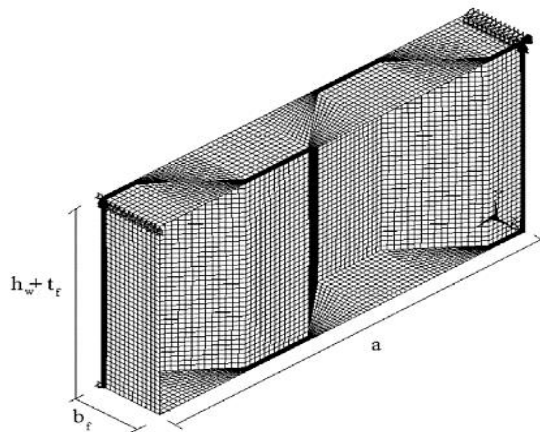
Figure 1.24. FE Model of Elgaaly and Seshadri

Table 1.6. Comparison between experimental and numerical results Elgaaly and Seshadri

Case (1)	Location of load (2)	Distribution width, N (in.) (3)	P_e (kips) (4)	P_t (kips) (5)	P_t/P_e (6)
Case 1	Parallel fold	5.75	29.50	24.05	0.815
Case 2	Parallel fold	0.00	18.50	17.74	0.959
Case 3	Inclined fold	4.10	23.00	20.03	0.871
Case 4	Inclined fold	0.00	21.50	19.40	0.902
Case 5	Junction between a parallel and an inclined fold	0.00	16.50	20.89	1.266

Another parametric analysis was conducted on this FE Model by B. Kövesdi et al were other aspects such as the Influence of the loading length, overall web, and local fold ratios, corrugated webs, Failure modes were studied. (Kövesdi et al. 2010)
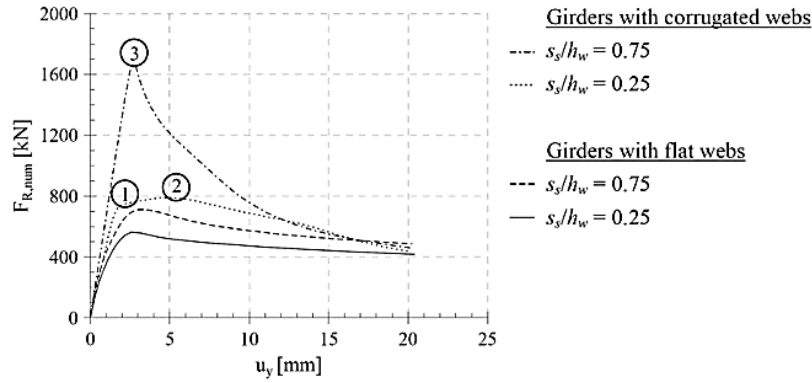
Figure 1.25. Comparison of load displacement curves. (Kövesdi et al. 2010)
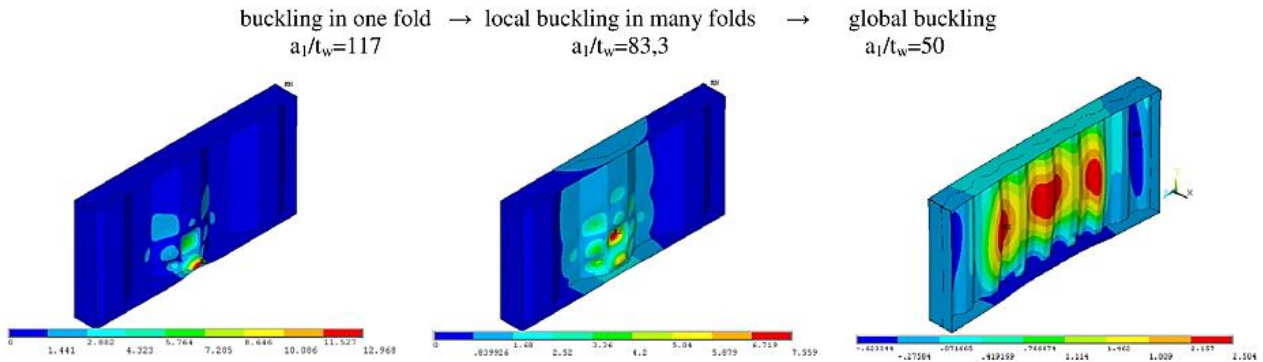
Figure 1.26. Different buckling failure modes. (Kövesdi et al. 2010)
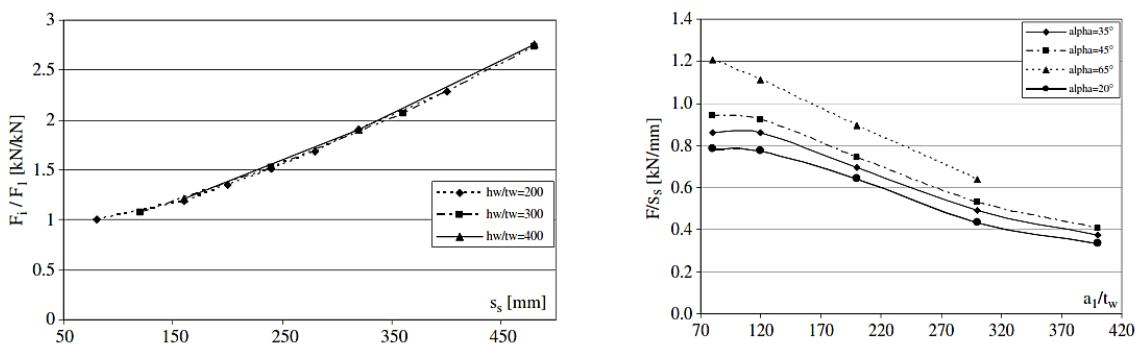
Figure 1.27. Influence of the loading length and web slenderness.

- **The behavior of corrugated webs**

The corrugation of the web provides effective out-of-plane stiffening and increases the buckling strength. It can be seen that the load-carrying capacity of girders with corrugated webs with the

same thickness as girders with flat webs can be multiples of the resistance. For both cases, an increase in loading length significantly increases the resistance.

- **Failure modes**

The failure mode mainly depends on the corrugation profile. For small overall web and high fold ratios, the failure mode is mainly the local buckling of the fold (web crippling). For a short loading length, the local buckling occurs only in one-fold, for longer loading length in several folds. For small fold ratios, the buckling mode can change to global buckling of the whole web

- **Influence of the loading length**

With increasing loading length, the load-carrying capacity increases nearly linearly. The increase is due to the activation of more web parts in the case of long loading lengths.

- **Influence of overall web and local fold ratios**

The relationship shows a part of the typical reduction curve for all corrugation angles, that is the load-carrying capacity decreases with higher fold ratios

- **Corrugation angle influence**

The corrugation angle has a significant influence on the patch loading resistance. For higher corrugation angles the patch loading resistance increases. The character of the relationship between corrugation angle and patch loading resistance can be hardly studied Eccentric patch loading

Eccentric patch loading is a research field where only a few investigations are conducted till now, however during the launching of the bridge structural eccentricities of the patch load are unavoidable in practice.
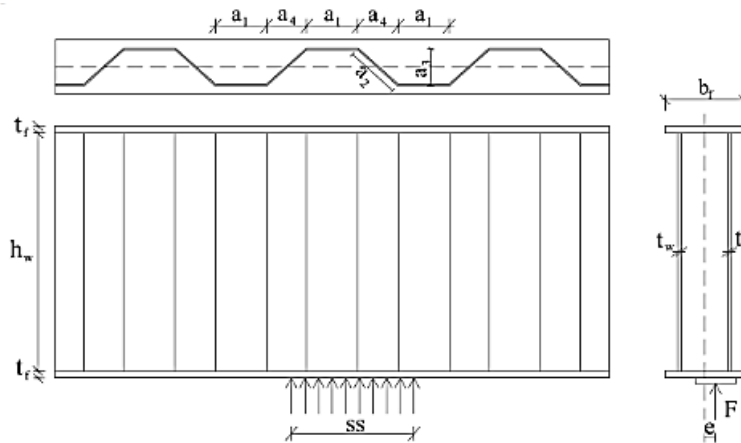
Figure 1.28. Eccentric patch loading of corrugated web girders.

There is no standard design method to determine the resistance reduction due to eccentricities and only a few investigations and research recommendations can be found in literature dealing with this topic even for flat web girders. In eccentric loading, the load is not centered about the normal axis as soon before but applied at a specific distance from the neutral axis

In the last decades, researchers investigated only scarcely this research field. All the previous investigations are conducted on steel girders with flat webs and no available investigations were dealing with corrugated web girders. Experimental research in the field of eccentric patch loading was started by Oxford and Weber in 1979. 6 tests were conducted on flat web I-girders and the effect of the eccentric patch loading was studied. In the experiments, the flange rotated along its longitudinal axis, and therefore, it ensured softer support for the web plate. Due to the softer support conditions, the web buckled at a lower ultimate load level. Experiments showed that the resistance decrease did not depend significantly on the flange size and the longitudinal web stiffener had a much smaller efficiency in case of eccentric loading. Elgaaly and his team conducted a comprehensive experimental program on 35 steel I-girders with flat webs under eccentric patch loading between 1988 and 1990. The investigated parameters in the experiments are the loading mode (loading plate or loading rod), $t_f/t_w, L/h_\omega, {}^e/_{b_f}$ ratios. A numerical model is developed to determine the patch loading resistance and a numerical parametric study is conducted to analyze the patch loading resistance reduction due to eccentricities. Based on the test results and numerical calculations design model is developed in the form of an equation which can be applied in the parameter range between $1 < t_f/t_w < 4$ and ${}^e/_{b_f} < 1/2$

$$\frac{F_R^{red}}{F_R} = \left[-0 \cdot 45 \cdot \left(\frac{t_f}{t_w}\right)^2 + 4 \cdot 45 \cdot \left(\frac{t_f}{t_\omega}\right) - 12 \cdot 75 \right] \cdot \left(\frac{e}{b_f}\right) + \left(\frac{e}{b_f}\right) + 1.15 - 0.025 \cdot \left(\frac{t_f}{t_w}\right) \quad (1.21)$$

Other research was later carried out by Scepanovic and co-researchers between 2001 and 2009 to analyze the eccentric patch loading resistance of flat web girders with the main aim of the tests and numerical modeling was to enlarge the previously analyzed parameter and the equation was later modified.

$$\frac{F_R^{red}}{F_R} = \left[-0 \cdot 32 \cdot \left(\frac{t_f}{t_w}\right)^2 + 3.60 \cdot \left(\frac{t_f}{t_\omega}\right) - 7.67 \right] \cdot \left(\frac{e}{b_f}\right) + \left(\frac{e}{b_f}\right) + 1.00 - 0.0025 \cdot \left(\frac{t_f}{t_w}\right) \quad (1.22)$$

A FE was then developed and the structural behavior and failure mechanism were studied under three different loading conditions. These are centric patch loading along the whole flange width, along a smaller loading width, and under eccentric loading. Load-deflection and load-horizontal displacement diagrams are studied and compared in the three analyzed cases
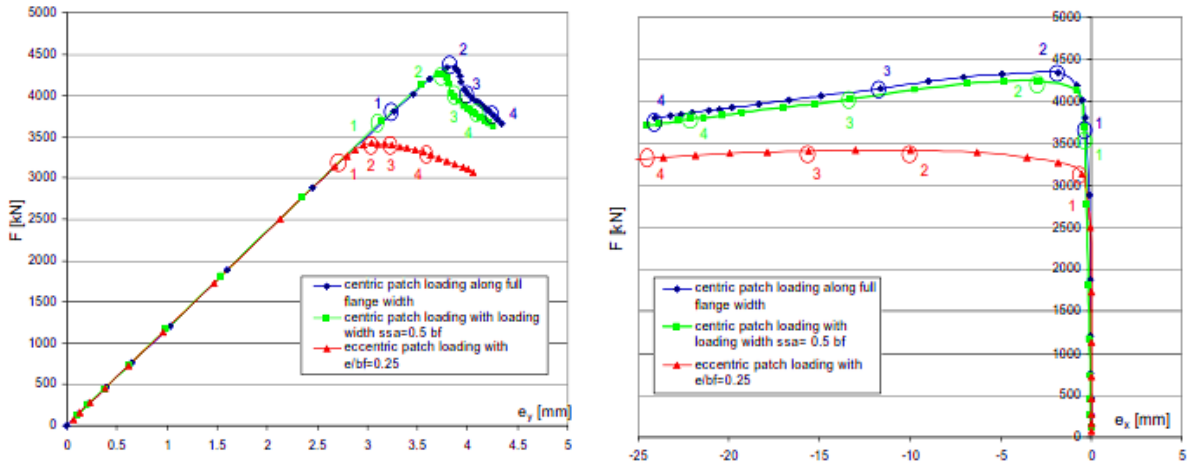
Figure 1.29. Load deflection and Load -Lateral displacement diagrams

Conclusion

This chapter aimed to present an overview of plate girders and the state of research works

investigating their behaviors. This was done starting with the definition of plate girders and presenting their typical longitudinal and transversal geometry. After this was the definition of plate girders and their general application in construction. This was followed by the presentation of the different patch loading scenarios in steel construction Stating their origin and imposed problems. Then the criteria for the classification of plate girder sections as compact, non-compact and slender sections as a function of the slenderness parameter according to Eurocode standards was done. This was followed by the description of the general behavior of plate girders elaborating on their ultimate resistance and their elastic buckling and failure modes. After this was the general aspects and research works for flat plate girders and Finally, for plate girders with corrugated webs, the types of corrugations, failure modes, and their design parameters were presented. Also, research works investigating the behavior of plate girders with corrugations together with some profiles of corrugated steel webs for bridges constructed and their properties were presented.

CHAPTER 2. METHODOLOGY

Introduction

This chapter presents the methodology used in this study to evaluate the Patch loading resistance of plate girders with flat webs and trapezoidal corrugated webs. To attain the objectives of this chapter is divided into five parts. In the four-part of this chapter, the geometry, the methodology used to derive the numerical models of the individual members are discussed. This is followed by discussing the methods of defining the material properties of steel according to EN 1993-1-1. Later in this chapter are discussed the theoretical methods of evaluating the Patch loading strength using formulations according to EN 1993-1-5 specifications and also empirical formulations from other authors. This part is immediately followed by the FEM for Patch loading analysis. Finally, the last part of this chapter presents the modeling methodology using the ABAQUS/CAE finite element package.

2.1. GEOMETRIC CLASSIFICATION OF NUMERICAL MODELS

The geometry of flat and trapezoidal corrugated web girders used in this study together with initial input parameters of cross-sections will be discussed in this section. The analytical models used in the current study consists of plate girders with flat and trapezoidal corrugated webs with geometry defined in **Error! Reference source not found.**.
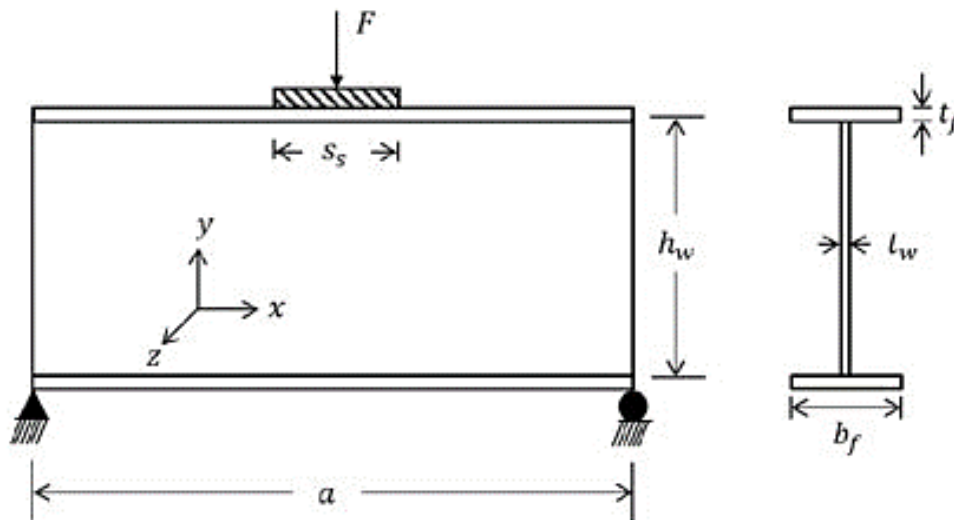
Figure 2.1. Geometry of plate girder with flat web.
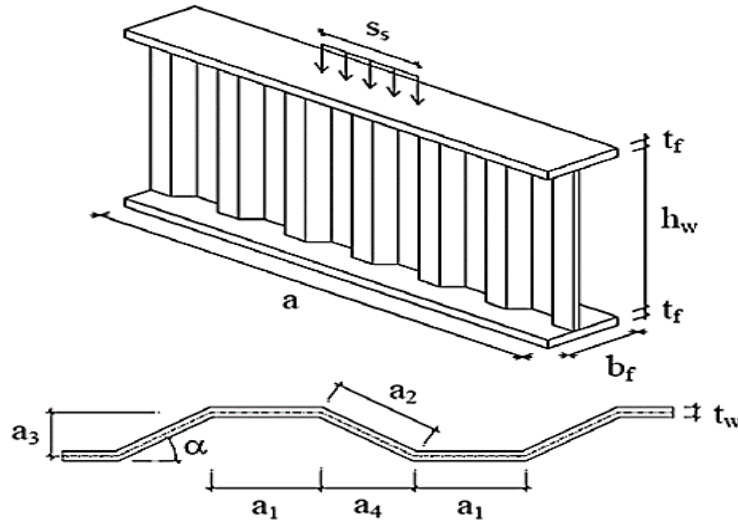
Figure 2.2. Geometry of plate girder with corrugated web.

2.1.1. Numerical models

The input parameters for the models are web thickness (t_ω), Stiffener separation (a), Web depth (h_ω), flange width (b_f), flange thickness (t_f), corrugation widths ($a_1, a_2, a_3, a_4,$) and the corrugation angle (α).

2.1.2. Classification of girder sections

Members of plate girders are classified according to EC3 Part 1-1, Section 5.5 where cross-sections of plate girders are classified to identify the extent to which the resistance and rotation capacity of cross-sections is limited by its local buckling resistance as printed in the literature above.

2.1.3. Input parameters for Plate girders.
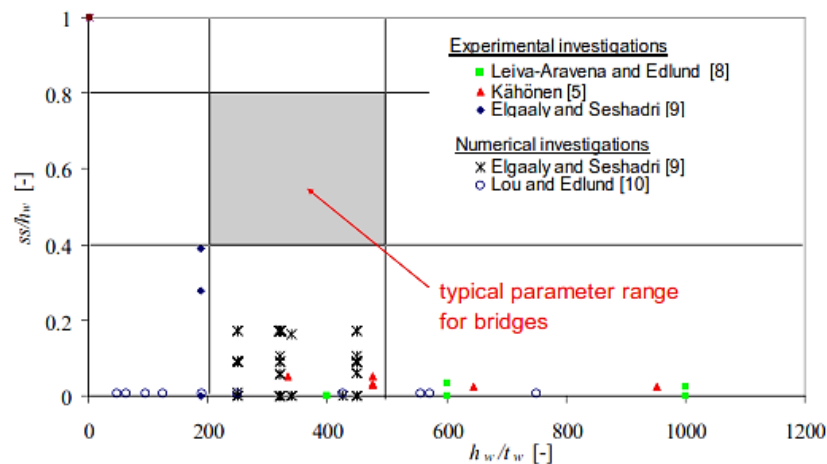
Figure 2.3. Typical Parametric range for bridges

The input parameters considered are those near the characteristic range for bridge Construction as shown in Figure 2.3 above

$$h_w/t_w = 200 - 600 \qquad s_s/h_w = 0.4 - 0.8$$

From these parameters, 35 plate girders are generated considering variations in loading length, loading width, Slenderness, Aspect ratio corrugation width, Corrugation angle, Local and global fold ratios.

2.1.4. Comparative model

A Comparative model will be derived considering equal values of ultimate Patch loading resistance for Flat and corrugated Plate girders. The developed models will be used to analyze the percentage of material reduction in the use of corrugated webs over flat webs. Equation (2.1) gives the expressions to compute the volume of material.

$$
\begin{aligned}
&a \; x \; h_w \; x \; t_w \qquad for \; flat \; web \\
&n \; x \; b \; x \; h_w \; x \; t_w \quad for \; \text{corrugated web}
\end{aligned}
\qquad (2.1)
$$

Where:

n is the total number of horizontal and inclined folds in corrugated members.

This is a cost conservative method as the cost of material is directly proportional to the volume of material used according to (Rajkumar et al. 2017)

2.1.5. Material properties

The steel material is modeled as a Von Mises material with isotropic hardening. The ductility requirements of structural steel used in this study are defined by section 3.2.2 of EC3 part 1-1. The nominal values of the yield and ultimate strength of steel conforming to these requirements are given on Table

Table 2.1. Yield strength (fy) and ultimate tensile strength (fu) of hot-rolled structural steel

Standard and steel grade	Nominal thickness of the element t (mm)			
	$t \leq 40\ mm$		$40\ mm < t < 80mm$	
	$f_y\ [N/mm^2]$	$f_u\ [N/mm^2]$	$f_y\ [N/mm^2]$	$f_u\ [N/mm^2]$
EN10025-2				
S 235	235	360	215	360
S 275	275	430	255	410
S 355	355	510	335	470
S 450	440	550	410	550

S355 steel is used in this study (typical in bridge application) with stress/strain bilinear behavior and material coefficients are given by **Table 2.2** and **Table 2.3**respectively

Table 2.2. Stress/Strain bilinear behavior of steel

Properties	Stress	Strain
Elastic	$355N/mm^2$	0
Plastic	$510\ N/mm^2$	0.2

Table 2.3. Material Coefficients of steel

Property	*Expression*	*Value*
Elastic Modulus	E	$210000N/mm^2$
Shear Modulus	$G = E/2(1+v)$	$81000N/mm^2$
Poisson Ratio	v	0.3
Linear Thermal Expansion Coefficient	α	$12 \times 10^{-6}\ per\ K$

2.2. THEORETICAL METHODS OF PATCH LOADING RESISTANCE

For a safe and durable analysis of patch loading phenomena in steel plate girders, there exists a set of prescriptions and formulas to investigate this behavior. With the European Norms being our design manual, the following specifications will be used in the scope of this study. (En 2005)

Eurocode 3: Design of steel structures

- Part 1-1: General rules and rules for buildings
- Part 1-5: Plated structural elements

2.2.1. Patch loading resistance for members with flat webs

- Critical Load

$$F_{Cr} = K_F \frac{\Pi^2 E}{12(1-v^2)} \frac{t_w^3}{h_w} \approx 0{,}9K_F \frac{Et_w^3}{h_w} \qquad (2.2)$$

where the coefficient K_F depends on the type of loading and the geometry as shown in figure

The loading length (Ss) was taken as 80mm along the whole width of the flange as recommended by EN 1993-1-5.

$$k_F = 6 + 2\left(\frac{h_w}{a}\right)^2 \qquad k_F = 3{,}5 + 2\left(\frac{h_w}{a}\right)^2 \qquad k_F = 2 + 6\left(\frac{s_s + c}{h_w}\right) \le 6$$
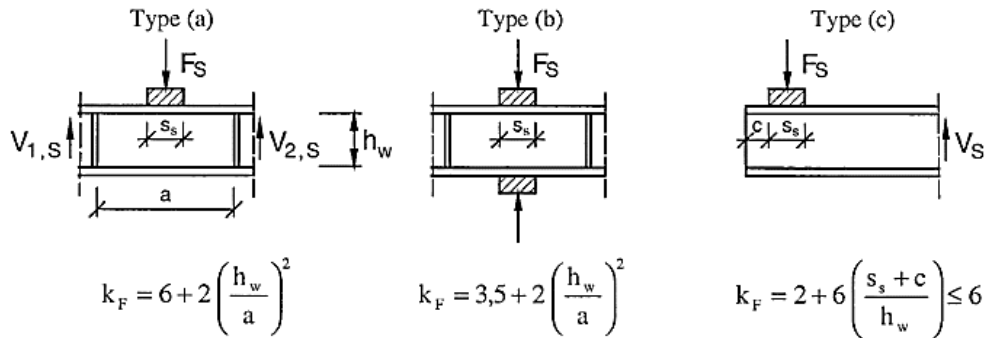
- Design resistance (EN 1993-1-5)

$$F_{Rd} = \frac{f_{yw} \cdot L_{eff} \cdot t_w}{\gamma_{M1}} \qquad (2.3)$$

Where

$$L_{eff} = \chi_F \cdot l_y \qquad l_y = s_s + 2 \cdot t_f \cdot \left(1 + \sqrt{m_1 + m_2}\right) \le a$$

$$m_1 = \frac{f_{yf} \cdot b_f}{f_{yw} \cdot t_w}$$

$$m_2 = 0.02\left(\frac{h_w}{t_f}\right)^2 \qquad for \quad \bar{\lambda}_F > 0.5$$

$$m_2 = 0 \qquad for \quad \bar{\lambda}_F \le 0.5$$

$$\chi_F = \frac{0.5}{\bar{\lambda}_F} \qquad \bar{\lambda}_F = \sqrt{\frac{l_y \cdot t_w \cdot f_{yw}}{F_{Cr}}} \qquad F_{Cr} = K_F \frac{\Pi^2 E}{12(1-v^2)} \frac{t_w^3}{h_w} \approx 0{,}9K_F \frac{Et_w^3}{h_w}$$

2.2.2. Patch loading resistance for members with Corrugated webs

No rules for patch loading resistance are given in EN 1993-1-5 but It has been studied by several authors and the results have however not been collated and merged into a design model. The EN1993-1-5 Annex D [4] deals with members with corrugated webs, but there is no

standard design method for patch loading of girders with trapezoidal corrugated webs.

- Ultimate resistance under Patch loading (Kähönen)

$$F = 2 \cdot \sqrt{4 \cdot M_{plf} \cdot t_w \cdot \chi \cdot f_{yw} + \chi \cdot t_w \cdot f_{yw} \cdot ss \cdot K_\alpha} \qquad (2.4)$$

$$M_{plf} = \frac{b_f \cdot t_f^2}{4} \cdot f_{yf}$$

$$\chi = \frac{1 \cdot 9}{\bar{\lambda}} - \frac{0 \cdot 798}{\bar{\lambda}^2} \quad if \ \bar{\lambda} > 1 \cdot 273 \qquad \chi = 1.00 \ \ if \ \bar{\lambda} \le 1 \cdot 273$$

Where

$$\bar{\lambda} = \sqrt{\frac{f_{yw}}{\sigma_{Cr}}}$$

$$\sigma_{Cr} = \frac{\Pi^2 E}{12(1 - v^2)} \cdot \left(\frac{t_w}{a_i}\right)^2 \qquad K_\alpha = \frac{1}{0 \cdot 9} = 1.11$$

Valid For

corrugation angles $15^0 \le \alpha \le 65^0$,

loading lengths in the range between $ss/h_w = 0 \cdot 4 \ and \ 0 \cdot 8$,

 inclined and parallel folds have the same length ($a_1 = a_2$).

web slenderness ratios $h_w/t_w = 200 - 500$

2.3. FINITE ELEMENT METHOD FOR PATCH LOADING RESISTANCE

Finite element analysis is a modern computerized method of predicting how a complex object or a simple object under complex conditions reacts to real live forces, vibrations, heat, fluid flow, and other physical effects. The principle theory of FEA is to simulate the real-life response of an object by breaking it down into a large number (thousands to hundreds of thousands) which can be little cubes, tetrahedral, octahedral, etc. depending on the overall geometry of the object. (Mathematics of FEM, 2017) Numerical analysis of I-girders with flat and corrugated webs will be performed in two phases. Firstly, a linear analysis (Eigenvalue buckling analysis or Euler buckling analysis). This will be done to evaluate the critical Patch loading resistance which corresponds to the load of the first Eigen mode. Again, a nonlinear analysis will be done and the force-displacement of each model will be plotted from which the ultimate (maximum) load is obtained. The loading and boundary conditions under which these analyses are carried out will be discussed as well as the model and mesh size verification adopted for this study.

2.3.1. Linear-buckling analysis

Linear-buckling is the most common type of analysis and it's easy to execute, but is limited in the results it provides. Linear buckling analysis calculates buckling load magnitudes that cause buckling and associated buckling modes. ("Buckling Analysis with FEA | Machine Design," n.d.). The applied loads can consist of pressures, concentrated forces, non-zero prescribed displacements and/or thermal loading. FEA programs provide calculations of a large number of buckling modes and the associated buckling-load factors (BFL). The BLF is expressed by a number by which the applied load must be multiplied by (or divided- depending on the FEA package) to obtain the buckling-load magnitude. The buckling modes present the shape the structure assumes when it buckles in a particular mode, but says nothing about the numerical values of the displacements or stresses. Theoretically, it is possible to calculate as many buckling modes as the number of degrees of freedom in the FEA model. However, only the first positive buckling mode and its associated BLF needs to be found. This is because higher buckling modes have no chances of taking place as buckling often cause catastrophic failure or renders the structure unusable. The nomenclature is "the first positive buckling mode" is because buckling modes are reported in ascending order according to their numerical values. Buckling modes with a negative BLF means the load direction must be reversed (in addition to multiplying by the BLF) for buckling to happen ("Buckling Analysis with FEA | Machine Design," n.d.).

In this study for the Linear Buckling analysis;

- Number of eigen values requested = 3
- Vectors per iteration = 18
- Maximum number of iterations = 300

However, FE models most often represent geometry with no imperfections. Also, loads and supports are applied with perfect accuracy with no offsets. However, in reality, loads are applied with offsets, faces are never perfectly flat and supports are never perfectly rigid. Even if the supports are modeled as flexible, their stiffness is never evenly distributed. Imperfections are always present in the reality.

2.3.2. Nonlinear-buckling analysis

Nonlinear-buckling analysis requires that a load be applied gradually in multiple steps rather than in one step as in a linear analysis. Each load increment changes the structure's shape and this in return changes the stiffness of the structure. Therefore, the structure's stiffness if updated at each increment ("Buckling Analysis with FEA | Machine Design," n.d.)Although the load-control method is used in most types of nonlinear analysis, it would be difficult to implement in buckling analysis. When buckling happens the structure undergoes a momentary loss in its stiffness and the load control method results in numerical instabilities. Nonlinear buckling analysis as a result requires another way of controlling load application. In contrast to linear-buckling analysis, which only calculates the potential buckling shape with no quantitative values of importance, nonlinear analysis calculates the actual displacements and their corresponding stresses. However, when real-life imperfections are absent in the FEA model, buckling will still happen but it will be initiated by imperfections introduced by discretizing errors. Therefore, non-linear buckling analysis requires a model with some initial imperfection. When no such imperfections are present, they must be added to control the onset of buckling.(Hibbitt, Karlsson & Sorensen 2012). In simple cases, the eigenvalue analysis is sufficient for design evaluation. But if there is concern about material nonlinearity, geometric nonlinearity before buckling, or unstable post-buckling response, a load-deflection analysis must be performed to investigate the problem further. The Static RIKS method uses the load magnitude as additional unknown. It solves simultaneously for loads and displacements. Therefore, another quantity must be used to measure the progress of the solution. Abaqus uses the "arc length method" along the static equilibrium path in load displacement space. This approach responds regardless of whether the response is stable or unstable. In this study the

static RIKS analysis which works on the arc-length method will be used to predict the non-linear buckling behavior with;

- Nonlinear geometry included
- Maximum number of increments = 1000
- Arc length increment = 0.01
- Estimated total arc length = 1

In the non-linear finite element analysis, the nonlinear geometry will be included in the models by considering material nonlinearity, geometric nonlinearity, and residual stresses. The assumptions in calculations that materials are linear and elastic are not valid especially for structural steel whose behavior is mostly plastic. In the FEA material non-linearity will be included .by the use of bi-linear stress-strain behavior of structural steel.(Šutić, Krolo, and Bulić 2018)
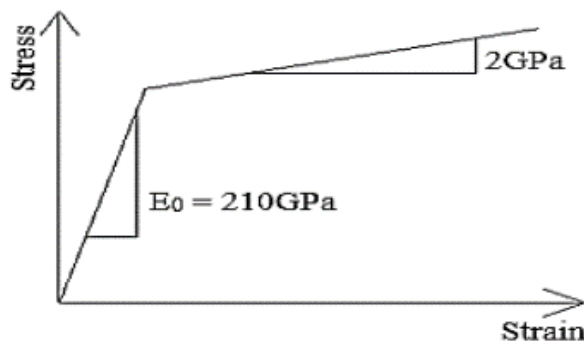
Figure 2.4. Bilinear stress-strain curve accounting for material nonlinearity

Geometrical nonlinearity on the other hand accounts for the fact that any kind of element is not perfect such that during its production it develops an initial bow as shown in Figure 2.5
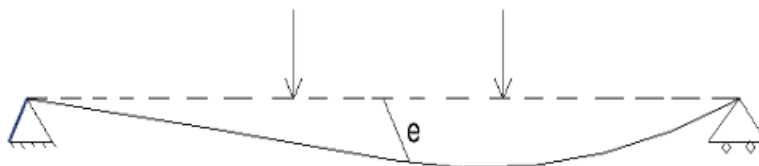
Figure 2.5. Initial bow showing geometric non-linearity

The residual stresses are always present as well, which occur because during the production of cross-section, not all the parts of the cross-section are cooled at the same rate leading to the development of residual stresses along the cross-section. Figure 2.6
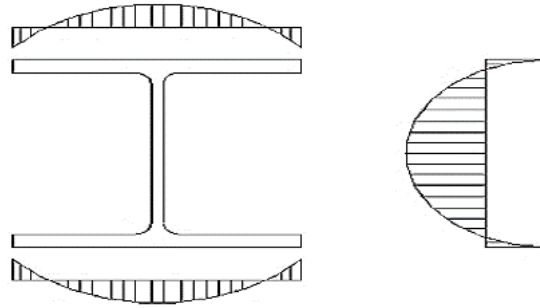
Figure 2.6. Stress distribution across beam section due to residual stress

However, residual stresses are much more complicated to include in the model and a simplified model will be used which is quite accurate. This is done by including both geometrical nonlinearity and residual stress by using "equivalent geometric imperfection" which is larger than the real live imperfection. These values of imperfections are obtained from EC3-Part 1-1 section 5.3.2
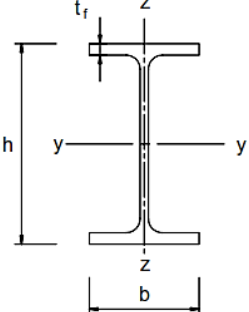
Table 2.4. Design values for initial local bow imperfection. e_0 / L

Buckling curve acc. to Table 6.1	elastic analysis e_0 / L	plastic analysis e_0 / L
a_0	1 / 350	1 / 300
a	1 / 300	1 / 250
b	1 / 250	1 / 200
c	1 / 200	1 / 150
d	1 / 150	1 / 100

Where

L is the length of the beam with the buckling curve is defined by the section properties of the element, buckling axis, and the steel grade as shown

Table 2.5. Selection of buckling curve for a cross-section

Cross section		Limits	Buckling about axis	Buckling curve S 235 S 275 S 355 S 420	S 460
Rolled sections	$t_f \le 40$ mm ($h/b > 1,2$)	$t_f \le 40$ mm	$y - y$ $z - z$	a b	a_0 a_0
		40 mm $< t_f \le 100$	$y - y$ $z - z$	b c	a a
	($h/b \le 1,2$)	$t_f \le 100$ mm	$y - y$ $z - z$	b c	a a
		$t_f > 100$ mm	$y - y$ $z - z$	d d	c c

From the Static RIKS analysis, the LPF (load vs arc length curve) for the whole model and the displacement vs arc length for all nodes of the web section is obtained. The displacement curve of the node corresponding to the maximum positive out-of-plane displacement will be obtained. The LPF together with the displacement vs arc-length curve is used to plot the load vs displacement behavior of the model from which the ultimate loads are obtained.

2.3.3. Load application and boundary conditions

The loads are modeled as Concentrated loads of magnitude 1kN on the patch area in the eigenvalue analysis and magnitude corresponding to the load of the first buckling mode for the nonlinear analysis. The Plate is Simple supported with lateral movements restricted along with one of its side edges without restraint in the plane of the Plate. The flanges were also restrained against vertical deformation at the ends of the girders provided by the support from a vertical stiffener as shown in Figure 2.7
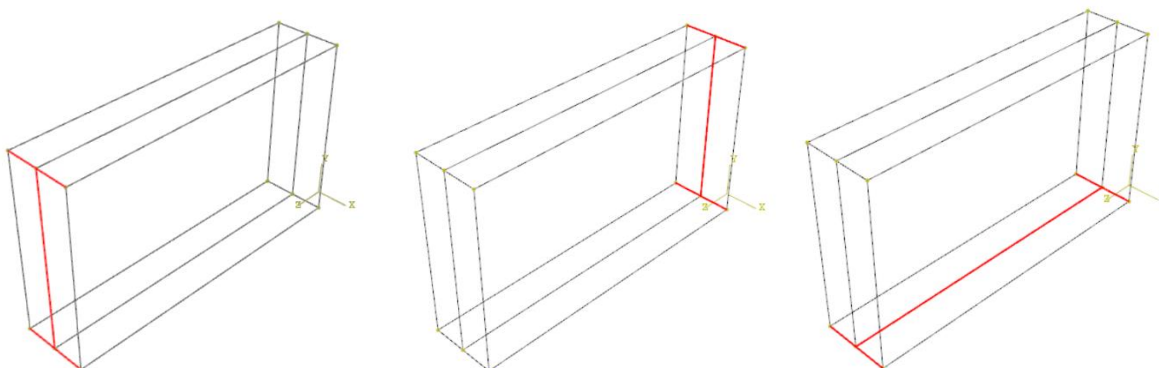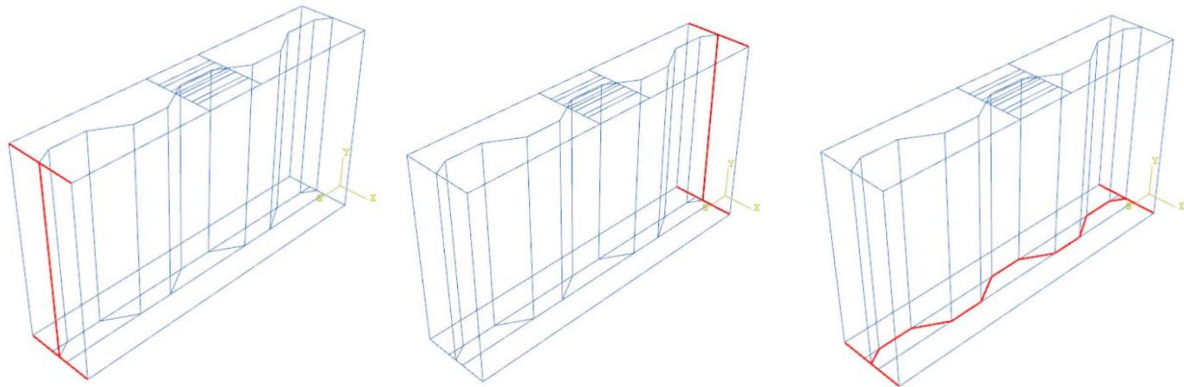
| Restrain Displacement X and Z | Restrain Displacement-X | Restrain Displacement-Y |

Figure 2.7. Model with boundary conditions as prescribed by EN 1993-1-5

2.3.4. Verification of finite element models and mesh

For Plate girders, FE results are compared with EN 1993-1-5 Specifications for the Critical and ultimate resistance under patch loading. Given that there are no specifications for Corrugated by EN 1993-1-5 the Experiment conducted by Elgaaly and Seshadri was used together with Empirical formulations produced by other Authors such as Kähönen, Lou, and Edlund for the verification of the FE Model. Based on the verified model a comprehensive parametric study is executed to analyze the effects of eccentricity on the patch loading resistance of corrugated plates near the parameter range used in bridges.

2.4. MODELLING METHODOLOGY

The software program used for Patch loading analysis in the study is ABAQUS/CAE. With ABAQUS/CAE you can quickly and efficiently create, edit, monitor, diagnose and visualize advanced ABAQUS analysis.

2.4.1. Interface of Abaqus/CAE

Abaqus/CAE is a complete Abaqus environment that provides a simple and consistent interface for creating, submitting, monitoring, and evaluating results from Abaqus/Standard and Abaqus /Explicit simulations. Abaqus/CAE is divided into modules, where each module defines a logical aspect of the modeling process including geometry definition, defining material properties, generating a mesh, and visualization of results.
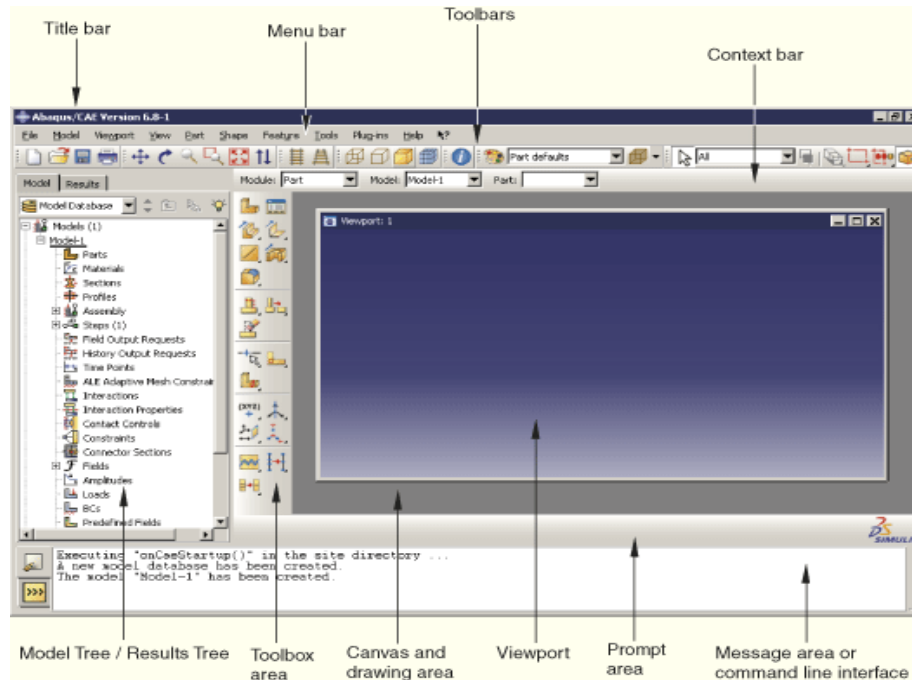
Figure 2.8. User Interface of Abaqus/CAE

2.4.2. Patch loading analysis using Abaqus

Patch loading analysis using Abaqus involves the 3 phases which are the pre-processing, processing, and post-processing phase.

2.4.2.1. Pre-processing stage

This is the first stage during which every input detail information including the section geometry, material properties, loads and boundary conditions, and the type of mesh needs to be defined. This stage involves 5 main steps.

a. **First step.** The first step involves creating the geometry (parts). The flanges, the web, and stiffeners are defined after creating the geometry by grouping them into different sets. This helps in the subsequent steps in sorting out different parts of the model to assign properties. The definition of geometry is shown in Appendix.1

b. **Second step.** The next step is to define the material properties. The elastic properties are defined for the linear analysis and the plastic properties are added for the nonlinear analysis.Appendix.2 shows the definition of nonlinear material properties and the definition of section properties

c. **Third step.** This step involves assembling the parts and creating the step. The eigenvalue analysis is defined for the linear buckling analysis and the Static RIKS analysis for the nonlinear buckling analysis as shown in Appendix.3

d. **Fourth step.** In this step, the loads and the boundary conditions are defined. The loads are modeled as surface Pressure and Concentrated loads and boundary conditions are displayed.Appendix.4

e. **Fifth Step.** In this step, the model is meshed and a job is created. The meshing involves defining the approximate global size as in Appendix.5. Keywords are then edited to create a file regarding the eigenmodes for the linear analysis and to include imperfection for the nonlinear analysis respectively in the message box as on and submitted for analysis.

2.4.2.2. Processing stage

In this stage, the software program solves the unknowns assigned in the processing phase. The eigenvalues for the first, second, and third eigenmodes are obtained for the linear analysis. On the other hand, LPF and the displacement versus arc-length graphs of the web are the main output data for the nonlinear buckling analysis and can be seen in.Appendix.6

2.4.2.3. Post-processing

The final stage is the post-processing stage. In this stage, engineering judgments are required, based on the results that the processing stage provides the analysis and reliability of the results are determined. The critical Patch load resistances are evaluated by multiplying the first eigenvalue by the load applied. In the nonlinear analysis, load versus out-of-plane displacements curves are plotted and the ultimate loads obtained as shown from Appendix.9

Conclusion

This chapter aimed to describe the methodology used to design the numerical models and to compute the Patch loading resistance for plate girders. This chapter began with the presentation of the geometry of plate girders with flat and trapezoidal corrugated webs, the derivation of the numerical models, and the classification of individual members of the cross-section according to EN 1993-1-1. This was followed by presenting the methods for choosing the material properties of the steel used in this study considering requirements by EN 1993-1-1. Later in this chapter, the theoretical formulations for the evaluation of Patch loading resistance according to the

specifications by EN 1993-1-5 and Annex-D of EN 1993-1-5 for plate girders with corrugations were also discussed. This was followed by the linear and the non-linear FEM of Patch loading resistance using the eigenvalue method of analysis and the Static RIKS method respectively. Finally, the modeling methodology where the 3 phases (pre-processing, processing, and the post-processing phases) of analysis using the FE package Abacus/CAE program was discussed.

CHAPTER 3. RESULTS ANALYSIS AND DISCUSSIONS

Introduction

This chapter presents results obtained using the methodology discussed in the previous chapter, which is made up of analysis and the discussion of the results obtained. This chapter is divided into three parts. In the first part of this chapter, 35 plate girder models will be presented consisting of 10 Flat plate girders and 25 Corrugated webs girders. This is followed by the presentation Model verification using Theoretical and FE results for Patch loading resistance in the linear and nonlinear elastic field. Finally, in the last part of this chapter, Parametric analysis carried out to evaluate the effects of centric and eccentric loading are presented followed by discussions and conclusions.

3.1. MODELS FOR CORRUGATED AND FLAT GIRDERS

Girders were selected to consider model verifications as specifications by EN 1993-1-5 and Annex D and also those appropriate for parametric and Comparative analysis.

3.1.1. Flat web Girders

Models were selected to consider variation in loading length, Slenderness, and aspect ratio as presented in **Table 3.1**

<div align="center">

Table 3.1. Models for Corrugated Flat web girders

</div>

Model	a	S_s	S_{sa}	h_ω	t_ω	b_f	t_f		Purpose
PG1	1400	80	300	800	4	300	20	slender	Model Verification
PG2	1400	80	300	800	6	300	20	slender	
PG3	1400	80	300	800	8	300	20	slender	
PG4	1400	80	300	800	10	300	20	slender	
PG5	1400	80	300	800	15	300	20	slender	
PG6	1400	80	60	800	4	300	20	slender	Slenderness Verification
PG7	1400	80	60	800	6	300	20	slender	
PG8	1400	80	60	800	8	300	20	slender	
PG9	1400	80	300	1000	6	300	20	slender	Aspect ratio Verification
PG10	1400	80	300	1200	6	300	20	slender	

3.1.2. Corrugated web girders

Models were selected to consider variations in Loading length, loading width, Corrugation angle, local and global fold ratio.

Table 3.2. Models for Corrugated web girders

Model	a	S_s	S_{sa}	h_ω	t_ω	b_f	t_f	α	a_1	a_2	a_3	a_4	
PG11	750	/	120	376	2	120	10	40^0	130	157	120	101	
PG12	1400	80	60	800	4	300	20	45^0	200	200	141	141	
PG13	1400	120	60	800	4	300	20	45^0	200	200	141	141	
PG14	1400	200	60	800	4	300	20	45^0	200	200	141	141	Loading Length
PG15	1400	250	60	800	4	300	20	45^0	200	200	141	141	
PG16	1400	300	60	800	4	300	20	45^0	200	200	141	141	
PG17	1400	450	60	800	4	300	20	45^0	200	200	141	141	
PG18	1400	80	300	800	4	300	20	15^0	200	200	141	141	
PG19	1400	700	300	800	4	300	20	15^0	200	200	141	141	
PG20	1400	250	60	800	4	300	20	15^0	200	200	51.8	193.2	
PG21	1400	250	60	800	4	300	20	30^0	200	200	100.0	173.2	Corrugation angle
PG22	1400	250	60	800	4	300	20	45^0	200	200	141.4	141.4	
PG23	1400	250	60	800	4	300	20	60^0	200	200	173	100.0	
PG24	1400	250	60	800	4	300	20	70^0	200	200	188	68.4	
PG25	1400	250	60	800	4	300	20	30^0	100	100	50	87	
PG26	1400	250	60	800	4	300	20	30^0	150	150	75	130	
PG27	1400	250	60	800	4	300	20	30^0	200	200	100	173	
PG28	1400	250	60	800	4	300	20	30^0	250	250	125	217	Local fold ratio
PG29	1400	250	60	800	4	300	20	30^0	200	200	100	173	
PG30	1400	250	60	800	4	300	20	30^0	200	150	75	130	
PG31	1400	250	60	800	4	300	20	30^0	200	100	50	87	
PG32	1400	250	60	800	4	300	20	30^0	200	250	125	217	

PG33	1400	250	60	800	4	300	20	30^0	200	150	75	130	
PG34	1400	250	60	800	6	300	20	30^0	200	150	75	130	Global fold ratio
PG35	1400	250	60	800	8	300	20	30^0	200	150	75	130	

The web of both flat and corrugated girders was seen to flow under class 4 (Slender) and class 2 for the flange (Compact) which made the overall model to be considered as slender.

3.2. MODEL VERIFICATION

Model verification was done using specifications from EN 1993-1-5, Experimental results, and other empirical formulations by different authors. A mesh size of 20mm was adopted to be used for the model as FE results were seen to converge around this size.
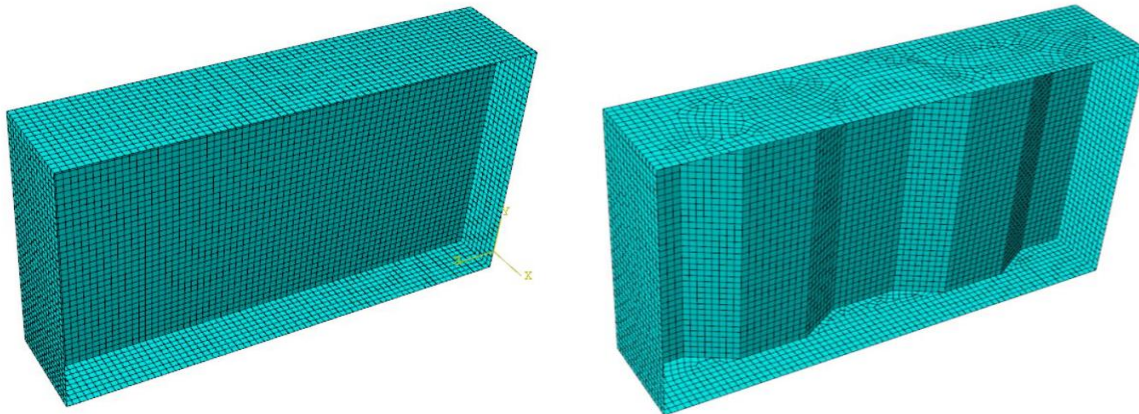
Figure 3.1. Meshing for FE Models

3.2.1. Plate girders with Flat web

Loading was considered following specifications from EN 1993-1-5 Annex C, where a centered distributed load of length (Ss=80mm) is applied along the whole width of the girder.

Table 3.3. FE results for model verification.

Model	$F_{cr(Theo.)}$ kN	$F_{cr(FE)}$ kN	$\dfrac{F_{Cr(Theo.)}}{F_{Cr(FE)}}$	$F_{u(Theo.)}$ kN	$F_{u(FE)}$ kN	$\dfrac{F_{u(Theo.)}}{F_{u(FE)}}$
PG1	100.594	84.590	1.20	121.924	238.552	0.51
PG2	339.506	274.529	1.24	260.747	553.395	0.47
PG3	804.754	610.643	1.32	449.520	696.133	0.65

A good correlation is obtained as the Critical load is always specified to have a percentage difference in the range of 20% for the Critical resistance and up to 50% in the case of Ultimate resistance.

3.2.2. Plate girders with Corrugated web

The experiment conducted by Elgaaly and Seshadri Consisted of a hybrid girder with the material and geometric properties as seen in Figure 3.2

Table 3.4. Geometrical properties for experimental model by Elgaaly

a	h_ω	t_ω	b_f	t_f	α	a_1	a_2	a_3	a_4
750	376	2	120	10	40^0	130	157	120	101
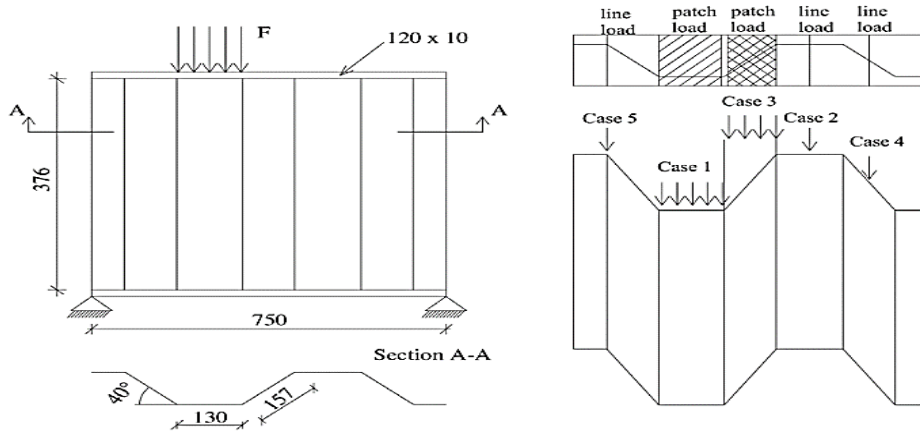
Figure 3.2. Test specimen of Elgaaly and Seshadri

Flange

Properties	Stress	Strain
Elastic (f_y)	389MPa	0
Plastic (f_u)	563MPa	0.2

Web

Properties	Stress	Strain
Elastic (f_y)	379MPa	0
Plastic (f_u)	413MPa	0.2

Young's modulus (E) = 200GPa   **Poissons ratio**(v) = 0.3

The model was reproduced and the following corresponding FE results were obtained as soon on Table 3.5.

Table 3.5. FE results for Elgaaly experimental Model

Case	Location of load	Load distribution width S_s (mm)	F_{Exp} (kN)	F_{FE} (kN)	F_{FE}/F_{Exp}
Case 1	Parallel fold	146.05	131.275	116.131	0.885
Case 2	Parallel fold	≈ 0	82.325	70.191	0.853
Case 3	Inclined fold	104.14	102.35	87.938	0.859
Case 4	Inclined fold	≈ 0	95.675	86.909	0.908
Case 5	Junction between parallel and Inclined fold	≈ 0	73.425	98.568	1.342

This showed a good correlation as the FE results where similar to that reproduced by other researchers such as Elgaaly, Kovesdi, and Inaam, where the ratio was seen to vary between 0.8 to 1.2 (Elgaaly and Seshadri 1997) (Inaam and Upadhyay 2020)

3.3. FINITE ELEMENT RESULTS FOR CENTRIC LOADING

Both flat and corrugated webs were seen to portray similar behavior even though there was a great difference in Ultimate resistance and failure mechanisms.
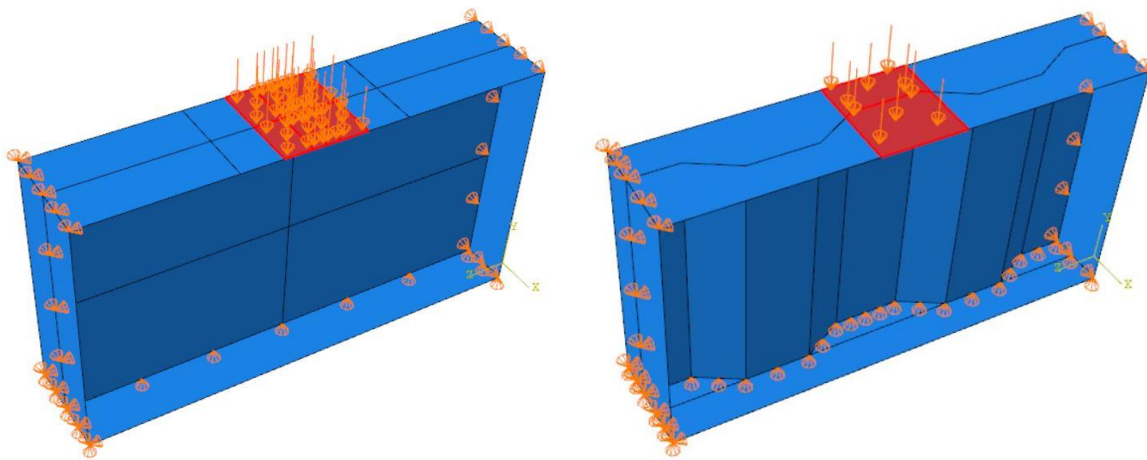
Figure 3.3. Centric loading for FE models

3.3.1. Flat web girders

Flat web girders were mostly characterized by Global web buckling, accompanied by Web buckling and crippling at failure for small slenderness ratios. Web yielding and flange buckling were very common at high slenderness ratios.

3.3.1.1. Critical and Ultimate load varying Slenderness ratio

The first, second, and third buckling modes of the PG1, PG2, PG5, PG6 are given by Figure 3.4 with their Eigenvalues which corresponds to their critical Patch load resistance.

a) **PG 1 ($t_w = 4$mm)**

Mode 1	**Mode 2**	**Mode 3**
Eigen Value = 84590N	Eigen Value = 134073N	Eigen Value = 2297780N
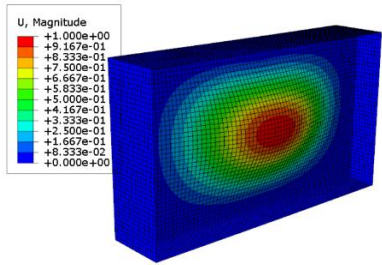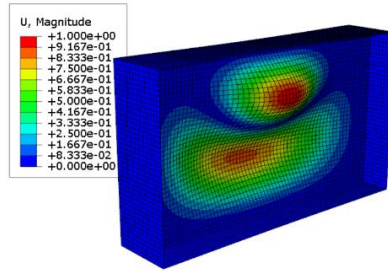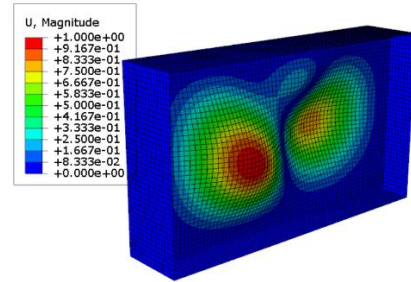
b) **PG 2 $t_w = 8$mm)**

Mode 1	**Mode 2**	**Mode 3**
Eigen Value = 274530N	Eigen Value = 432327N	Eigen Value = 745536N
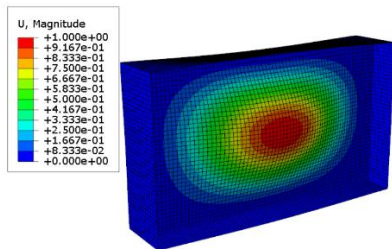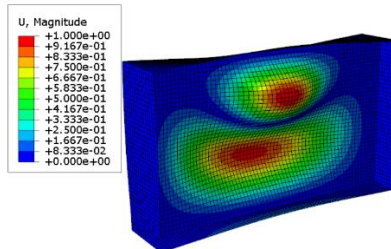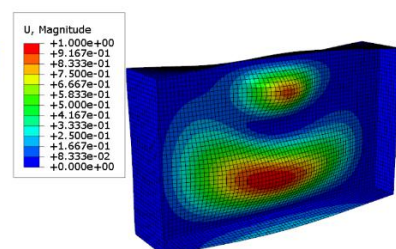
c) **PG 5 ($t_w = 10$mm)**

Mode 1	**Mode 2**	**Mode 3**
Eigen Value = 610644N	Eigen Value = 959474N	Eigen Value = 1647780N
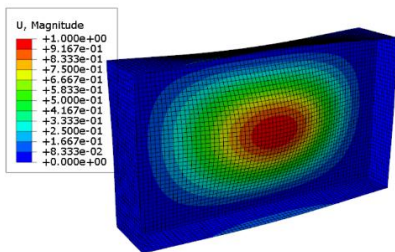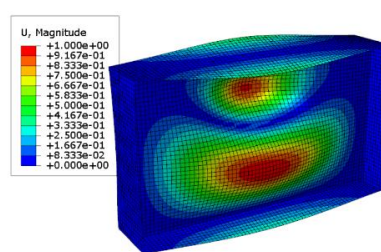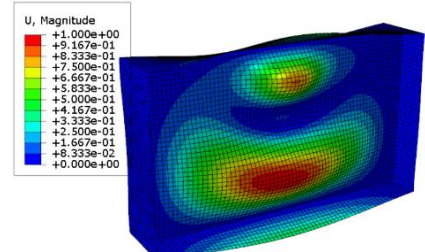
    d)   **PG 6 ($t_w = 15$mm)**

Mode 1

Eigen Value = 2772760N

Mode 2

Eigen Value = 4809800N

Mode 3

Eigen Value = 8243990N
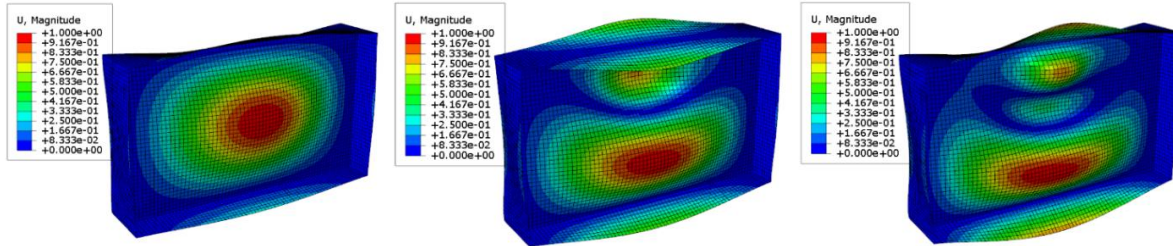
Figure 3.4. Linear buckling analysis for PG1, PG2, PG5, and PG6 Models

Failure is mostly characterized by web buckling and crippling for low slenderness and web yielding for higher slenderness.

    a) PG 1 ($F_u = 238.552$KN)
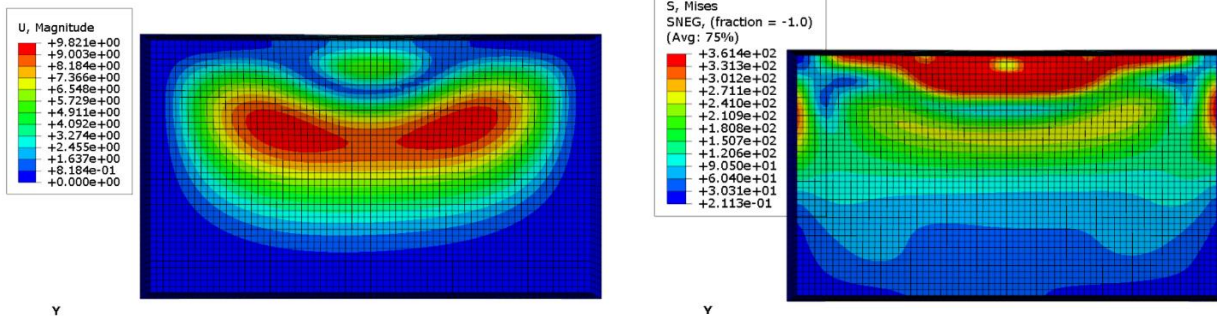
    b) PG 3 ($F_u = 696.133$KN)
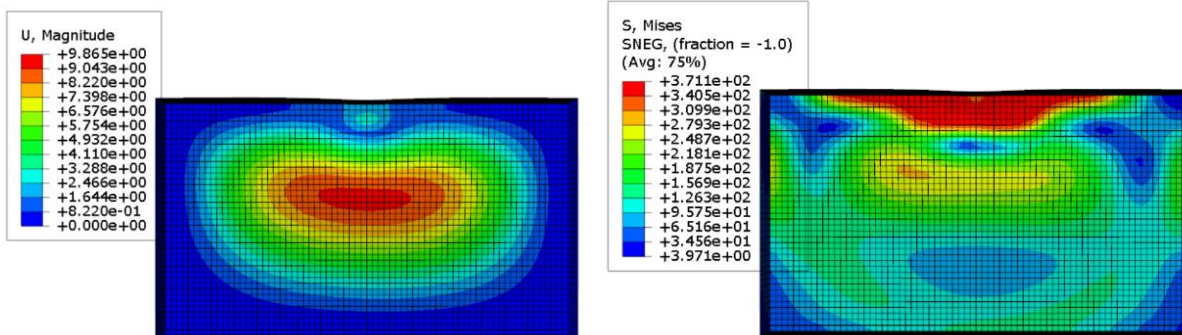
    c) PG 5 ($F_u = 968.995$KN)
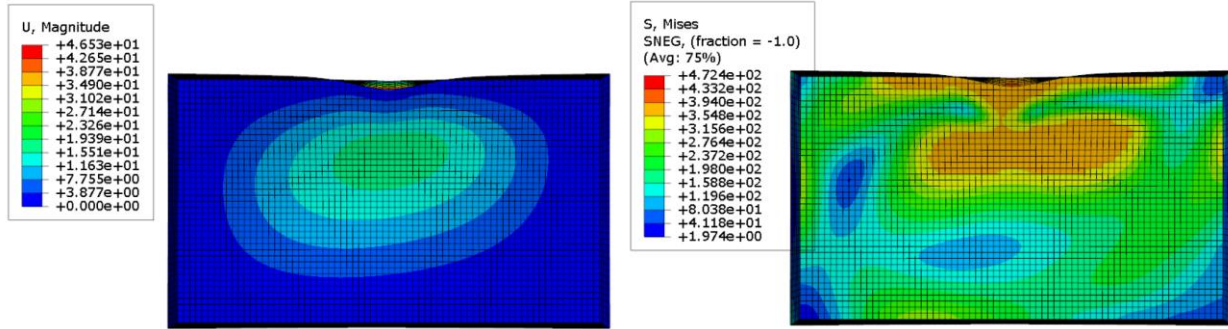
d) PG 6 ($F_u = 790.48$KN)
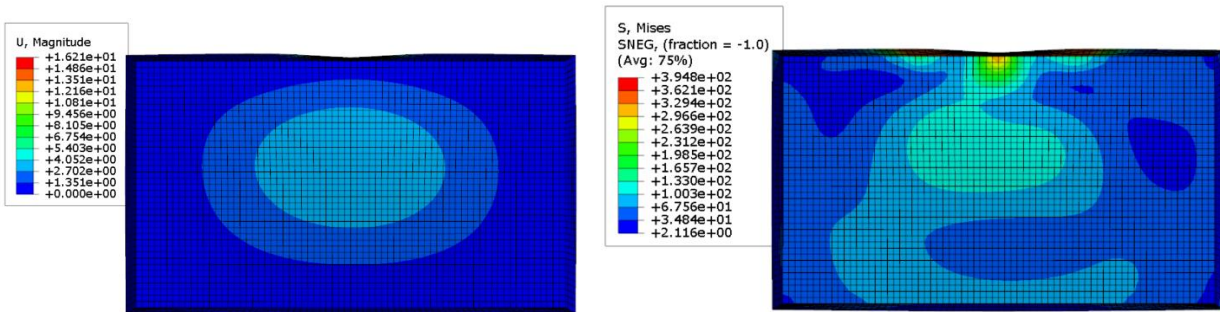
Figure 3.5. Nonlinear Static Riks analysis for PG1, PG2, PG5, and PG6 Models

Failure is seen to gradually change from Web buckling to Web yielding and finally flange bulking. This is evident from the gradual reduction of Post buckling reserve from PG1 to PG6 as soon in Figure 3.6 below.
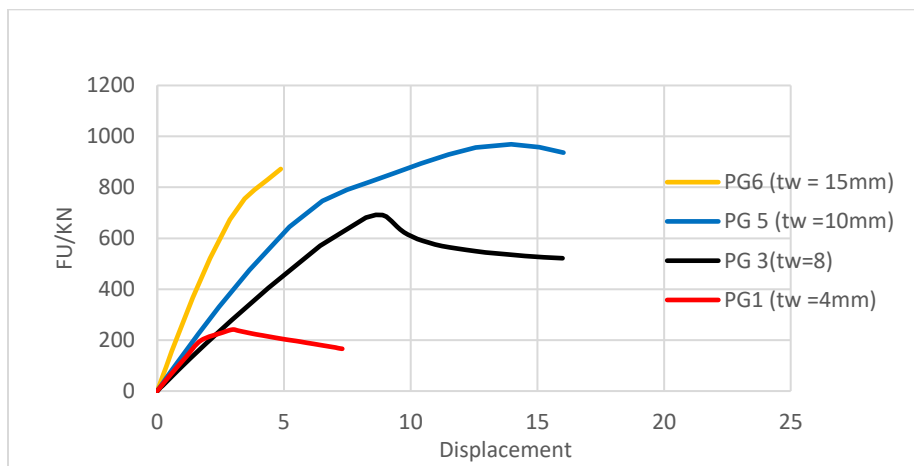
Figure 3.6. Load-displacement curve for PG1, PG3, PG5, PG6

3.3.1.2. Critical and Ultimate load with varying aspect ratio ($^a/h_w$)

Patch load resistance is seen to increases with a decrease aspect ratio. This is due to an increase in the web section which subsequently produces increase resistance to patch loading.

Table 3.6. Ultimate and critical loads forPG2, PG9, PG10.

Model	F_{cr}/kN	F_u/kN
PG2 (h_w = 800)	274.35	450.918
PG9 (h_w = 1000)	244.730	474.992
PG10 (h_w = 1200)	242.783	501.094
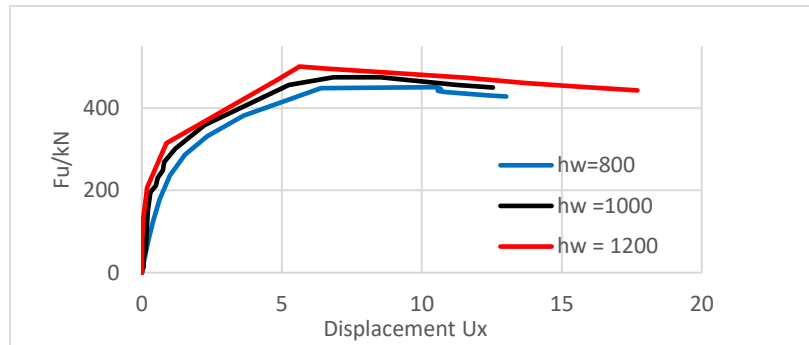
Figure 3.7. Load-Displace Curve for Varying aspect ratio.

Also, with Decreasing the aspect ratio the girder becomes more susceptible to buckling. This is evident from the gradual decrease in Critical buckling load as soon in **Figure 3.8**
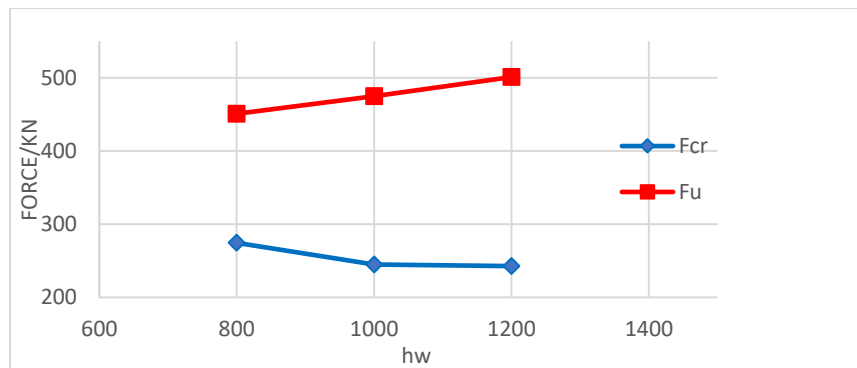
Figure 3.8. Variation of Ultimate and Critical Patch load resistance with aspect ratio

3.3.2. Corrugated Web

Corrugated webs on the other hand turn to show both Interactive and local buckling accompanied by web crippling and yielding for high slenderness ratios. Other parameters such as corrugated angle and Local fold ratio turn to play a very important role in its behavior.

a) PG 18 (Ss =80mm)

Mode 1

Eigen Value = 686763N

Mode 2

Eigen Value = 778864N

Mode 3

Eigen Value = 973757N
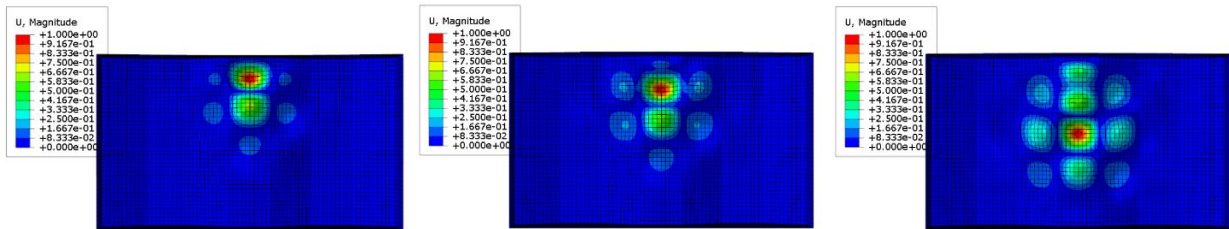
b) PG 19 (Ss= 700mm)

Mode 1

Eigen Value = 1231760N

Mode 2

Eigen Value = 1280770N

Mode 3

Eigen Value = 1363760N
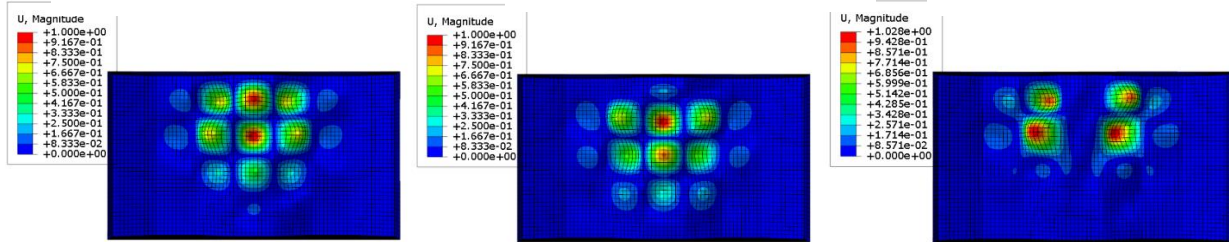
Figure 3.9. Linear buckling analysis for PG18 and PG19 Models
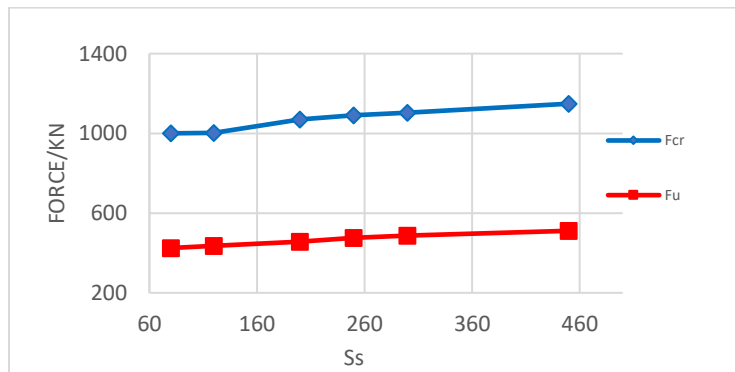
Figure 3.10. Variation of Critical and Ultimate resistance with Loading length.

EMECHEBE CLINTON CHISOM/*Master's Thesis in Civil engineering*

Corrugated girders are seen to mostly experience Web yielding at failure. This is evident from the fact that Critical loads are seen to be far greater than Ultimate loads which makes them fail before buckling is ever experienced. This is also evident from the reduction in post bulking reserve which makes failure occur immediately after the nonlinear elastic region is reached.
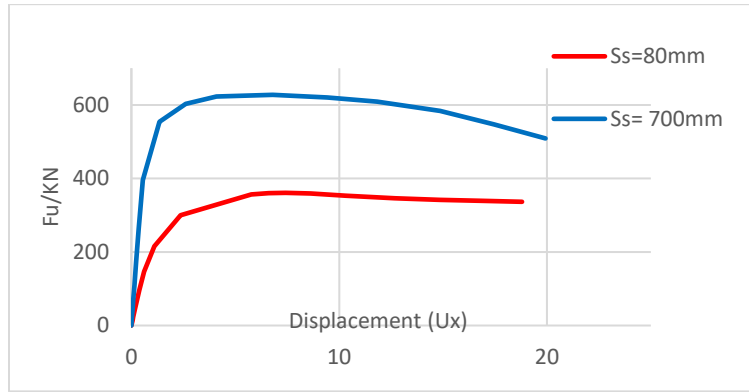
Figure 3.11. Loading displacement curve for PG18 and PG19

c) PG 10 (Ss = 80mm)
    Fu = 361.924KN
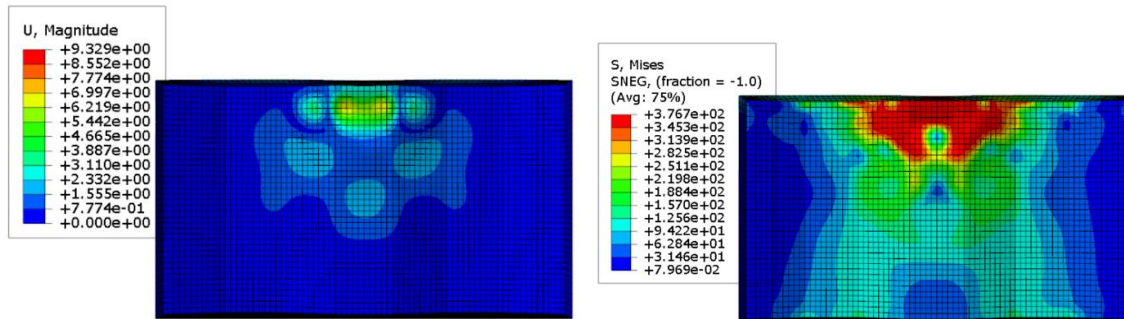
d) PG 18 (Ss = 700mm)
    Fu = 629.730KN
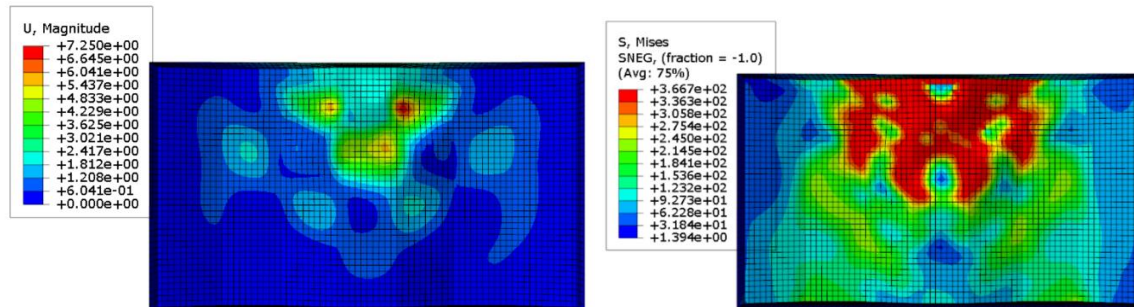
Figure 3.12. Nonlinear Static Riks analysis for PG10 and PG16 Models

EMECHEBE CLINTON CHISOM/*Master's Thesis in Civil engineering*

3.4. FINITE ELEMENT RESULTS FOR ECCENTRIC LOADING

Both Flat and Corrugated plates girders turn to show a resistance reduction under eccentric loading which are varied by the below-presented properties.

3.4.1. Effects of eccentricity on Flat web girders

Flat webs turn to show asymmetric behavior with respect to eccentric loading

3.4.1.1. Variation of Ultimate load with web slenderness

Resistance generally reduces with increasing eccentricity. Increase eccentricity generally leads to a change in failure mode from the web to flange buckling which is accompanied by very low resistance.
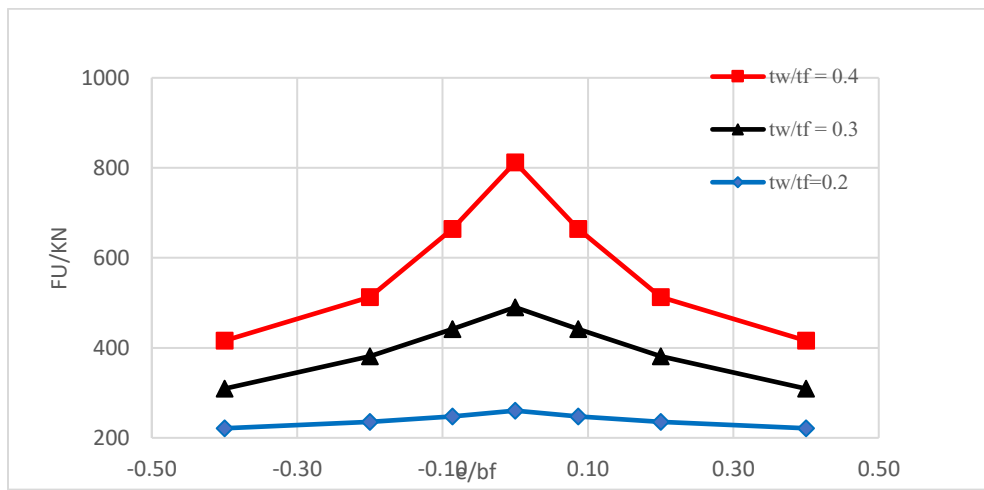
Figure 3.13. Variation of eccentric load with web slenderness
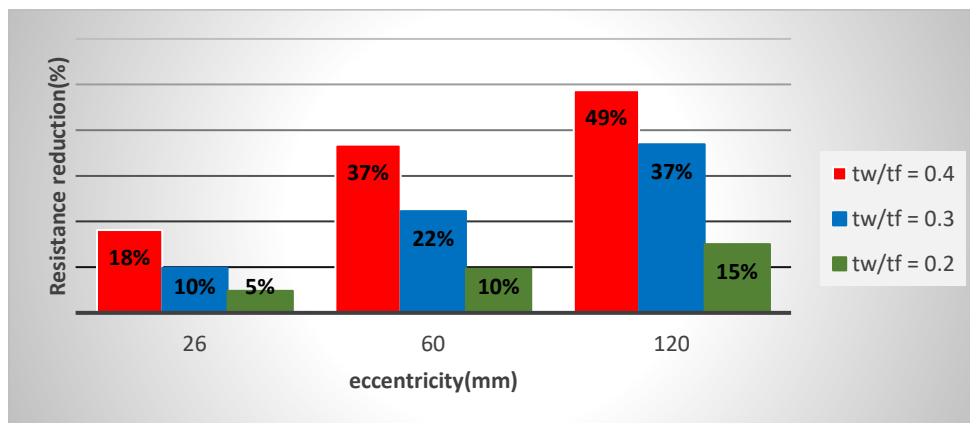
Figure 3.14. Load reduction with varying eccentricity for loading length

With high slenderness ratios, the web becomes more rigid. This causes ineffective load transmission from flange to web making the flange more susceptible to bulking. This is evident from a significant resistance reduction of 49% and 15% with high and low slenderness respectively.
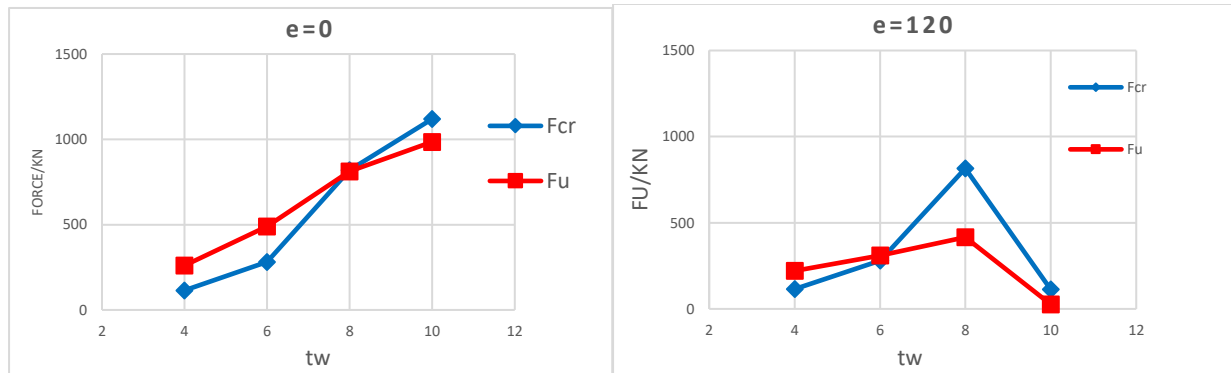
Figure 3.15. Variation of critical and Ultimate loads at for centric and eccentric loading

3.4.2. Effects of eccentricity on Corrugated web girders

Parametric analysis is conducted to analyze the effects of different geometric parameters such as Loading length, Corrugated angle, Local and global fold ratios on the eccentric loading resistance for corrugated Plate girders. Eccentricity was considered from the middle of the plate girder where Positive values were oriented towards the large flange outside and negative values towards the smaller flange outside.

3.4.2.1. Variation of ultimate load with Loading length

Resistance generally increases with increase loading length. This is due to the activation of more folds, resulting in a more effective stress distribution along the web of the corrugated girder leading to an increase in Patch load resistance.
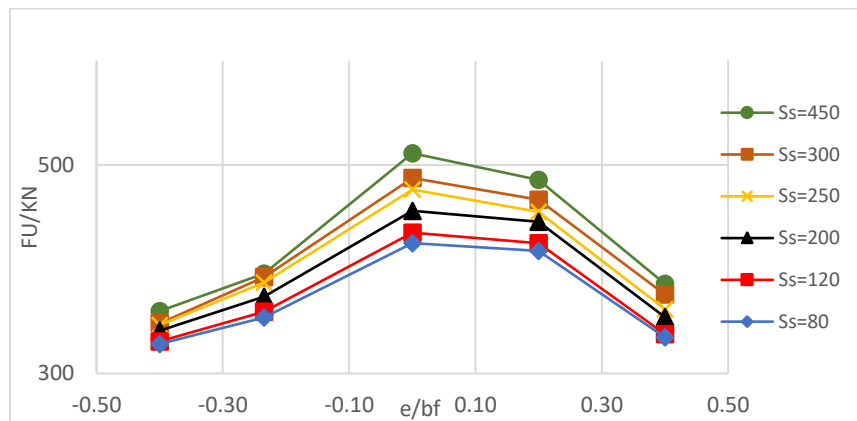
Figure 3.16. Variation of eccentric resistance reduction with loading length

For a specific eccentricity, a light change in gradient is observed which signifies a change from Short to Long loading lengths as observed by other researchers. (Inaam and Upadhyay 2020) where more folds are activated leading to more effective load transmission from the flange to the web.
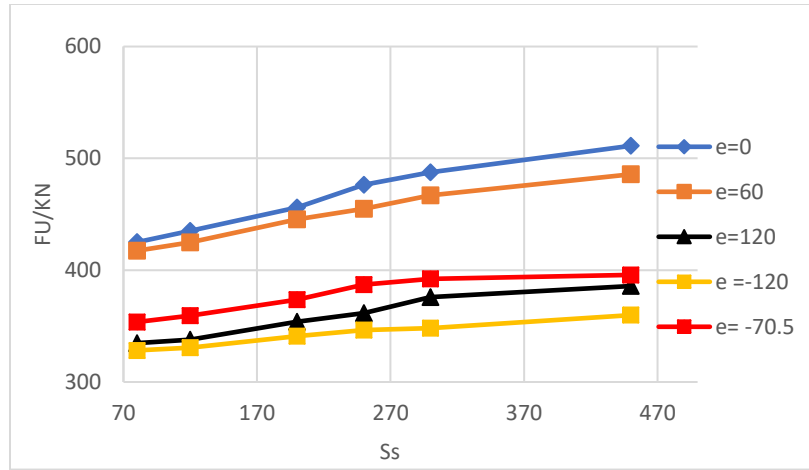
Figure 3.17. Variation of eccentric resistance reduction with loading length

Eccentricity effects are generally seen to increase with increasing loading length with 1.8% and 5% reductions at low eccentricities which is greatly increased to 21.2% and 24.5% and higher eccentricities.
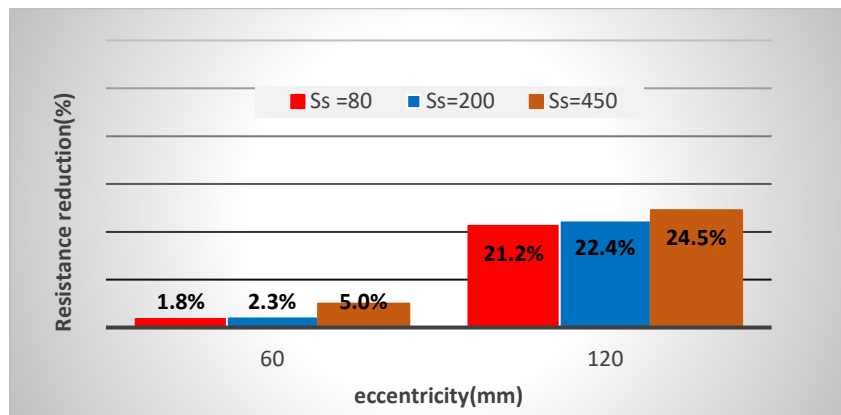
Figure 3.18. Load reduction with varying eccentricity for loading length

3.4.2.2. Variation of ultimate load with Corrugation angle

An increase in the corrugation angle results in a significant increase in the ultimate Patch load capacity. low corrugation angles are associated with low confinement which makes buckling propagate to surrounding folds with more ease as compared to when corrugation angles are higher.
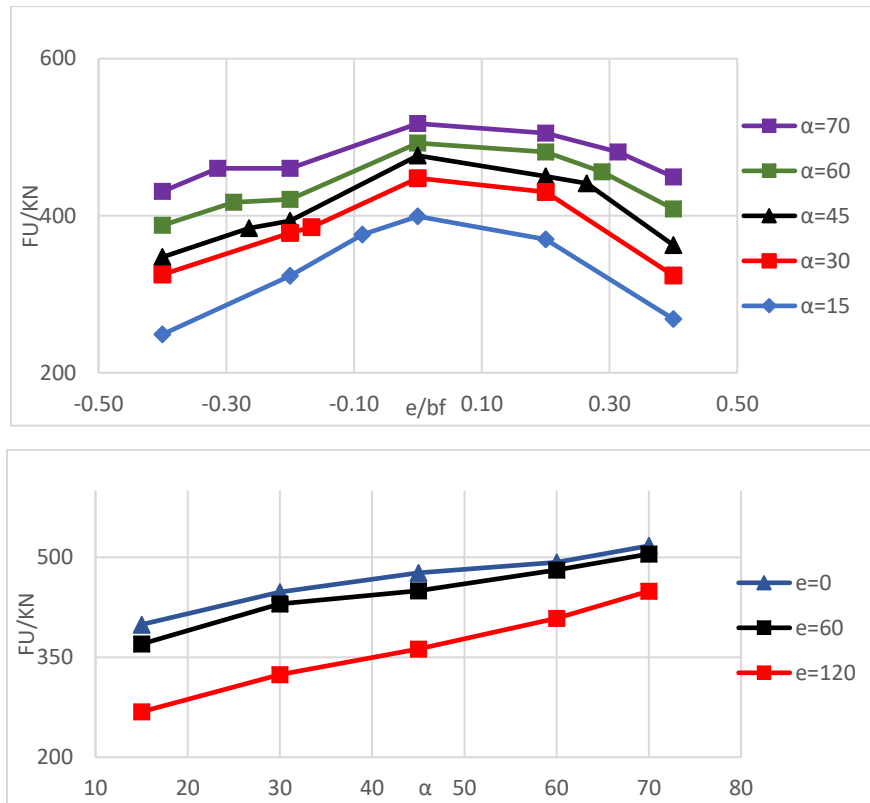
Figure 3.19. Variation of eccentric resistance reduction with corrugated angle

This is also evident in eccentricity reduction where a difference of 4% is seen at low eccentricities and 19% and high eccentricities.
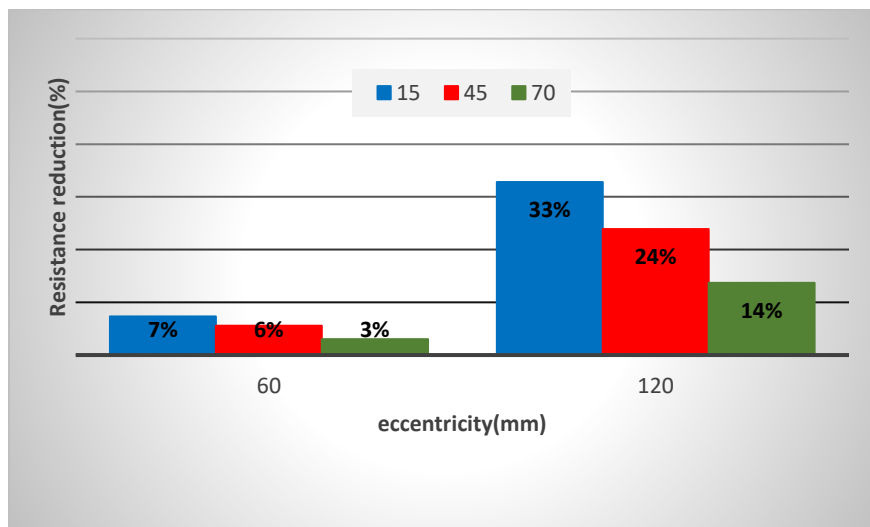
Figure 3.20. Load reduction with varying eccentricity for corrugation angles
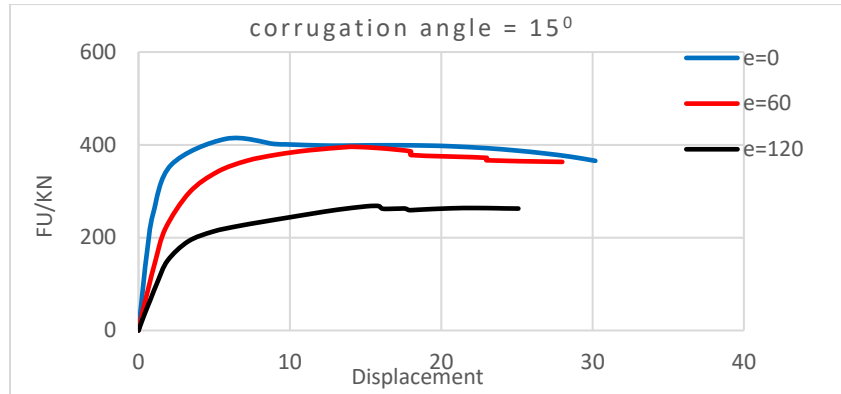
Figure 3.21. Force-displacement curve for variation corrugated angles

3.4.2.3. Variation of ultimate load with Local fold ratio

a) Considering equal length for inclined and parallel folds ($a_1=a_2$)

Local fold ratio is defined as the ratio of the individual fold to web thickness ($^{a_i}/_{t_w}$).

Patch loading capacity is lower for higher fold ratios and higher for lower fold ratios.
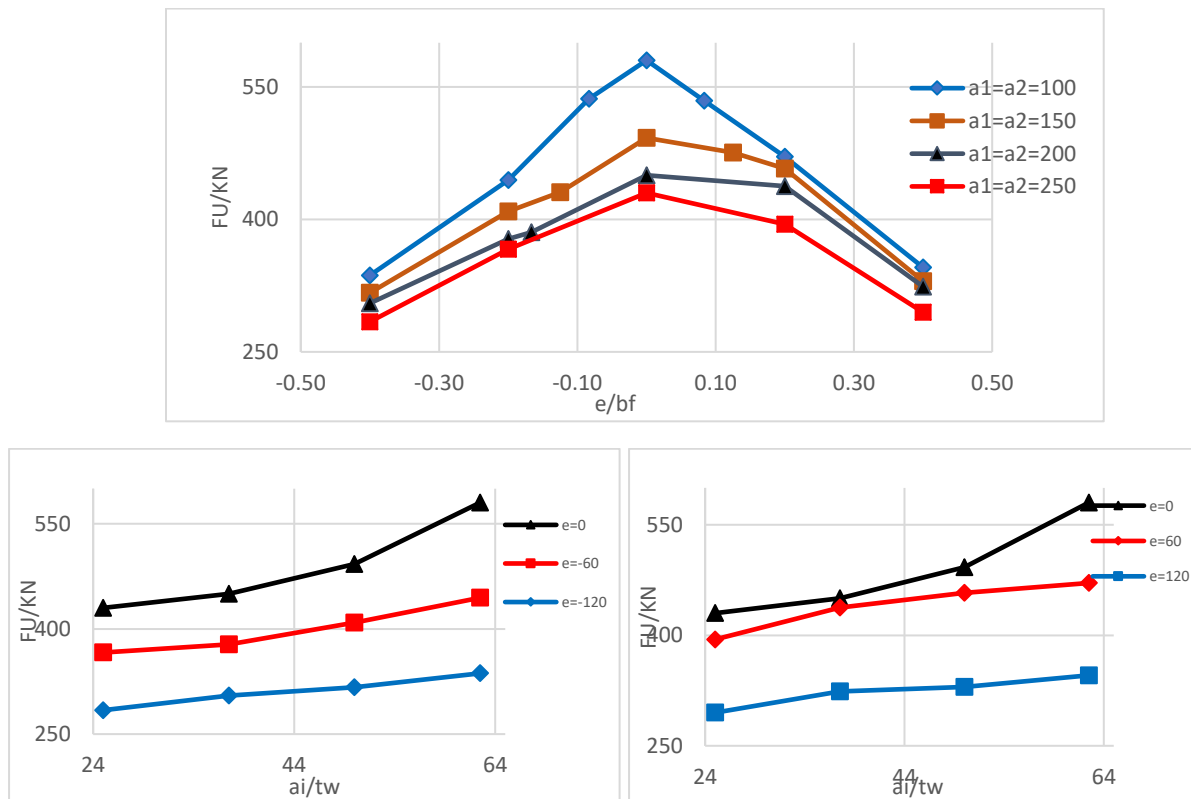
Figure 3.22. Variation of eccentric resistance reduction with Local fold ratio

This is also evident for resistance reduction where a 16% difference is seen for low eccentricities and an 18% difference for high eccentricities.
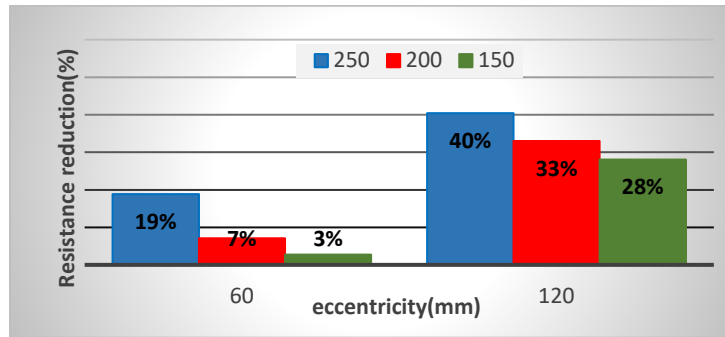
Figure 3.23. Load reduction with varying eccentricity for local fold ratio (equal folds)
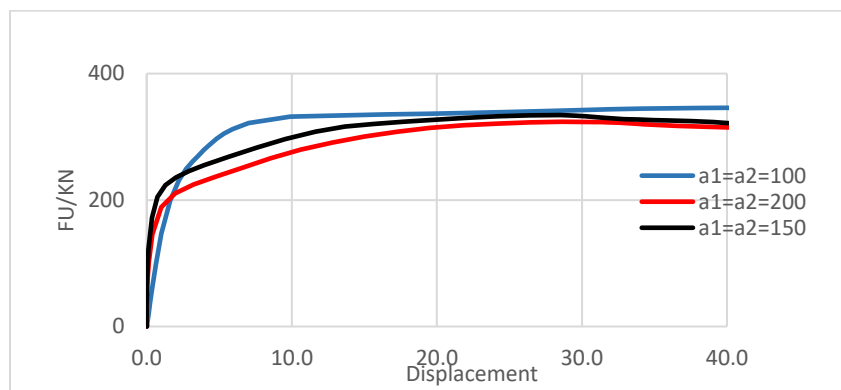
Figure 3.24. Load displacement curves for varying local fold ratio (equal folds).

b) Considering Varying the length for inclined and parallel folds

Unequal fold width generally results in higher loading resistance per unit corrugation length. The gain in loading resistance is higher for lower fold ratio and lower for higher fold ratio.
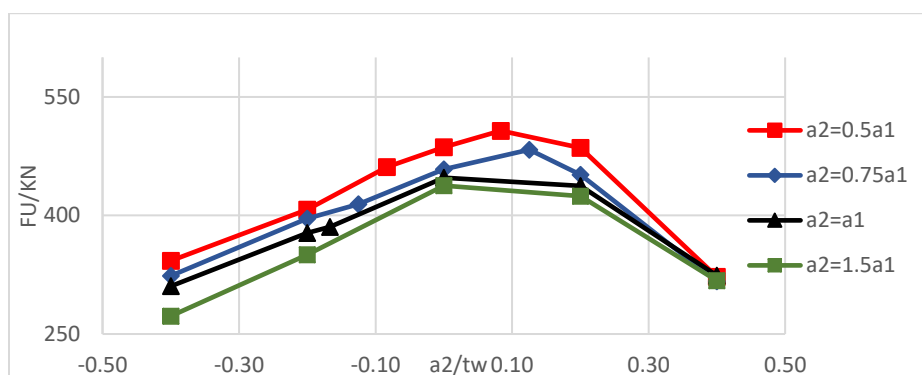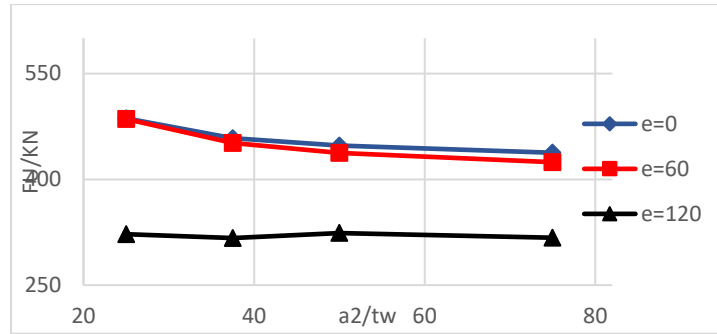
Figure 3.25. Variation of eccentric resistance reduction with unequal fold length.

Using unequal fold lengths are seen not to have only a slight effect on eccentricity reduction as changes within the range of 1-2% are obtained.
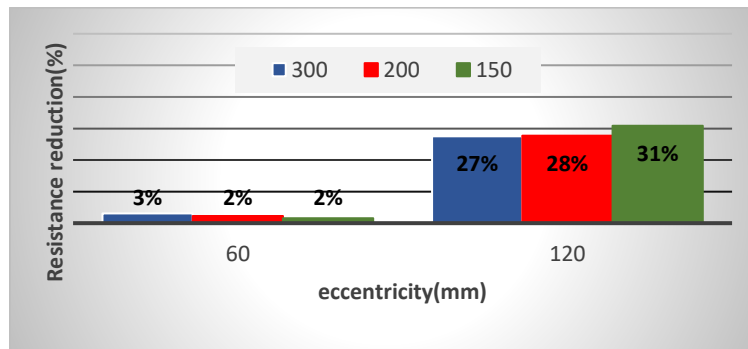
Figure 3.26. Load reduction with varying eccentricity for local fold ratio (unequal folds)

3.4.2.4. Variation of Ultimate load with Global fold ratio

The ultimate capacity Increases as the slenderness of the web decreases. This confirms the fact that the ultimate patch load capacity is inversely proportional to the global web ratio. The failure mode is limited to the local domain.
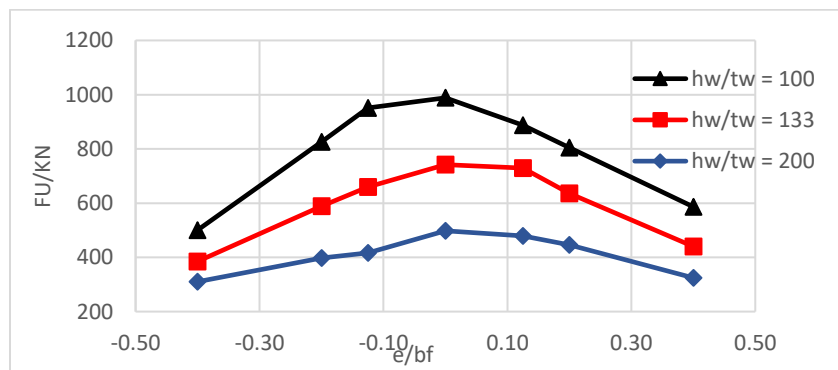
Figure 3.27. Variation of Ultimate load with global fold ratio
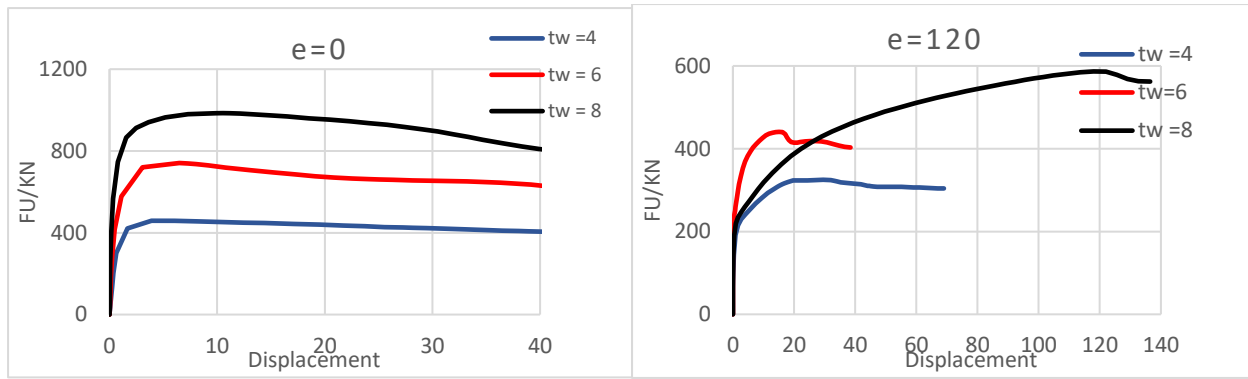
Figure 3.28. Load displacement curves for varying global fold ratio.
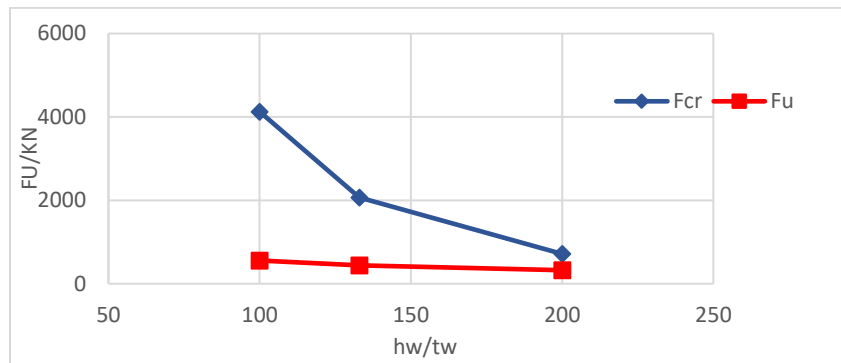
Figure 3.29. Ultimate and critical load variation with global fold ratio.

For smaller thickness failure occurs in slender steel web, whereas for higher web thickness flange buckling occurs resulting in a greater resistance capacity as corrugated webs are in a much better state to handle flange buckling due to a higher degree of confinement.
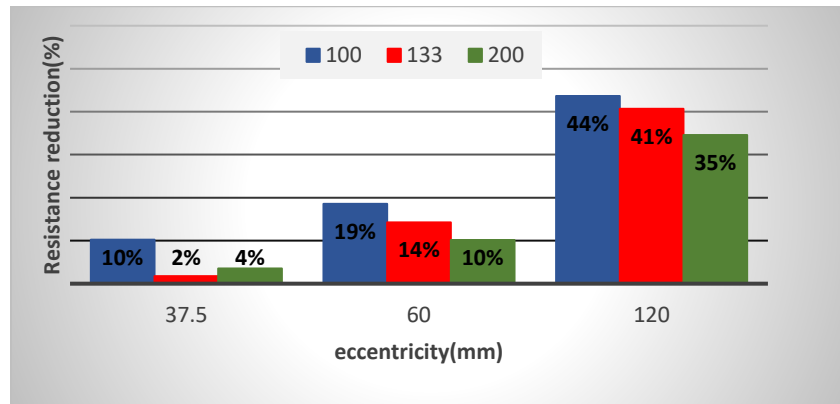
Figure 3.30. Load reduction with varying eccentricity for global fold ratio.

This is also evident with eccentric loading where only a 6% resistance reduction difference is seen for low and high eccentricities.

3.4.3. Comparative analysis

Taking a reference Ultimate resistance of 740kN a 19% reduction in the material is seen if Corrugated girders are used over Flat web girders.
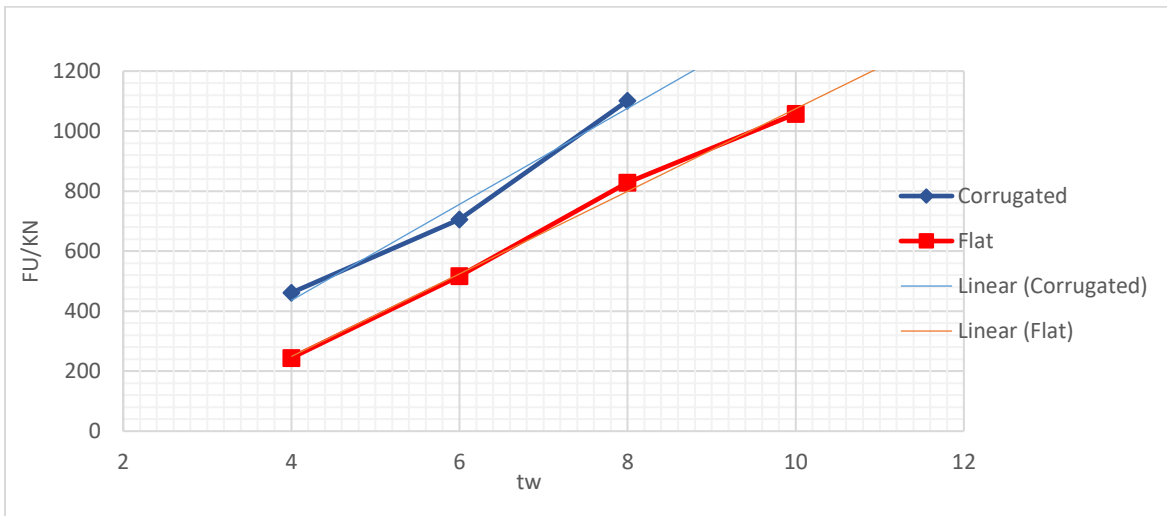
Figure 3.31. Comparative ultimate resistance for Flat and corrugated plate girders

Table 3.7. Comparative Material analysis Flat-Corrugated girders

	Total Web Length(mm)	Web Height (mm)	Web Thickness (mm)	Material Volume (mm³)	Percentage Reduction
Flat	1400	800	7.8	873,6000	19%
Corrugated	1480.38	800	6	710,5824	

An equivalent reduction in the dead load of the structure will also be obtained which makes it suitable for long-span bridges, industrial buildings, and other related structures.

Conclusion

This chapter aimed to display the results obtained using the methodology in the previous chapter. Firstly, 35 plate girder models were presented showing their section characteristics.

Amongst these models were 10 plate girder models with flat webs and 25 with corrugated webs.

The theoretical and FE results of the patch loading resistance for the models were presented. From the findings, the elastic buckling strength increases with a decrease in aspect ratio and slenderness parameter. It increases with increase loading length and loading width. In addition, for corrugated members, the elastic buckling strength increases with an increase in the angle of corrugation. It also increases with decreasing global and local fold ratios. Ultimate patch load resistance varies similarly. With Flat plate girders, Ultimate resistance was seen to be greater than Critical buckling loads which made them more susceptible to buckling at failure unlike in corrugated girders where web yielding was so common because of a higher critical than ultimate load. For flat plate girders, global buckling is very common at failure, with web yielding and crippling very typical for low slenderness ratios. Corrugated girders on the underhand turn to show both local and interactive buckling accompanied by web yielding and flange buckling at failure. The effects of eccentricity are seen to increase with increase Loading length and local fold ratio. Also, it decreases with increase Corrugation angle and global fold ratio. The smaller outstand for parallel fold is a more critical location as the maximum reduction in patch load capacity occurs when the patch load is kept adjacent to the edge of the shorter overhang which always accounts for a difference of 3% to 10% as compared to the longer overhang. Plate girders with corrugated webs show higher critical and ultimate patch load resistance under the same loading and boundary conditions than equivalent members with planar webs. This could account for up to about 15% material reduction per unit length in the use of members with corrugated webs over flat members considering equal patch loading resistance.

GENERAL CONCLUSION

The main objective of this study was to analyze and compare the effects of patch loading and loading eccentricities on the linear elastic and the nonlinear elastic field of plate girders with planar and corrugated webs under the same loading and boundary conditions. This was done considering variations in aspect ratio, slenderness parameter, loading length and width, angle of corrugation, local and global fold ratios. To attain these objectives, 35 plate girders models consisting of 10 flat web and 25 corrugated web girders were developed by varying geometric parameters of the girder cross-section. For the 10 flat plate girders, 4 were used for model verification,3 for slenderness verification, and 3 for aspect ratio verification. For the 25 corrugated plat girders, 3 were used for the model verification,6 for loading length,5 for corrugated angle,8 for local fold ratio, and 3 for global fold ratio. In addition, 4 samples were selected for each case considering varying slenderness parameters for the evaluation of the material reduction for equivalent corrugated and flat plate girders. The eigenvalue elastic buckling analysis and the static RIKS nonlinear buckling analysis were performed where a total of about 200 numerical analyses were carried out using a FEA package ABAQUS/CAE to reach results. Theoretical results using Eurocode and specifications from other authors were evaluated using MS Excel program and compared with results from FEA.

According to results obtained;

The elastic buckling strength increases with decreasing aspect ratio and slenderness parameter. It increases with increase loading length and loading width. In addition, for corrugated members, the elastic buckling strength increases with an increase in the angle of corrugation. It also increases with decreasing global and local fold ratios. Ultimate patch load resistance was seen to vary in the same manner. With Flat plate girders, Ultimate resistance was seen to be greater than Critical buckling loads which made them more susceptible to buckling at failure unlike in corrugated girders where web yielding was so common because of a higher critical than ultimate load. For flat plate girders global buckling is very common at failure, with web yielding and crippling very typical for low slenderness ratios. Corrugated girders on the underhand turn to show both local and interactive buckling accompanied by web yielding and flange buckling at failure. For loading length, a change of gradient is noticed with increasing loading length which signifies a change from short to long loading length. The use of unequal fold length for corrugation is seen to have a significant increase in resistance when shorter inclined and longer parallel folds are used.

Under eccentricities, flange buckling is very common for flat webs unlike in corrugated webs where web and flange yielding is very typical. The effects of eccentricity are seen to increase with increase loading length and local fold ratio. Also, it decreases with increase Corrugation angle and global fold ratio. The smaller outstand for parallel fold is a more critical location as the maximum reduction in patch load capacity occurs when the patch load is kept adjacent to the edge of the shorter overhang which always accounts for a difference of 3% to 10% as compared to the longer overhang. Plate girders with corrugated webs show higher critical and ultimate patch load resistance under the same loading and boundary conditions than equivalent members with planar webs. This could account for up to about 15% material reduction per unit length in the use of members with corrugated webs over flat web members considering equal patch loading resistance. However, in this study extensive parametric analysis on different static forms was not carried out which is found to have a considerable effect on the Patch loading resistance for steel girders.

Finally, trapezoidal corrugations were used in this work to investigate the patch loading resistance. Research investigating the behaviors of zigzag, rectangular, and sinusoidal corrugations as well is recommended.

REFERENCES

Abbas, M., Ibrahim, S. M., & Korashy, M. M. 2019. "Lateral Torsional Buckling of Partial Corrugated Web in Steel." (June).

Ajeesh, S. .. 2016. "Shear Behaviour of Stiffened Plate Girders." (April).

Alinia, M. M., A. Gheitasi, and Maryam Shakiba. 2011. "Postbuckling and Ultimate State of Stresses in Steel Plate Girders." *Thin-Walled Structures* 49(4):455–64. doi: 10.1016/j.tws.2010.12.008.

Basiński, W. 2019. "Shear Buckling of Plate Girders with Corrugated Web Restrained by End Stiffeners."

Buckling Analysis with FEA | Machine. n.d. "Buckling Analysis with FEA." (https://www.machinedesign.com/3d-printing-cad/fea-andsimulation/article/21831716/buckling-analysis-with-fea).

Chi, L. 2014. "A Beginner ' s Guide to Simple Plate Girder Design to EC3 Part 1-5." 1–44.

Egziabher, Tewolde Berhan Gebre, and Sue Edwards. 2013. 済無*No Title No Title*. Vol. 53.

Elgaaly, M., A. Seshadri, R. Rodriguez, and S. Ibrahim. 2000. "Bridge Girders with Corrugated Webs." *Transportation Research Record* 1(1696):162–70. doi: 10.3141/1696-19.

Elgaaly, Mohamed, and Anand Seshadri. 1997. "Girders with Corrugated Webs under Partial Compressive Edge Loading." *Journal of Structural Engineering* 123(6):783–91. doi: 10.1061/(asce)0733-9445(1997)123:6(783).

En, B. S. 2005. "Eurocode 3 : Design of Steel Structures." 3–1.

Ghadami, A., & Broujerdian, V. 2019. "Shear Behavior of Steel Plate Girders Considering Variations in Geometrical Properties." *Journal of Constructional Steel Research, 153, 567–577. Https://Doi.Org/10.1016/j.Jcsr.2018.11.009.*

Gozzi, Jonas. n.d. *Patch Loading Resistance of Plated Girders-Ultimate and Serviceability Limit State.*

Hibbitt, Karlsson & Sorensen, I. 2000. 2012. "ABAQUS User's Manual." *In ABAQUS/CAE User's Manual.*

Ibrahim, By Sherif Abdel-basset. 2015. "Steel Plate Girders with Corrugated Webs, Past Present and Future Steel Plate Girders with Corrugated." 79.

Inaam, Qazi, and Akhil Upadhyay. 2020. "Behavior of Corrugated Steel I-Girder Webs Subjected

to Patch Loading: Parametric Study." *Journal of Constructional Steel Research* 165:105896. doi: 10.1016/j.jcsr.2019.105896.

Jáger, Bence, Balázs Kövesdi, and László Dunai. 2020. "Design Method Improvements for Trapezoidally Corrugated Web Girders." *Proceedings of the 9th International Conference on Advances in Steel Structures, ICASS 2018* (December). doi: 10.18057/ICASS2018.P.143.

Johansson, B., R. Maquoi, G. Sedlacek, C. Müller, and D. Beg. 2007. "Commentary and Worked Examples To En 1993-1-5 ' Plated Structural Elements .'" *October* 3(October).

Kala, Z., & Kala, J. 2019. "Resistance of Thin-Walled Plate Girders under Combined Bending and Shear." (November).

Kilardj, Madina, Ghania Ikhenazen, Tanguy Messager, and Toufik Kanit. 2016. "Linear and Nonlinear Buckling Analysis of a Locally Stretched Plate." *Journal of Mechanical Science and Technology* 30(8):3607–13. doi: 10.1007/s12206-016-0721-5.

Kövesdi, B., B. Braun, U. Kuhlmann, and L. Dunai. 2010. "Patch Loading Resistance of Girders with Corrugated Webs." *Journal of Constructional Steel Research* 66(12). doi: 10.1016/j.jcsr.2010.05.011.

Maiorana, Emanuele, Cyrille Denis Tetougueni, Paolo Zampieri, and Carlo Pellegrino. 2019. "Interaction between Patch Loading , Bending Moment , and Shear Stress in Steel Girders." 20(6):389–410.

NSHANJI, SHEY Louis. 2020. "SHEAR BUCKLING ANALYSIS OF PLATE GIRDERS CONSIDERING VARIATIONS IN GEOMETRIC PARAMETERS."

Rajkumar, R., R. Aravindh, B. Gokula Krishanan, and B. Mukul Anand. 2017. "Study on the Behaviour of Plate Girder with Plane Web and Corrugated Web." *Advances in Computational Sciences and Technology* 10(9):2745–64.

Roberts, T. M. 1979. "81 99 A." 155–75.

da Silva, Luís Simões, Rui Simões, and Helena Gervásio. 2010. "Eurocode 3: Part 1-1: General Rules and Rules for Buildings." 3(1).

Sreekumar, S. 2014. "Effect of Imperfection on Shear Behaviour of Hybrid Plate Girder." 4(May):43–48.

Supervisors, Economics. 2010. "Patch Loading Resistance of Girders with Corrugated Webs PhD Dissertation Balázs KÖVESDI Budapest University of Technology and Economics

Supervisors : László DUNAI , DSc Budapest University of Technology and Economics , Hungary University of Stuttgart , G."

Šutić, Izabela, Paulina Krolo, and Mladen Bulić. 2018. "Nelinearna Analiza Vitkih Čeličnih Greda." *Zbornik Radova* 20(1):127–40. doi: 10.32762/zr.20.1.8.

APPENDIX

Appendix.1   Definition of Parts
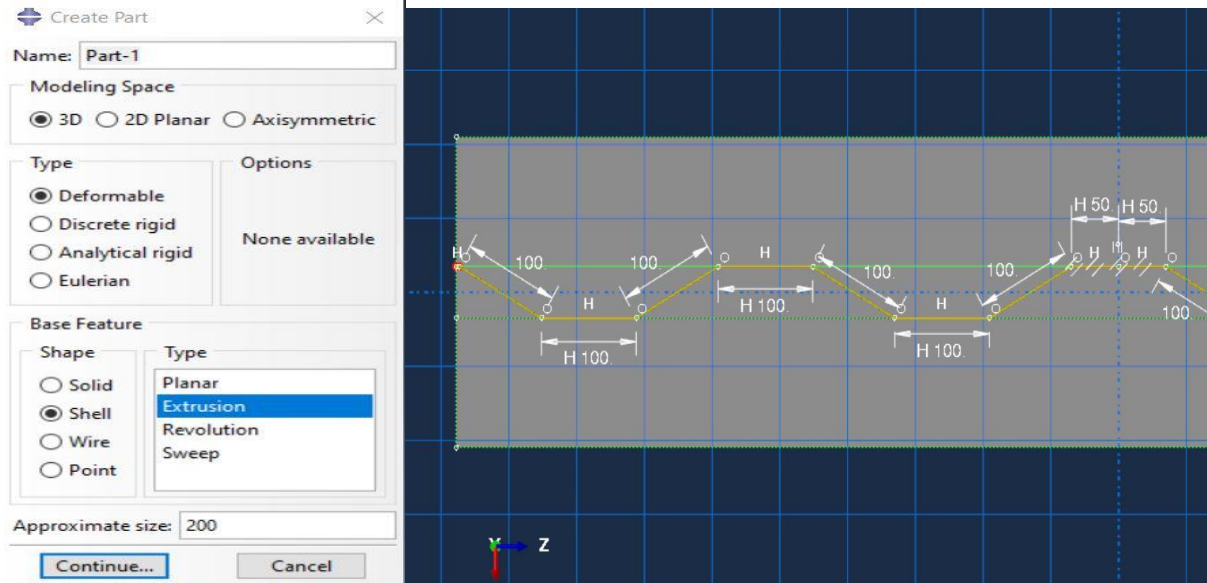
Geometry creation
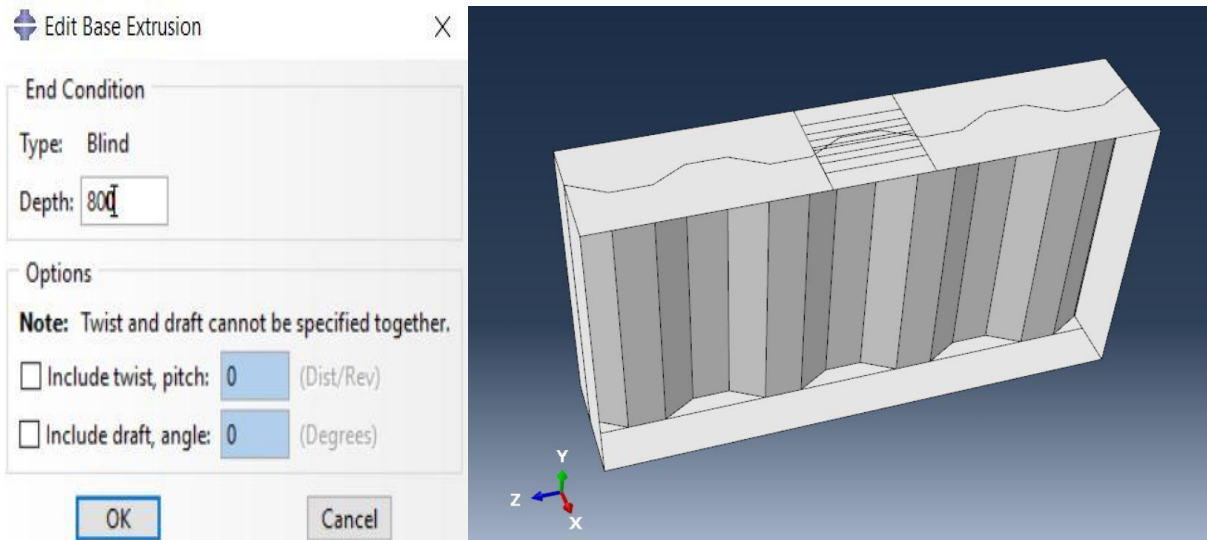
Geometry extrusion

Appendix.2   Definition of material properties and creation of section
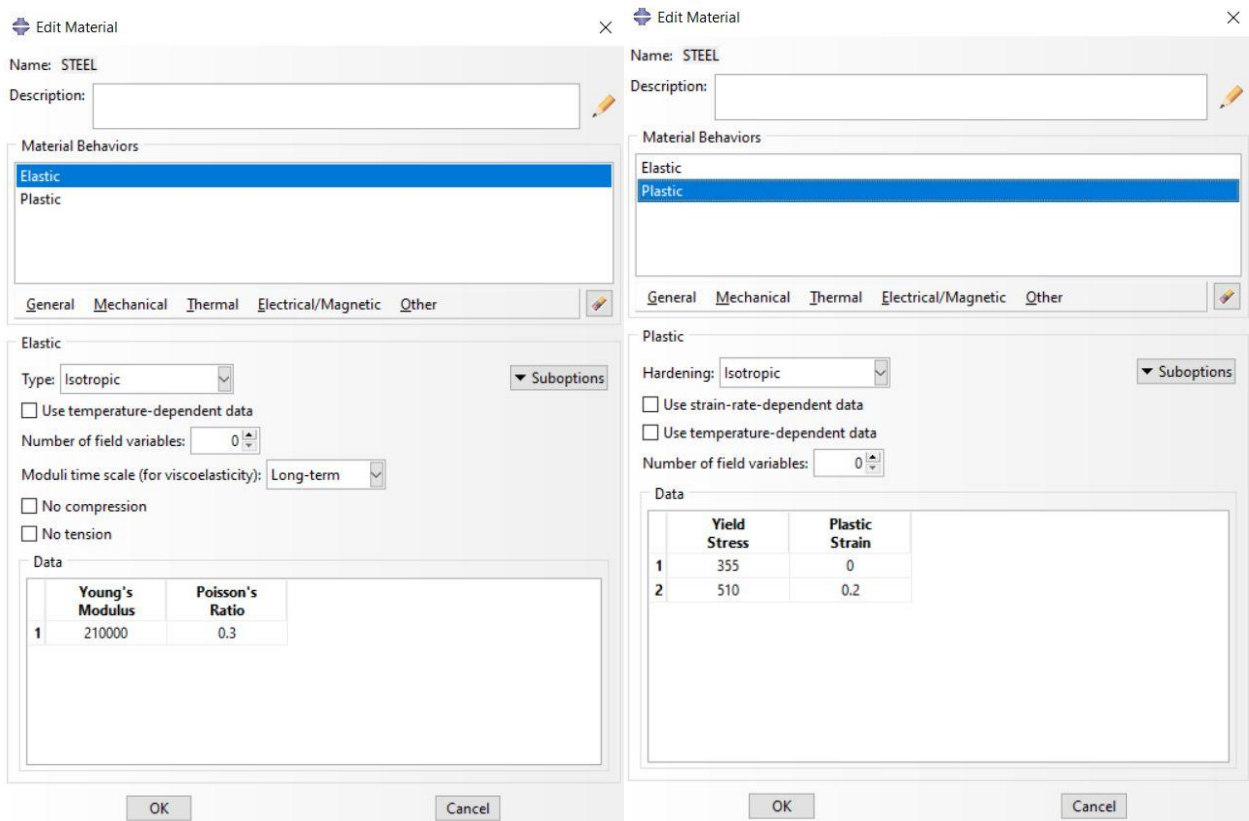
Elastic and Plastic material properties definition
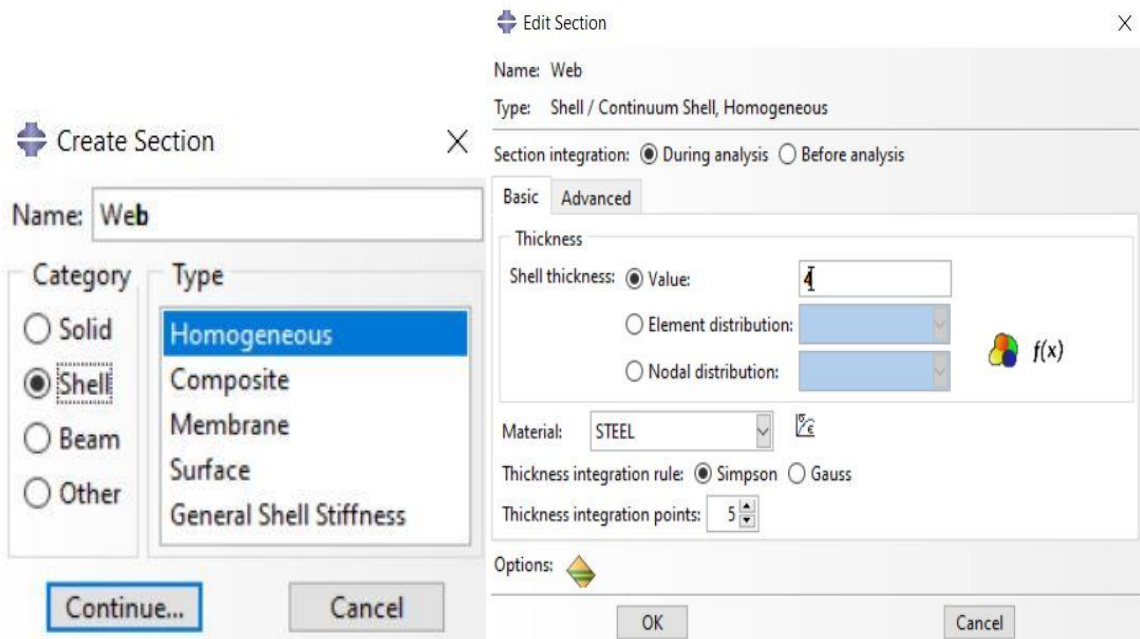
Section creation and assignment

Appendix.3   Creating the step
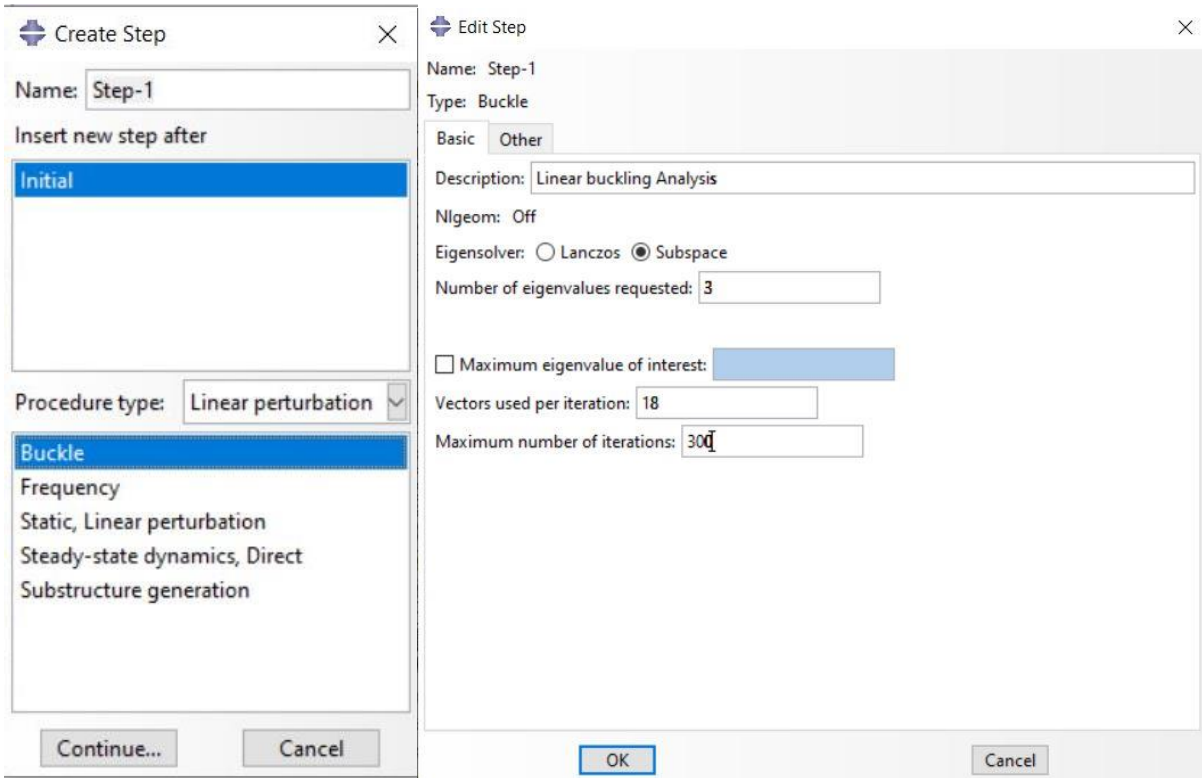
Creation of step for linear Eigenvalue buckling Analysis
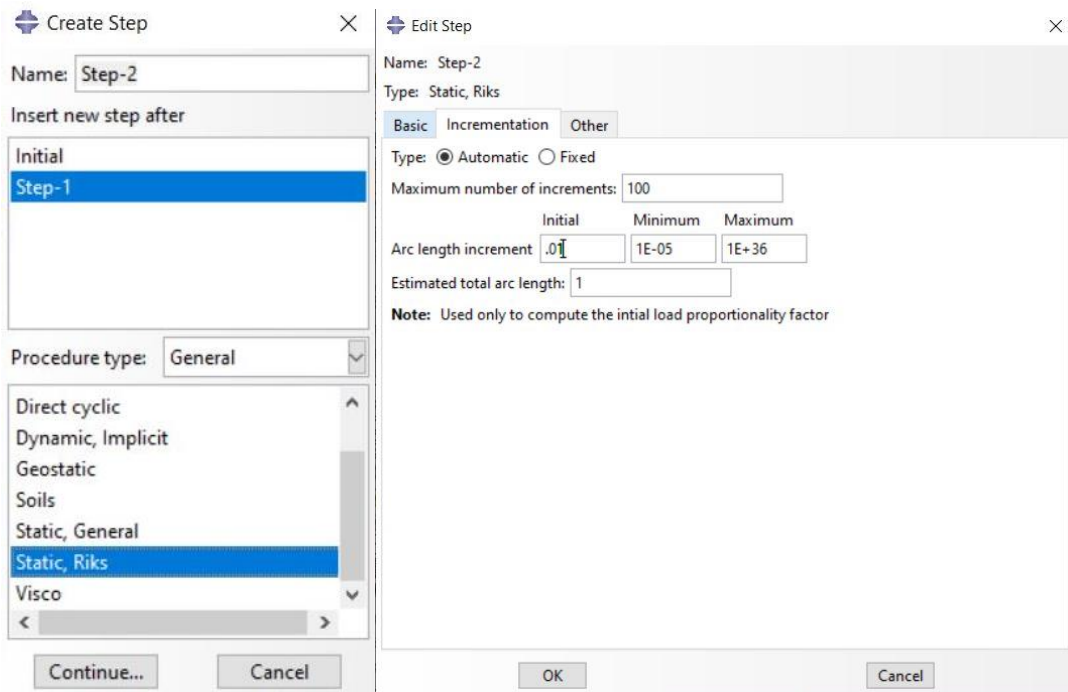
Creation of step for Non-linear Static, Riks Analysis

Appendix.4   Load and Boundary condition definition
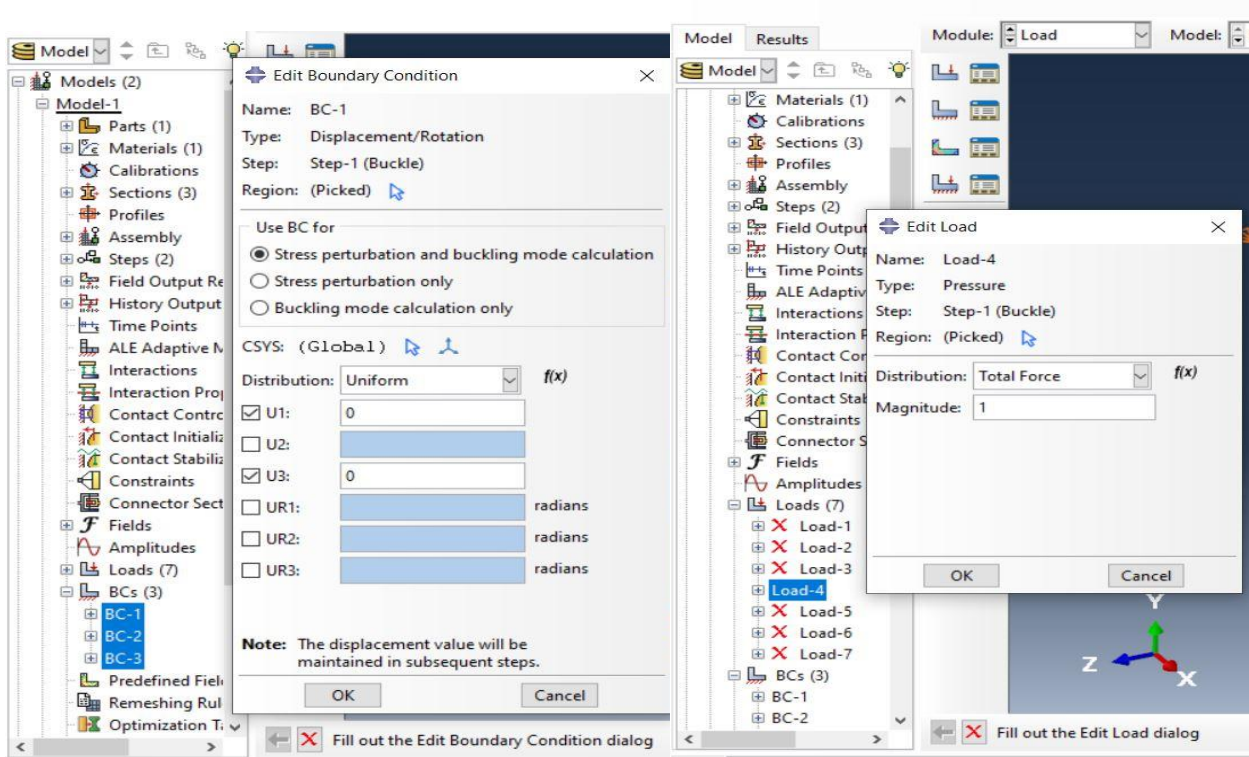
Boundary conditions and load definition
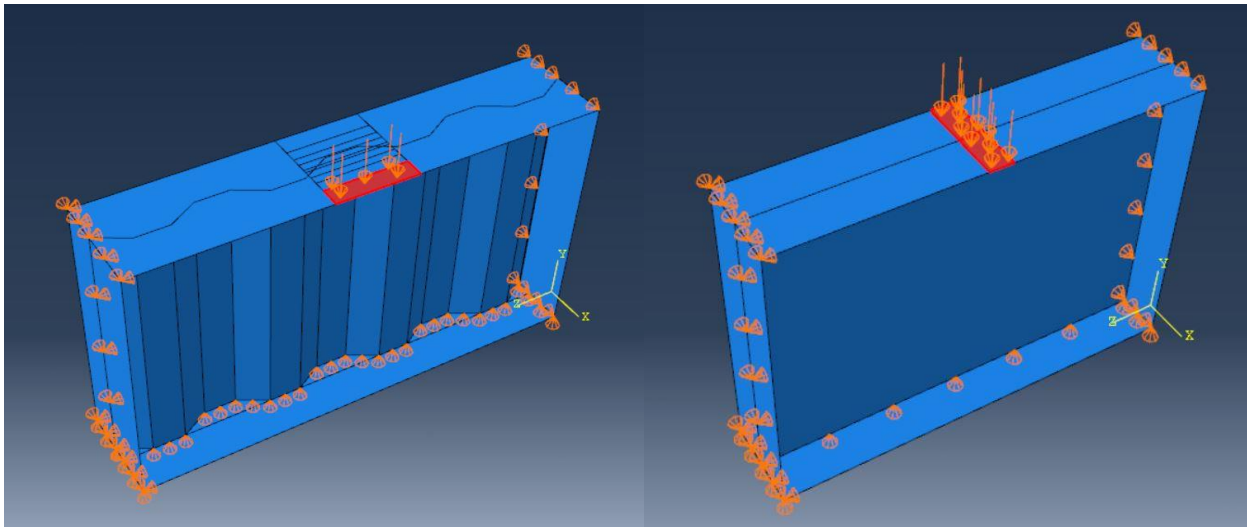
Model with Boundary conditions and loads

Appendix.5   Meshing and Keywords editing to include imperfections
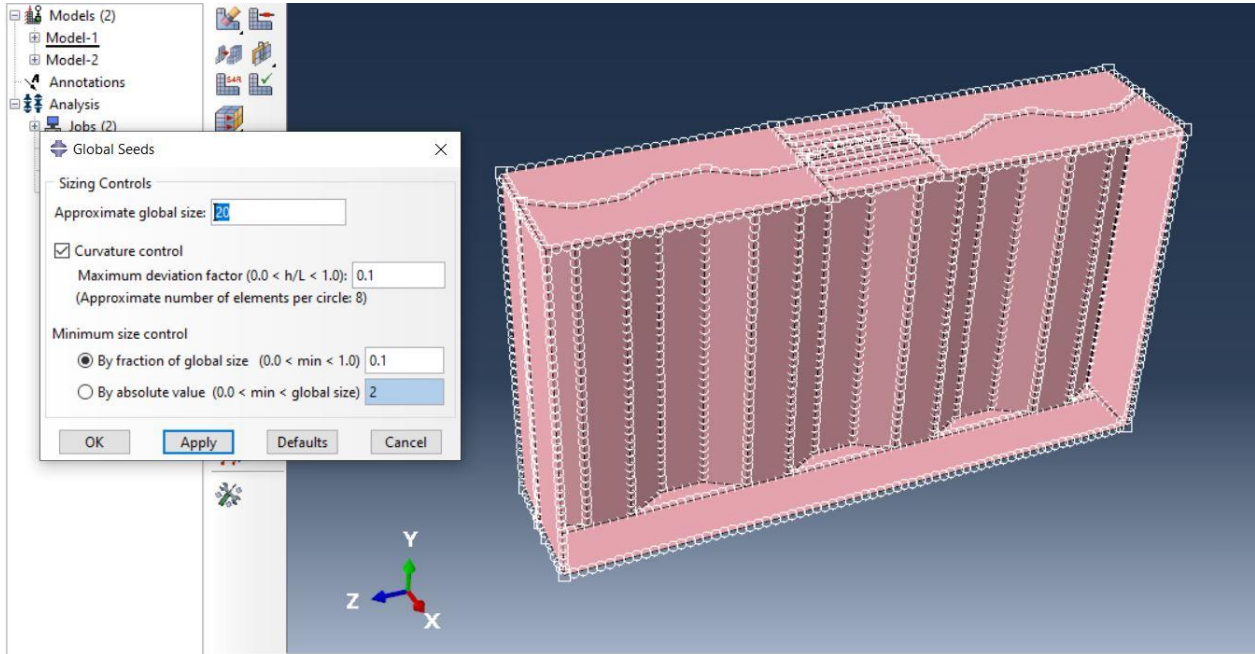
Model seeding at 20mm
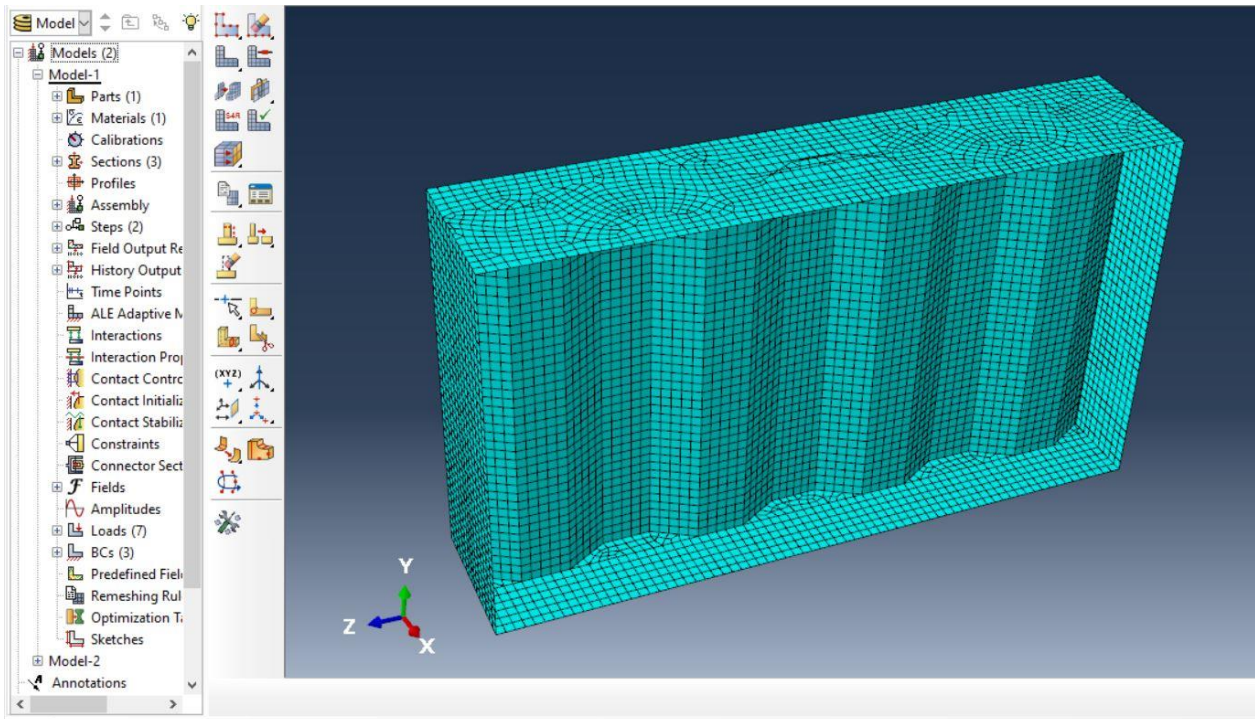
Meshed Model

Appendix.6   Post-processing of non-linear analysis results
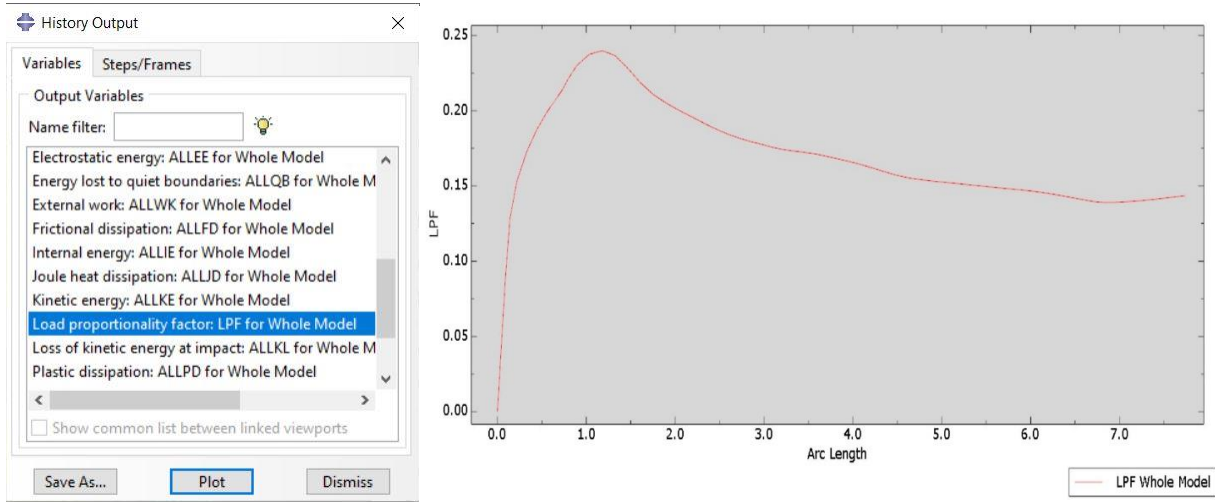
Load-proportionality factor of the whole model
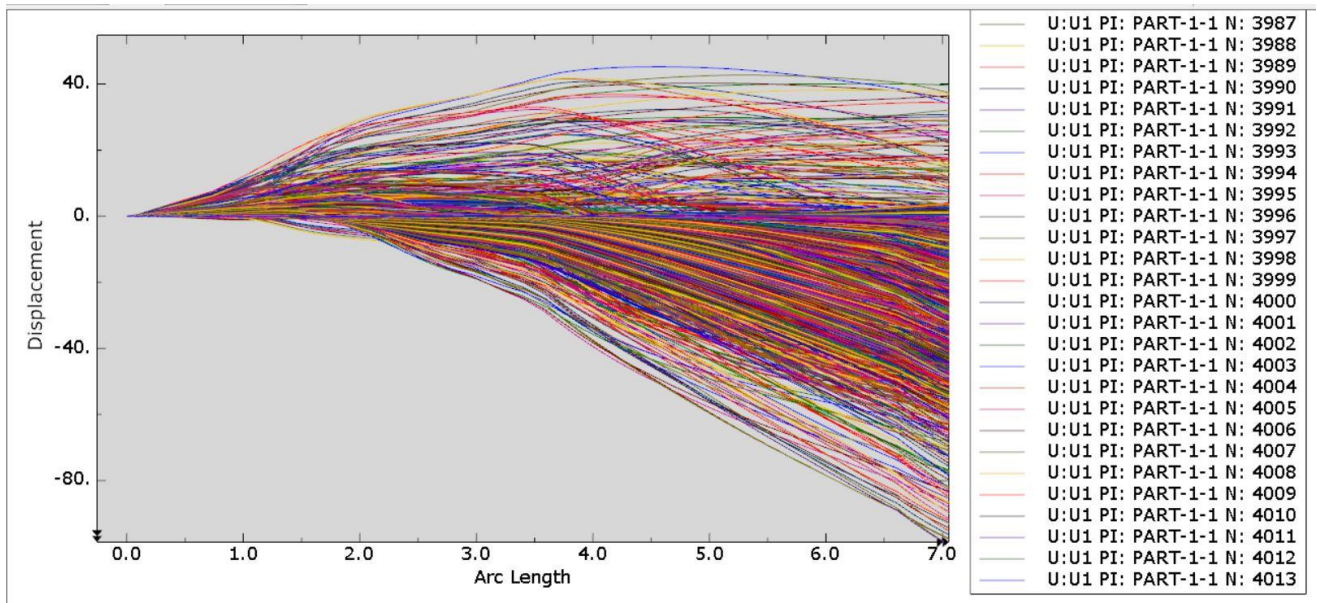
Displacement curves for all the nodes present on the Model
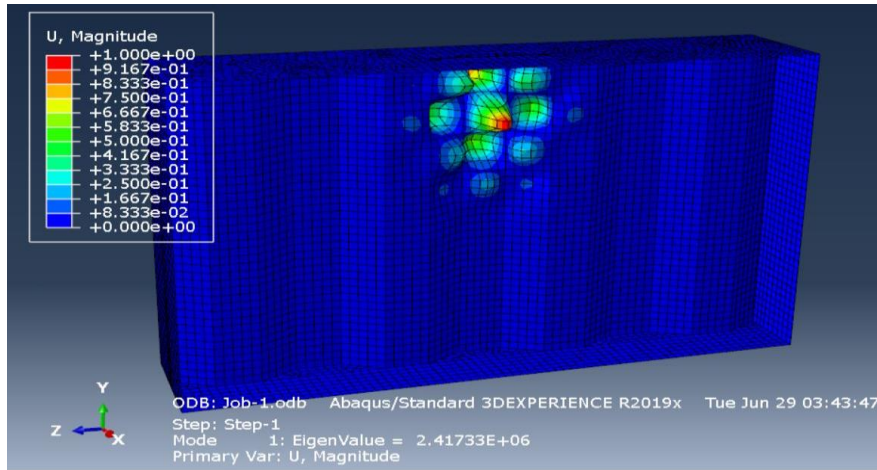
Eigenvalue analysis deformation spectrum
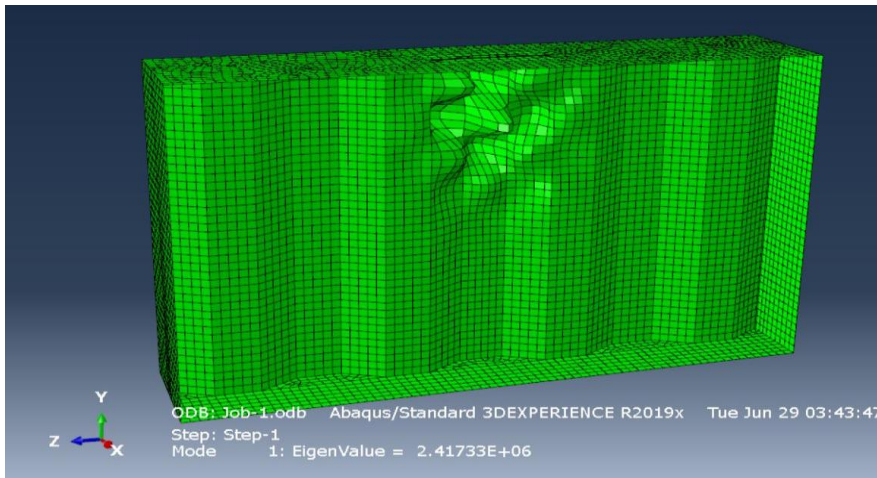
Eigenvalue analysis deformed shape
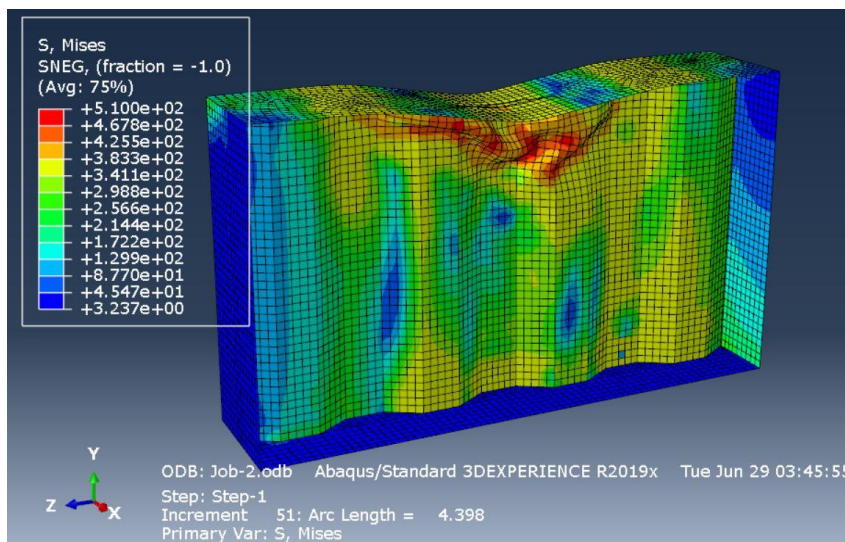
STATIC RIKS analysis deformed shape

Appendix.7   Load displacement values for PG1, PG3, PG5, PG6

PG1			PG3			PG5			PG6		
Ux	LPF	Fu	Ux	LPF	Fu	Ux	LPF	Fu	Ux	LPF	Fu
0.00	0.01	0.845	0.00	0.00	0.000	0.00	0.000	0.000	0.0	0.00	0.00
0.01	0.02	1.690	0.06	0.01	6.093	0.07	0.010	10.863	0.1	0.01	27.61
0.02	0.03	2.954	0.12	0.02	12.159	0.15	0.020	21.661	0.2	0.02	54.98
0.04	0.06	4.846	0.21	0.03	21.208	0.26	0.035	37.740	0.3	0.03	95.59
0.06	0.09	7.673	0.34	0.06	34.673	0.43	0.057	61.600	0.6	0.06	155.53
0.09	0.14	11.892	0.55	0.09	54.633	0.68	0.089	96.832	0.9	0.09	243.14
0.14	0.21	18.174	0.85	0.14	84.069	1.06	0.136	148.498	1.4	0.13	367.40
0.22	0.33	27.497	1.29	0.21	127.170	1.62	0.205	223.545	2.1	0.19	521.50
0.33	0.49	41.280	1.96	0.31	189.712	2.44	0.303	330.541	2.9	0.24	673.44
0.50	0.73	61.566	2.94	0.46	279.305	3.64	0.437	475.706	3.5	0.27	755.62
0.76	1.08	91.302	4.39	0.66	405.227	5.22	0.592	645.113	3.8	0.29	790.48
1.14	1.59	134.794	6.43	0.93	570.066	6.52	0.685	746.202	4.3	0.30	829.50
1.72	2.35	198.404	8.24	1.11	680.838	7.50	0.725	790.014	4.9	0.31	872.09
2.58	2.72	230.039	8.62	1.13	691.847	8.40	0.755	822.076	5.5	0.33	923.15
2.91	2.84	240.476	8.89	1.13	691.628	9.36	0.786	856.113	6.1	0.35	979.44
3.03	2.85	241.419	9.04	1.12	684.917	10.40	0.820	893.111	6.8	0.37	1037.06
3.08	2.84	240.593	9.15	1.11	676.166	11.49	0.852	928.233	7.4	0.39	1093.09
3.14	2.82	238.471	9.24	1.09	667.275	12.56	0.877	955.792	8.1	0.41	1146.35
3.25	2.79	236.042	9.33	1.08	658.696	13.97	0.889	968.995	8.6	0.43	1196.65
3.35	2.76	233.854	9.46	1.06	646.202	15.08	0.879	957.720	9.4	0.46	1267.74
3.45	2.74	231.720	9.59	1.04	634.679	16.03	0.859	936.357	10.2	0.48	1334.45
3.56	2.71	229.563	9.74	1.02	623.974	16.91	0.837	911.515	10.8	0.50	1397.71
3.66	2.69	227.438	9.89	1.01	614.210	17.74	0.813	886.286	11.3	0.53	1458.47
3.76	2.66	225.376	10.08	0.99	605.461	18.52	0.791	861.596	11.7	0.55	1516.46
3.86	2.64	223.414	10.27	0.98	597.227	19.27	0.769	837.855	11.8	0.55	1530.85
3.97	2.62	221.573	10.49	0.97	589.696	19.98	0.748	814.835	11.9	0.56	1545.20
4.07	2.60	219.835	10.72	0.95	582.575	20.66	0.728	792.703	12.0	0.57	1566.63
4.17	2.58	218.141	10.97	0.94	576.000	21.30	0.708	771.561	12.1	0.58	1598.69
4.27	2.56	216.286	11.24	0.93	569.843	21.93	0.690	751.339	12.2	0.59	1630.45
4.38	2.54	214.465	11.53	0.92	564.052	22.55	0.672	732.217	12.2	0.60	1662.22
4.48	2.51	212.674	11.86	0.92	558.745				12.2	0.61	1693.75
4.58	2.49	210.846	12.21	0.91	553.734				12.2	0.62	1725.36
4.68	2.47	209.069	12.57	0.90	548.981				12.1	0.63	1756.98
4.79	2.45	207.282	12.96	0.89	544.579				12.0	0.65	1788.54
4.89	2.43	205.555	13.39	0.89	540.439				11.9	0.66	1819.61
4.99	2.41	203.887	13.82	0.88	536.401				11.7	0.67	1850.37
5.09	2.39	202.253	14.51	0.87	530.860				11.6	0.68	1880.84
5.20	2.37	200.688	15.24	0.86	525.764				11.4	0.69	1910.85
5.30	2.35	199.203	16.00	0.85	521.001						

Appendix.9   Load displacement table for varying aspect ratio

PG2			PG9			PG10		
Ux	LPF	Fu	Ux	LPF	Fu	Ux	LPF	Fu
0.00	0.000	0.000	0.00	0.000	0.000	0.0	0.000	0.000
0.01	0.010	2.742	0.00	0.010	2.444	0.0	0.099	24.061
0.01	0.020	5.476	0.01	0.020	4.880	0.0	0.197	47.715
0.03	0.035	9.565	0.01	0.035	8.522	0.0	0.340	82.517
0.04	0.057	15.665	0.06	0.057	13.951	0.0	0.550	133.411
0.07	0.090	24.742	0.06	0.090	22.021	0.2	0.854	207.417
0.10	0.139	38.182	0.05	0.139	33.943	0.9	1.296	314.627
0.16	0.211	57.910	0.12	0.210	51.366	4.8	1.929	468.314
0.26	0.315	86.410	0.15	0.312	76.265	5.6	2.064	501.094
0.40	0.460	126.264	0.18	0.449	109.988	6.4	2.045	496.603
0.64	0.649	178.221	0.21	0.611	149.639	7.7	2.025	491.599
1.00	0.859	235.807	0.30	0.800	195.784	9.4	1.993	483.833
1.54	1.043	286.461	0.50	0.862	210.899	11.7	1.949	473.102
2.33	1.210	332.052	0.56	0.943	230.674	13.7	1.899	461.074
3.63	1.391	381.863	0.75	1.015	248.406	15.7	1.860	451.608
6.40	1.633	448.220	0.80	1.100	269.174	17.7	1.825	442.960
10.53	1.643	450.918	1.20	1.231	301.346	19.6	1.792	434.972
10.68	1.626	446.496	2.25	1.467	358.936	21.5	1.762	427.711
10.57	1.612	442.496	5.25	1.866	456.546	23.3	1.734	421.005
10.61	1.608	441.312	6.84	1.940	474.796	25.1	1.708	414.758
10.82	1.599	439.042	8.52	1.941	474.992	26.7	1.684	408.813
12.42	1.569	430.828	11.25	1.865	456.514	28.3	1.660	402.996
13.02	1.561	428.558	12.54	1.839	450.103	29.8	1.637	397.358

Appendix.10 Load displacement table for PG18 and PG19

PG18			PG19		
Ux	LPF	Fu	Ux	LPF	Fu
0.0	0.000	0	0.0	0.000	0.0
0.0	0.010	7	0.0	0.010	12.3
0.1	0.020	14	0.0	0.020	24.6
0.1	0.035	24	0.1	0.035	43.0
0.2	0.057	39	0.1	0.057	70.5
0.2	0.091	62	0.1	0.091	111.5
0.4	0.141	97	0.2	0.140	172.6
0.6	0.214	147	0.4	0.214	263.0
1.1	0.314	216	0.5	0.321	395.9
2.4	0.437	300	1.4	0.450	554.3

5.8	0.520	357		2.6	0.490	603.4
6.6	0.525	360		4.1	0.506	623.3
7.4	0.526	361		6.8	0.510	627.7
8.6	0.523	359		9.4	0.504	620.5
10.3	0.515	354		11.8	0.495	609.5
12.7	0.504	346		14.9	0.474	583.9
14.9	0.498	342		17.4	0.445	547.8
16.9	0.493	339		19.9	0.413	508.7
18.8	0.490	337		22.2	0.382	470.8
20.6	0.488	335		22.8	0.375	461.8
22.3	0.486	334		23.3	0.368	452.8

Appendix.11 Load Displacement table for varying Corrugation angle

PG12									
e= 0				**e =60**			**e =120**		
x	LPF	Force		x	LPF	Force	x	LPF	Force
0.0	0.00	0		0.00	0.00	0	0.0	0.00	0
0.0	0.01	8		0.07	0.01	11	0.1	0.01	8
0.1	0.02	16		0.14	0.02	21	0.2	0.02	15
0.1	0.03	28		0.25	0.03	37	0.3	0.03	26
0.1	0.06	46		0.43	0.06	61	0.5	0.06	43
0.2	0.09	72		0.70	0.09	97	0.8	0.09	68
0.4	0.14	112		1.11	0.14	149	1.3	0.14	105
0.6	0.21	170		1.79	0.21	221	1.9	0.20	151
1.0	0.32	252		3.37	0.28	298	3.3	0.25	192
2.2	0.45	357		5.20	0.32	342	4.9	0.28	213
5.8	0.52	413		7.14	0.34	366	6.6	0.30	225
9.0	0.51	402		9.14	0.35	379	8.2	0.31	234
9.7	0.50	401		11.27	0.36	388	9.8	0.32	243
10.4	0.50	400		13.69	0.37	395	11.4	0.33	252
11.4	0.50	399		14.2	0.37	396	13.2	0.34	260
12.8	0.50	398		16.0	0.37	393	15.0	0.35	268
14.2	0.50	399		18.0	0.36	386	15.5	0.36	268
15.5	0.50	399		18.0	0.35	378	15.9	0.35	268
17.3	0.50	399		23.0	0.35	372	16.0	0.35	265
19.1	0.50	398		23.0	0.34	367	16.1	0.35	263
20.7	0.50	397		28.00	0.34	363	16.3	0.35	262
22.9	0.49	393					16.6	0.35	262
25.0	0.49	388					17.3	0.35	263
26.8	0.48	381					17.6	0.35	263
28.6	0.47	374					17.8	0.34	260
30.2	0.46	366					18.0	0.34	259

Appendix.12 Load-displacement table for Local fold ratio variation

PG25			PG26			PG27		
Ux	LPF	Fu	Ux	LPF	Force	Ux	LPF	Force
0.0	0.000	0	0.0	0.000	0	0.0	0.000	0
0.1	0.010	11	0.0	0.010	9	0.0	0.010	7
0.1	0.020	22	0.0	0.020	18	0.0	0.020	15
0.2	0.035	38	0.0	0.035	31	0.0	0.035	26
0.4	0.057	62	0.0	0.057	51	0.0	0.057	42
0.6	0.090	98	0.0	0.091	81	0.0	0.091	67
1.0	0.135	147	0.1	0.138	123	0.1	0.139	102
1.6	0.184	199	0.4	0.193	172	0.4	0.198	146
2.2	0.214	231	0.7	0.230	205	1.0	0.257	189
2.7	0.230	249	1.3	0.251	224	2.0	0.287	211
3.2	0.241	261	2.0	0.265	236	3.2	0.306	225
3.6	0.249	270	2.9	0.276	246	4.8	0.323	237
3.9	0.258	279	3.9	0.286	255	6.6	0.342	251
4.4	0.266	288	5.7	0.301	269	8.5	0.362	266
4.8	0.274	297	7.6	0.317	283	10.6	0.381	280
5.3	0.282	305	9.6	0.333	297	12.8	0.396	291
5.9	0.288	312	11.6	0.346	308	15.0	0.410	301
7.0	0.297	322	13.7	0.354	316	17.3	0.420	308
9.9	0.307	332	15.6	0.359	320	19.6	0.428	314
16.5	0.309	335	17.7	0.363	324	21.8	0.433	318
18.0	0.310	336	19.8	0.367	327	24.1	0.437	321
19.5	0.311	337	21.9	0.370	330	26.4	0.440	323
21.6	0.311	337	24.1	0.373	332	28.6	0.441	324
24.5	0.313	339	26.4	0.375	334	30.8	0.441	324
27.2	0.314	341	28.5	0.375	334	31.4	0.440	323
29.6	0.316	342	29.0	0.375	334	31.9	0.440	323
31.9	0.317	343	29.5	0.374	334	32.6	0.439	322
34.1	0.318	345	30.3	0.373	333	33.7	0.437	321
36.1	0.319	345	31.3	0.370	330	34.3	0.436	320
38.1	0.319	346	32.0	0.369	329	35.2	0.434	319
39.9	0.319	346	32.9	0.368	328	36.6	0.432	317
42.4	0.318	345	33.9	0.367	327	38.1	0.430	316
44.8	0.316	343	34.9	0.366	327	39.5	0.429	315
46.9	0.314	340	36.0	0.366	326	41.0	0.428	314
49.0	0.310	336	37.6	0.364	325	42.6	0.427	313
51.0	0.308	334	39.1	0.363	323	44.1	0.426	313
53.0	0.306	332	40.6	0.360	321	45.6	0.426	313
55.0	0.305	331	41.9	0.357	318	47.9	0.425	312

Appendix.13 Load displacement table for Varying Global ratio

PG33 (e=120)			PG33 (e=0)		
Ux	LPF	Fu	Ux	LPF	Fu
0.00	0.000	0.000	0.0	0.000	0.000
0.00	0.010	7.154	0.0	0.010	9.479
0.00	0.020	14.300	0.0	0.020	18.950
0.00	0.035	25.004	0.1	0.035	33.142
0.01	0.057	41.026	0.1	0.057	54.396
0.04	0.091	64.895	0.1	0.091	86.200
0.11	0.139	99.513	0.2	0.141	133.688
0.31	0.201	144.229	0.4	0.215	203.495
0.82	0.267	191.340	0.6	0.317	300.798
1.63	0.301	215.314	1.7	0.445	421.582
2.73	0.321	229.566	3.9	0.483	458.276
4.10	0.338	241.636	6.1	0.484	458.488
5.70	0.355	254.223	8.2	0.480	455.105
7.47	0.374	267.661	10.4	0.477	452.490
9.38	0.393	281.028	12.4	0.474	449.911
11.38	0.409	292.999	14.4	0.472	447.265
14.51	0.431	308.289	17.1	0.467	443.158
15.30	0.435	311.345	19.5	0.464	439.549
16.07	0.439	314.010	21.7	0.459	435.443
16.85	0.442	316.466	23.7	0.455	431.482
18.02	0.447	319.688	25.5	0.451	428.127
19.72	0.452	323.339	27.2	0.449	425.350
21.98	0.452	323.797	28.2	0.447	424.060
24.43	0.452	323.480	29.5	0.445	422.087
26.95	0.453	324.299	31.4	0.442	418.900
29.52	0.454	325.059	33.2	0.439	415.875
31.98	0.452	323.828	34.9	0.436	413.108
32.56	0.451	323.146	36.5	0.433	410.543
33.13	0.450	322.297	38.0	0.430	408.179
33.97	0.448	320.894	38.9	0.429	407.019
35.28	0.446	319.083	40.1	0.427	405.268
37.37	0.443	317.209	41.9	0.425	402.695
39.60	0.441	315.933	43.6	0.422	400.031
41.87	0.439	313.873	45.2	0.418	396.785
44.05	0.434	310.594	45.5	0.417	395.888
44.58	0.433	309.980	45.9	0.416	394.881
45.12	0.432	309.464	46.5	0.415	393.090
45.93	0.431	308.802	47.0	0.412	390.799
47.19	0.431	308.187	47.4	0.409	388.067

PG34 (e=120)			PG34 (e=0)		
Ux	LPF	Fu	Ux	LPF	Fu
0.0	0.000	0.000	0.0	0.000	0.000
0.0	0.010	20.653	0.0	0.010	31.542
0.0	0.020	41.269	0.0	0.020	63.040
0.0	0.035	71.946	0.1	0.035	110.198
0.0	0.056	115.014	0.1	0.057	180.446
0.0	0.080	165.646	0.2	0.089	280.809
0.2	0.101	209.099	0.5	0.132	416.277
0.3	0.111	229.573	1.1	0.183	577.639
0.4	0.113	233.577	3.1	0.228	719.363
0.5	0.115	237.346	6.5	0.235	741.068
0.6	0.117	242.815	7.3	0.234	739.158
0.7	0.121	250.956	8.0	0.233	735.575
0.9	0.126	259.626	9.2	0.231	729.120
1.1	0.130	268.965	10.8	0.228	719.202
1.3	0.137	284.223	13.1	0.224	705.631
1.7	0.145	299.360	15.2	0.220	694.466
2.0	0.152	313.908	17.2	0.217	684.977
2.6	0.162	334.101	19.1	0.214	677.076
3.3	0.171	353.084	20.9	0.212	670.656
4.0	0.179	369.028	22.5	0.211	665.756
4.8	0.185	382.409	24.2	0.210	661.987
5.7	0.190	393.665	25.0	0.209	660.501
6.6	0.195	403.317	26.3	0.209	658.585
7.6	0.199	411.888	28.1	0.208	656.331
8.6	0.203	419.578	29.9	0.207	654.443
9.7	0.206	426.405	31.6	0.207	652.789
10.8	0.209	432.099	33.2	0.206	650.781
11.9	0.211	436.202	34.8	0.205	648.212
12.9	0.212	438.776	36.3	0.204	644.979
14.0	0.213	440.154	37.7	0.203	640.689
15.1	0.213	440.737	39.2	0.201	635.191
16.2	0.213	440.309	41.1	0.198	624.474
17.1	0.211	435.278	43.0	0.194	611.718
17.3	0.209	432.828	44.8	0.189	597.750
17.5	0.208	430.064	46.5	0.185	584.201
17.8	0.206	425.953	48.1	0.181	572.578
18.3	0.204	420.917	49.6	0.178	563.143
19.1	0.201	416.175	51.0	0.176	555.349
20.0	0.201	414.666	52.3	0.174	548.796
21.0	0.201	414.995	53.6	0.172	543.064

PG35 (e=120)			PG35 (e=0)		
Ux	LPF	Force	Ux	LPF	Force
0.0	0.000	0.000	0.0	0.000	0.000
0.0	0.010	41.219	0.0	0.010	72.572
0.0	0.020	82.065	0.0	0.020	144.993
0.1	0.033	135.971	0.1	0.035	251.518
0.4	0.046	190.095	0.2	0.054	392.166
1.0	0.053	218.734	0.3	0.078	566.106
1.7	0.057	234.568	0.8	0.103	746.093
2.7	0.060	247.129	1.5	0.119	866.112
3.9	0.063	259.134	2.5	0.126	912.790
5.2	0.066	272.326	3.6	0.129	940.224
6.7	0.070	287.145	5.2	0.133	963.937
8.3	0.073	302.743	7.3	0.135	980.600
10.0	0.077	318.610	9.9	0.136	984.859
12.8	0.083	340.884	10.5	0.136	985.106
15.8	0.088	361.961	11.2	0.136	984.786
19.0	0.092	381.786	12.1	0.135	983.297
22.3	0.097	399.606	13.6	0.135	978.936
25.6	0.101	415.269	15.1	0.134	973.718
29.0	0.104	429.229	16.5	0.133	968.399
32.4	0.107	441.624	18.5	0.132	960.230
35.9	0.110	452.848	20.5	0.131	952.520
39.3	0.112	463.117	22.3	0.130	944.707
42.8	0.115	472.619	24.1	0.129	936.525
46.2	0.117	481.328	25.8	0.128	927.789
49.7	0.119	489.373	27.4	0.126	918.029
53.1	0.120	496.873	29.0	0.125	906.918
56.4	0.122	503.898	30.5	0.123	894.672
59.8	0.124	510.523	31.9	0.121	881.737
63.1	0.125	516.797	33.3	0.119	868.314
66.5	0.127	522.728	34.7	0.118	855.298
69.7	0.128	528.379	36.5	0.115	837.159
73.0	0.129	533.778	38.3	0.113	821.898
76.3	0.131	538.934	40.0	0.111	809.471
79.5	0.132	543.858	41.5	0.110	799.304
82.7	0.133	548.592	43.0	0.109	791.056
85.9	0.134	553.157	44.4	0.108	784.479
89.1	0.135	557.557	45.7	0.107	779.370
92.2	0.136	561.797	46.9	0.107	775.627
95.4	0.137	565.862	48.1	0.106	772.866

Appendix.14 Variation of eccentricity with loading length, Figure 3.16

PG12					PG13				
e (mm)	e/bf	F_{cr} (kN)	LPF	F_u (kN)	e (mm)	e/bf	F_{cr} (kN)	LPF	F_u (kN)
-120	-0.40	457.818	0.717	328.256	-120	-0.40	465.884	0.710	330.778
-70.5	-0.24	585.496	0.604	353.640	-70.5	-0.24	602.789	0.596	359.262
0	0.00	1000.170	0.413	425.000	0	0.00	1002.361	0.425	435.000
60	0.20	944.296	0.442	417.379	60	0.20	943.944	0.450	424.775
120	0.40	735.702	0.455	334.744	120	0.40	737.413	0.458	337.735

PPG14					PPG15				
e (mm)	e/bf	F_{cr} (kN)	LPF	F_u (kN)	e (mm)	e/bf	F_{cr} (kN)	LPF	F_u (kN)
-120	-0.40	487.100	0.700	340.970	-120	-0.40	502.094	0.690	346.445
-70.5	-0.24	644.379	0.580	373.740	-70.5	-0.24	670.762	0.577	387.030
0	0.00	1070.410	0.426	455.995	0	0.00	1090.090	0.437	476.369
60	0.20	943.593	0.472	445.376	60	0.20	945.929	0.481	454.992
120	0.40	743.399	0.476	353.858	120	0.40	750.380	0.482	361.683

PPG16					PPG17				
e (mm)	e/bf	F_{cr} (kN)	LPF	F_u (kN)	e (mm)	e/bf	F_{cr} (kN)	LPF	F_u (kN)
-120	-0.40	516.360	0.674	348.027	-120	-0.40	562.170	0.640	359.789
-70.5	-0.24	694.299	0.565	392.279	-70.5	-0.24	761.108	0.520	395.776
0	0.00	1102.810	0.442	487.442	0	0.00	1148.770	0.445	511.203
60	0.20	948.738	0.492	466.779	60	0.20	987.240	0.492	485.722
120	0.40	757.832	0.496	375.885	120	0.40	795.444	0.485	385.790

Appendix.15 Variation of eccentricity with Corrugation angle Figure 3.19

PG20					PG21				
e (mm)	e/bf	F_{cr} (kN)	LPF	F_u (kN)	e (mm)	e/bf	F_{cr} (kN)	LPF	F_u (kN)
-120	-0.40	372.114	0.669	248.944	-120	-0.40	444.124	0.732	325.099
-60	-0.20	516.402	0.626	323.268	-60	-0.20	626.773	0.603	377.944
-26	-0.09	649.303	0.579	375.946	-50	-0.17	671.592	0.574	385.494
0	0.00	795.146	0.502	399.163	0	0.00	995.168	0.450	447.826
60	0.20	1071.350	0.369	370.000	60	0.20	976.712	0.448	430.000
120	0.40	755.657	0.355	268.258	120	0.40	734.325	0.441	323.837

PPG22					PPG23				
e (mm)	e/bf	F_{cr} (kN)	LPF	F_u (kN)	e (mm)	e/bf	F_{cr} (kN)	LPF	F_u (kN)
-120	-0.40	502.672	0.691	347.346	-120	-0.40	545.791	0.710	387.730
-79.3	-0.26	670.747	0.573	384.338	-86.5	-0.29	666.247	0.626	417.071
-60	-0.20	722.076	0.545	393.531	-60	-0.20	800.284	0.526	420.949
0	0.00	1090.550	0.437	476.570	0	0.00	1104.220	0.446	492.482
60	0.20	946.095	0.482	450.000	60	0.20	958.209	0.502	481.021
79.3	0.26	906.243	0.487	441.341	86.5	0.29	885.146	0.515	455.850
120	0.40	750.809	0.483	362.641	120	0.40	796.304	0.513	408.504

PPG24				
e (mm)	e/bf	F_{cr} (kN)	LPF	F_u (kN)
-120	-0.40	569.876	0.756	430.826
-94	-0.31	668.237	0.689	460.415
-60	-0.20	846.372	0.544	460.426
0	0.00	1107.740	0.470	520.638
60	0.20	994.173	0.520	505.000

94	0.31	912.807	0.527	481.049
120	0.40	839.807	0.535	449.297

Appendix.1 Variation of eccentricity with local fold ratio for equal folds Figure 3.22

PG25					PG26				
e (mm)	e/bf	F_{cr} (kN)	LPF	F_u (kN)	e (mm)	e/bf	F_{cr} (kN)	LPF	F_u (kN)
-120	-0.40	748.215	0.450	336.697	-120	-0.40	538.883	0.588	316.863
-60	-0.20	1139.650	0.390	444.464	-60	-0.20	794.213	0.515	409.020
-25	-0.08	1671.590	0.321	536.580	-37.5	-0.13	967.620	0.445	430.591
0	0.00	2417.310	0.240	580.154	0	0.00	1443.700	0.341	492.302
25	0.08	2581.650	0.207	534.402	37.5	0.13	1486.410	0.320	475.651
60	0.20	1790.710	0.263	470.957	60	0.20	1307.470	0.350	457.615
120	0.40	1083.586	0.319	345.664	120	0.40	891.778	0.370	329.958
PPG27					**PPG28**				
e (mm)	e/bf	F_{cr} (kN)	LPF	F_u (kN)	e (mm)	e/bf	F_{cr} (kN)	LPF	F_u (kN)
-120	-0.40	444.124	0.732	305.000	-120	-0.40	382.862	0.742	284.084
-60	-0.20	626.773	0.603	377.944	-60	-0.20	512.376	0.715	366.349
-50	-0.17	671.592	0.574	385.494	0	0.00	716.796	0.612	430.000
0	0.00	995.168	0.450	450.000	60	0.20	787.148	0.501	394.361
60	0.20	976.712	0.448	437.567	120	0.40	606.957	0.486	294.981
120	0.40	734.325	0.441	323.837					

Appendix.2 Variation of eccentricity with local fold ratio for unequal folds Figure 3.25

PG29					PG30				
e (mm)	e/bf	F_{cr} (kN)	LPF	F_u (kN)	e (mm)	e/bf	F_{cr} (kN)	LPF	F_u (kN)
-120	-0.40	424.150	0.732	310.478	-120	-0.40	420.358	0.770	323.676

-60	-0.20	626.773	0.603	377.944		-60	-0.20	558.970	0.709	396.310
-50	-0.17	671.592	0.574	385.494		-37.5	-0.13	663.779	0.624	414.198
0	0.00	995.168	0.450	447.826		0	0.00	949.205	0.483	458.466
60	0.20	976.712	0.448	437.567		37.5	0.13	1353.690	0.357	483.267
120	0.40	734.325	0.441	323.837		60	0.20	1030.830	0.438	451.504
						120	0.40	708.664	0.447	316.773

PPG31						PG32				
e (mm)	e/bf	F_{cr} (kN)	LPF	F_u (kN)		e (mm)	e/bf	F_{cr} (kN)	LPF	F_u (kN)
-120	-0.40	400.297	0.856	342.654		-120	-0.40	489.571	0.557	272.691
-60	-0.20	488.775	0.834	407.638		-60	-0.20	687.033	0.510	350.387
-25	-0.08	659.017	0.700	461.312		0	0.00	900.701	0.486	437.741
0	0.00	879.776	0.553	486.516		60	0.20	748.361	0.567	424.321
25	0.08	1264.990	0.401	507.261		120	0.40	585.549	0.542	317.368
60	0.20	892.493	0.544	485.516						
120	0.40	550.136	0.586	322.380						

Appendix.3 Variation of eccentricity with Global fold ratio **Figure 3.27**

PG33						PG34				
e (mm)	e/bf	F_{cr} (kN)	LPF	F_u (kN)		e (mm)	e/bf	F_{cr} (kN)	LPF	F_u (kN)
-120	-0.40	392.664	0.790	310.205		-120	-0.40	1184.600	0.325	384.995
-60	-0.20	559.672	0.711	397.927		-60	-0.20	1756.010	0.335	588.263
-37.5	-0.13	664.144	0.627	416.418		-37.5	-0.13	2128.940	0.310	659.971
0	0.00	948.264	0.524	496.890		0	0.00	3156.650	0.235	741.813
37.5	0.13	1361.560	0.352	479.269		37.5	0.13	4117.020	0.177	728.713
60	0.20	1110.270	0.402	446.329		60	0.20	3260.940	0.195	635.883

120	0.40	715.782	0.454	324.965		120	0.40	2067.200	0.213	440.314

PG35										
e (mm)	e/bf	F_{cr} (kN)	LPF	F_u (kN)						
-120	-0.40	2490.020	0.201	500.494						
-60	-0.20	3839.800	0.215	825.557						
-37.5	-0.13	4755.330	0.200	951.066						
0	0.00	7267.260	0.136	988.347						
37.5	0.13	8291.190	0.107	887.157						
60	0.20	6540.840	0.123	804.523						
120	0.40	4127.640	0.135	557.231						